Energy-efficient solutions for non-orthogonal multiple access systems aided by ambient backscattering

Hajar El Hassani

Doctoral Thesis

Doctoral School : EM2PSI (n° 405)

Domain : STIC

Specialty : Telecommunications

Establishment : CY Cergy Paris University

Research Lab : ETIS - UMR 8051

Thesis presented and defended by :

Hajar EL HASSANI

Thesis Topic :

Energy-efficient solutions for non-orthogonal multiple access systems aided by ambient backscattering

Thesis defended on 02/12/2022

Jury members :

E. VERONICA BELMEGA	Professor, Université Gustave Eiffel, France	Thesis director
ANNE SAVARD	Associate professor, IMT Nord Europe, France	Thesis supervisor
MICHÈLE WIGGER	Professor, Télécom ParisTech, France	Reviewer
ROBERT SCHOBER	Professor, University of Erlangen-Nuremberg, Germany	Reviewer
MARCO DI RENZO	DR CNRS, Université Paris-Saclay, France	Examiner
MARIA-GABRIELLA DI BENEDETTO	Professor, Sapienza University of Rome, Italy	Examiner
JEAN-MARIE GORCE	Professor, INSA Lyon, France	Examiner
PHILIPPE MARY	Associate professor, INSA Rennes, France	Examiner
RODRIGO C. DE LAMARE	Professor, PUC-Rio and University of York, Brazil	Invited member

Acknowledgments

I would like to thank my advisors Prof. Veronica Belmega and Dr. Anne Savard for giving me the opportunity to work on this thesis. I am sincerely thankful for all your help, support and continuous encouragement. Without your valuable suggestions, comments and guidance, this research work would not have been possible.

I also would like to take this opportunity to thank Prof. Rodrigo C. de Lamare for sharing his ideas and helpful suggestions for my work.

I am grateful to my husband and my two beautiful amazing children for their great support and patience. They have been a great source of strength, motivation and energy.

Words cannot express the appreciation and gratitude for my parents, for their unconditional love and support throughout all these years. Without believing in me, motivating me and supporting me with everything they can, I would not have been able to accomplish any of this.

Also, I would like to thank my sisters for their support and encouragements. A special thought for my grandfather and my grandmother, may God have mercy on their souls, for all their love and blessings.

I also thank all the departmental staff, particularly Annick Bertinotti, for helping me during these years of my PhD.

Abstract

Recent advances in wireless communications have paved the way to a tremendous increase in the number of connected devices. As this number continues to grow, so do the challenges of achieving massive connectivity and higher energy efficiency. On the one hand, Non-Orthogonal Multiple Access (NOMA) is a promising technology enabling massive connectivity where multiple users are served on the same radio resources by superposing their signals. On the other hand, Ambient Backscatter Communication (AmBC) has been introduced as a low-energy technology allowing both a passive transmission of data and energy harvesting. Since resource management plays a significant role in improving the systems performance, we focus in this thesis on maximizing the energy efficiency in NOMA systems aided by ambient backscattering with perfect knowledge or unknown channel state information at the transmitter (CSIT).

First, assuming perfect knowledge of the CSIT, we investigate the energy-efficiency maximization for a downlink multi-user NOMA system, which is formulated as a trade-off between the sum rate versus the overall power consumption. Considering the power budget at the transmitter and the minimum quality of service requirements at each user, the optimal power allocation is obtained in closed form and characterizes the entire Pareto-optimal boundary of the rate vs. power trade-offs. In the special case of maximizing the ratio sum rate vs. overall power, our solution reduces the complexity of the Dinkelbach procedure to a univariate bisection method. The benefit of NOMA over Orthogonal Multiple Access (OMA) in terms of the rate vs. power optimal trade-off is highlighted via simulation results.

We then extend our investigation to include AmBC where an ambient backscatter device modulates its own information by reflecting the incident signal coming from the transmitter. First, we consider the special case of a fixed backscattering state where the ambient backscatter device is fully cooperative and can be considered as a passive relay. We also extend this investigation to multiple ambient backscattering devices. The optimal resource allocation policies are obtained in closed form, simplifying Dinkelbach's algorithm. In the general case in which the ambient backscatter is not always in a fixed backscattering state, we derive the achievable rate region using information-theoretic tools and analytically obtain the optimal energy-efficient resource allocation policy. The proposed solution is shown to achieve higher energy efficiency than other benchmark schemes. We also highlight that the energy efficiency increases with the number of

cooperative backscatter devices. To complete our study, we also investigate the impact of imperfect CSIT on our solution and show its pertinence when the quality of the estimation is sufficient.

Our analytical solutions, which rely on the CSIT, do not require the use of expensive iterative algorithms in terms of computing power, thus contributing to greener communications. However, the perfect CSIT is challenging to obtain in practice. Therefore, we further investigate a two-user NOMA system in a time-varying channel that is unknown at the transmitter side (in state and distribution) and propose an online reinforcement learning method, relying only on a 1-bit feedback to minimize the overall system outage probability and outage-based energy efficiency. Remarkably, our proposed scheme requires only a single bit of feedback from each user and is still able to outperform OMA in many settings of interest including stochastic and even non-stationary ones as demonstrated by the numerical results.

Résumé

Le progrès récent des communications sans fil a ouvert la voie à une explosion du nombre de dispositifs connectés. Cette croissance sans précédent pose de nombreux défis en termes de connectivité massive et d'efficacité énergétique. D'une part, l'accès multiple non-orthogonal (NOMA) est une technologie prometteuse permettant une connectivité massive où plusieurs utilisateurs sont servis sur les mêmes ressources radio en superposant leurs signaux. D'autre part, la communication par rétrodiffusion ambiante (AmBC) a été introduite en tant que technologie à faible consommation d'énergie permettant à la fois une transmission passive de données et une récupération d'énergie. Étant donné que la gestion des ressources joue un rôle important dans l'amélioration des performances des systèmes de communication, nous nous concentrons dans cette thèse sur la maximisation de l'efficacité énergétique dans les systèmes NOMA aidés par la rétrodiffusion ambiante avec ou sans connaissance parfaite du canal au niveau de l'émetteur.

Dans un premier temps, en supposant une connaissance parfaite du canal, nous maximisons l'efficacité énergétique pour un système NOMA multi-utilisateurs en liaison descendante, formulée comme le compromis entre le débit somme et la consommation totale de puissance. Compte tenu du budget de puissance au niveau de l'émetteur et des exigences minimales de qualité de service de chaque utilisateur, l'allocation de puissance optimale est obtenue analytiquement et celle-ci caractérise l'ensemble de la frontière Pareto-optimale des compromis débit versus (vs.) puissance. Dans le cas particulier de la maximisation du ratio débit somme vs. puissance totale, notre solution réduit la complexité de l'algorithme Dinkelbach à une méthode de recherche par dichotomie. L'avantage de NOMA par rapport à l'accès multiple orthogonal (OMA) en termes du compromis optimal débit vs. puissance est mis en évidence numériquement.

Ensuite, nous étendons notre étude en incluant un dispositif de rétrodiffusion ambiante qui module sa propre information à transmettre en reflétant le signal incident provenant de l'émetteur. Premièrement, nous considérons le cas particulier d'un état de rétrodiffusion fixe où le dispositif agit comme un relais passif. Nous étendons également cette étude à plusieurs dispositifs de rétrodiffusion ambiante. Les politiques optimales d'allocation de ressources sont obtenues analytiquement, simplifiant ainsi l'algorithme de Dinkelbach. Dans le cas général où le dispositif n'est pas toujours dans un état de rétrodiffusion fixe, nous dérivons les régions de débits atteignables en exploitant les outils de la théorie de l'information et, ensuite, nous obtenons analytiquement la

politique optimale d'allocation de ressources. Nous montrons que la solution proposée atteint une efficacité énergétique supérieure à celle d'autres systèmes de référence. Nous soulignons également que l'efficacité énergétique augmente avec le nombre de dispositifs de rétrodiffusion coopératifs. Pour compléter notre étude, nous montrons également la pertinence de notre solution en cas de connaissance imparfaite du canal.

Nos solutions analytiques, qui s'appuient sur la connaissance parfaite du canal à l'émetteur, ne nécessitent pas l'utilisation d'algorithmes itératifs coûteux en termes de puissance de calcul. Cependant, la connaissance parfaite du canal est difficile à obtenir en pratique. Par conséquent, nous étudions un système NOMA à deux utilisateurs dans un canal variant dans le temps et inconnu au niveau de l'émetteur. Nous proposons ainsi une méthode d'apprentissage par renforcement en ligne, reposant uniquement sur un seul bit de feedback. Remarquablement, notre solution proposée ne nécessitant qu'un seul bit de feedback de chaque utilisateur est toujours capable de surpasser OMA dans plusieurs contextes d'intérêt, y compris ceux stochastiques et même non-stationnaires, comme le démontrent nos résultats numériques.

Contents

List of Figures

List of Acronyms

1G	First Generation
2G	Second Generation
3G	Third Generation
4G	Fourth Generation
5G	Fifth Generation
B5G	Beyond 5G
6G	Sixth Generation
AMPS	Advanced Mobile Phone System
TACS	Total Access Communication System
NMT	Nordic Mobile Telephone
J-TACS	Japanese-TACS
GSM	Global System for Mobile Communications
GPRS	General Packet Radio Service
ITU	International Telecommunication Union
LTE	Long Term Evolution
eMBB	enhanced mobile broadband
URLLC	ultra-reliable and low latency communications
mMTC	massive machine type communications
IoT	Internet of Things
IMT	International Mobile Telecommunications
OMA	Orthogonal Multiple Access
NOMA	Non-Orthogonal Multiple Access
SCMA	Sparse Code Multiple Access
SC	Superposition Coding
SIC	Successive Interference Cancellation
SUD	Single User Detection
BS	base station
AmBC	Ambient Backscatter Communication
CSI	channel state information

CSIT	channel state information at the transmitter
CDIT	channel distribution information at the transmitter
MAB	Multi-Armed Bandit
RIS	Reconfigurable Intelligent Surfaces
QoS	quality of service
ACK	acknowledgment
CS	circuit switched
PS	packet switching
3GPP	Third Generation Partnership Project
5G-PPP	5G Infrastructure Public Private Partnership
LDS-CDMA	Low Density Spreading Code Division Multiple Access
LDS-OFDM	Low Density Signature-Orthogonal Frequency Division Multiplexing
ML	Machine Learning
AF	Amplify-and-Forward
AWGN	additive white Gaussian noise
NAICS	network-assisted interference cancellation and suppression
LTE-A	LTE Advanced
KKT	Karush-Kuhn-Tucker
UCB	Upper Confidence Bound
EXP3	Exponential-weight algorithm for Exploration and Exploitation
RF	radio frequency
OOK	on-off keying
SINR	signal-to-interference-plus-noise ratio
SNR	signal-to-noise ratio

Mathematical Notations

Notations

$\boldsymbol{X}$, $\boldsymbol{x}$	Uppercase (Lowercase) and bold face for matrix (vector)
x, X	Scalar value
$\mathcal{X}$	Calligraphic letter for set
$\lvert\mathcal{X}\rvert$	Number of elements in the set $\mathcal{X}$

Functions and operators

$\mathrm{E}[\cdot]$	Expectation function
∇	Vector differential operator
$\arg\max(.)$	Elements of the domain of the function at which the function values are maximized
$\log_2(.)$	Log function with base 2
$\exp(\cdot)$	Exponential function
$\max(.)$	Maximum value of the function
$\min(.)$	Minimum value of the function
$C(\cdot)$	Shannon capacity
$\mathbb{I}(\cdot;\cdot)$	Mutual information
$\mathbb{H}(\cdot)$	Entropy
$\mathbb{1}[\cdot]$	Indicator function
$\mathbb{P}(\cdot)$	Probability of an event

Chapter 1

Introduction

Contents

1.1 Background and motivation

The evolution of communication systems has revolutionized the way people communicate, enabling an abundance of data and information to be transferred at faster rate all across the world with limitless boundaries. The first wireless network dates way back to the Stone Age when smoke signals, drums, signal flares or whistles were used to transmit information [1]. Towers and hilltop stations were set along roads to relay messages over long distances. These primitive communications were replaced by the telegraph in 1838, which is the first great breakthrough in the field of telecommunication, and later on by the telephone. The first radio transmission was demonstrated in 1895 from the Isle of Wight to a tugboat located 29 km away. Since then, wireless communication has rapidly evolved from one generation to the other, enabling transmission with better quality, higher volumes of data and less power consumption via smaller and cheaper devices [2].

The First Generation (1G) of mobile communication systems were independently developed systems used in different countries, (e.g. Advanced Mobile Phone System (AMPS) used in America, Total Access Communication System (TACS) and Nordic Mobile Telephone (NMT) used in parts of Europe and Japanese-TACS (J-TACS) used in Japan and Hong Kong). The key technology was the implementation of cells and frequency reuse. However, there were major concerns regarding the incompatibility, security and lack of roaming. As a result, the Second Generation (2G) of mobile communication

systems was deployed and commercially launched in 1991 in Finland based on the Global System for Mobile Communications (GSM) standard specifying the operation of the 2G mobile network (e.g., frequency bands, modulation techniques, access methods, etc.). The benefits of 2G over 1G systems were the digital encryption and higher spectrum efficiency. These standards were all circuit switched (CS)-based networks. To achieve a higher data rate, a service called General Packet Radio Service (GPRS) was developed reaching up to 160 Kbps and allowing data transmission based on packet switching (PS) [3]. In the late 1990s, the Third Generation (3G) of mobile communication systems was developed by the International Telecommunication Union (ITU) providing Mbps data rates for hungry applications such as broadband Internet access and high-quality audio and video entertainment [2]. As the technology evolved, the services started expanding and the first commercial Long Term Evolution (LTE) standard deployment for the Fourth Generation (4G) systems took place by the end of 2009 in northern Europe. The key features of 4G systems were reduced transmission latency, increased user data rate and improved spectral efficiency [4].

In recent years, the concept of the Internet of Things (IoT) is gaining a great momentum, estimated to reach 75 billion IoT connected devices by the year 2025 [5]. In fact, the emergence of new applications with different quality of service (QoS) has led to a significant evolution of future networks. New services are categorized by the ITU and the Third Generation Partnership Project (3GPP), currently 5G Infrastructure Public Private Partnership (5G-PPP), into three main use cases with different stringent requirements, namely: enhanced mobile broadband (eMBB), ultra-reliable and low latency communications (URLLC), and massive machine type communications (mMTC) [6]. These scenarios, supported by the Fifth Generation (5G), aim to overcome the limitations of previous technologies regarding capacity, latency and connectivity capacity respectively [7, 8]. The International Mobile Telecommunications (IMT)-2020 requirement for 5G use cases are illustrated in Figure 1.1.

The mMTC use case is considered as one of the key ingredients to provide wireless connectivity to tens of billions of machine-type devices, and hence, improving and impacting all aspects of our daily lives, from our health to our travels and business transactions. This massive connectivity is both an opportunity and a great challenge for the telecommunications industry. The first four generations of mobile communication systems have focused primarily on optimizing the data rate or latency, but over the past decade, new performance metrics, such as network energy efficiency and connection density, have emerged for mMTC.

One of the main performance requirements for a mMTC network service, as illustrated in Figure 1.1, is to support a high connection density of up to 1 million devices per km^2. All previous generations of cellular systems have relied on Orthogonal Multiple Access (OMA) to coordinate and guarantee services for multiple users [1, 2, 7]. With this access technology, a unique radio resource (e.g., frequency band, time slot, etc.) is

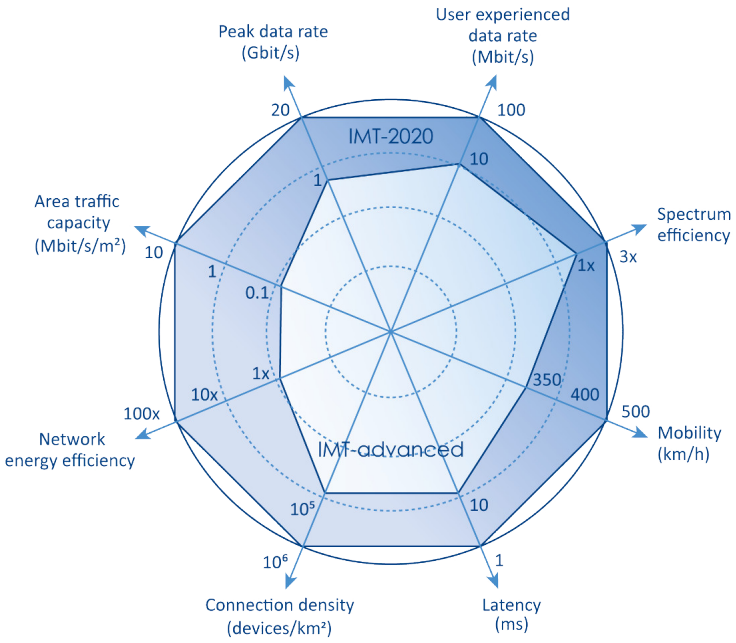

Figure 1.1: 4G vs. 5G key performance indicators (Source: ITU-R WP5D, 2015).

allocated per user. However, in the context of massive connectivity, applying OMA over limited and scarce radio spectrum is challenging and cannot fully realize the goal of the required connection density [9].

One of the promising technologies for alleviating the radio resources scarcity and enabling massive connectivity is Non-Orthogonal Multiple Access (NOMA) which, unlike conventional OMA, allows simultaneous communications via the same radio resources [10, 11]. This technology has attracted the attention of both academia and industry because of its efficient usage of resources. Although there are several different categories of NOMA such as Sparse Code Multiple Access (SCMA), Low Density Spreading Code Division Multiple Access (LDS-CDMA), Low Density Signature-Orthogonal Frequency Division Multiplexing (LDS-OFDM), etc., which all fall within the category of code domain NOMA [7, 9, 12], we focus squarely on the power domain NOMA scheme that has received great attention so far [7, 9, 12–14], and will be simply denoted by NOMA throughout this dissertation. In NOMA, the resulted multiple access interference is alleviated by superposing the signals of the multiplexed users in the power domain at the transmitter, and performing Successive Interference Cancellation (SIC) at the receiver side to decode those signals.

An important metric for mMTC is energy efficiency which has emerged as an important new figure of merit due to economic, operational, and environmental concerns. The telecommunications industry represents 1.4% of global CO_2 emissions [15] and the deployment of thousands of stations (base station (BS), small-cells, relays, etc.) needed for IoT networks will result in huge power consumption and more carbon emissions [16]. Hence, new green technologies need to be adopted in future networks to efficiently power

devices and improve their battery lifetime. Recently, Ambient Backscatter Communication (AmBC) has emerged as a very promising low-energy technology [17–20]. Using an antenna connected to a tunable impedance, the ambient backscatter device (tag) exploits the modulated existing radio frequency (RF) signals, coming from ambient RF sources, to transmit its own information, by reflecting a portion of these signals. The remaining portion of the same ambient signals is used to harvest energy for its circuit operation. In its simplest implementation, the ambient backscatter device switches between two states: a backscattering state, in which the ambient signal coming from a source is reflected; and a transparent state, in which no signal is reflected. These states result in power level variations of the ambient signal at the receiver side and the message of the ambient backscatter device can be detected by a simple energy detector [17, 21–23].

While 5G is globally deployed, and in addition to the ongoing evolution of its initiated three use cases [6], researchers in academia and industry start to think about possible Beyond 5G (B5G) and Sixth Generation (6G) wireless networks [24, 25] to pave the way for the development of intelligent networks. Machine Learning (ML) is a promising tool to enable intelligent resource allocation and will play a defining role in simplifying the network management in real time in future communication networks [26].

The performance of a wireless communication system relies on the resource allocation policy, e.g., the power allocation over the multiple users or frequency carriers, the reflection coefficient for NOMA and AmBC systems, etc. In this context, we aim to develop energy-efficient resource allocation policies in two extreme cases in terms of channel dynamics and the available channel state information at the transmitter (CSIT): the ideal case, where the channels are static and perfect CSIT is assumed to be known at the transmitter (an assumption often made in the relevant literature), and the worst case, where the channels are arbitrarily varying in time (including non-stationary and adversarial settings) and neither CSIT nor channel distribution information at the transmitter (CDIT) is available. In the static case with perfect CSIT, the analytical solutions can be obtained via traditional convex optimization tools and do not require the use of iterative algorithms that are costly in terms of computing power and therefore CO_2 emissions, thus, contributing to energy-efficient communications. In the worst case, the adaptive solutions obtained using reinforcement learning tools, require only one bit of feedback information and, although iterative, they are relatively inexpensive in terms of computational complexity, thus, conserving the energy of the system.

1.2 Thesis outline and contributions

In this PhD manuscript, the main contributions concern the three following topics:

- ▷ Energy efficiency in multi-user downlink NOMA with perfect CSIT
- ▷ Energy efficiency in multi-user downlink NOMA aided by ambient backscattering

- ▷ Adaptive resource allocation policies in downlink NOMA in time-varying networks with no CSIT/CDIT

Chapter 2 introduces some fundamental concepts. We first describe the principle of NOMA including the SIC decoding technique. We then provide an information-theoretic background behind NOMA that has been established several decades ago. We also analyze the performance gain of NOMA over conventional OMA scheme. We then introduce the basic principle of AmBC and highlight the key differences and similarities with other cooperative technologies such as Amplify-and-Forward (AF) relaying and Reconfigurable Intelligent Surfaces (RIS). We then define various energy-efficiency metrics. Finally, we discuss the different optimization frameworks used to solve our resource allocation problems.

In Chapter 3, we investigate the energy efficiency of a multi-user downlink NOMA system under the assumption of perfect CSIT. The energy efficiency maximization representing the trade-off between the sum rate versus the overall power consumption is formulated as a bi-criterion optimization problem. Assuming the transmitter power budget and the minimum users QoS constraints, and since the energy efficiency optimization problem is convex, we prove that the solution can be obtained in closed form. Hence, our solution characterizes the entire Pareto-optimal boundary of the sum rate vs. power consumption trade-offs. We also study the special case of maximizing the ratio sum rate vs. overall power consumption, where our previous closed-form solution reduces the complexity of the Dinkelbach algorithm to a univariate bisection method. At last, our simulation results highlight the benefit of NOMA over OMA in terms of the sum rate vs. power optimal trade-off.

In Chapter 4, the system model of the previous chapter is extended to include AmBC. More precisely, we consider the presence of an ambient backscatter device which modulates its own binary information by reflecting the incident signal coming from the NOMA transmitter. Before delving into detailed analysis of this problem, we investigate the special case of a fixed backscattering state where the ambient backscatter device is fully cooperative and acts as a passive relay (the backscatter device does not transmit any information). In this special case, the resource allocation policies maximizing the sum rate vs. overall power consumption trade-off are obtained in closed-form and lead to a simplified Dinkelbach's algorithm when maximizing the ratio between the sum rate and the overall power consumption. We further extend this investigation to multiple ambient backscattering devices.

In the general case, in which the ambient backscatter device transmits information and is not always in fixed reflective state, because of the multiplicative operation resulting from reflecting the transmitter's signal, obtaining the achievable sum rate of the system is not trivial. Therefore, we start by deriving the information-theoretic achievable rate region for discrete memoryless channels and, subsequently, for Gaussian channels. We

then propose a joint optimization framework for maximizing the system energy efficiency as the trade-off and ratio between the sum rate and the overall power consumption. To solve this non-convex optimization problem, we propose a simplifying modification, which enables us to obtain the optimal reflection coefficient and power allocation policy analytically. Our numerical results demonstrate the negligible impact of the introduced modification on the optimality of our solution. The ambient backscatter-aided NOMA is proven to outperform its OMA counterpart. At last, we show the pertinence of our solution also in the case of imperfect channel state information (CSI) assuming that the channel estimation quality is sufficiently high.

In Chapter 5, we investigate reinforcement learning to cope with the channel dynamics and the absence of CSIT and CDIT. Here, we consider a downlink NOMA system composed of one transmitter and two users where the transmitter does not have access to perfect CSI and cannot decide without error which of the two users encounters better channel conditions. Hence, it cannot perfectly decide the users' decoding schemes nor their optimal power allocation, and will inevitably lead to outage events. We derive a novel adaptive NOMA scheme that jointly allocates the power to the two users and decides which user performs SIC to minimize the overall system outage probability and outage-based energy efficiency. To circumvent the lack of channel knowledge at the transmitter, our novel scheme exploits Multi-Armed Bandit (MAB) algorithms, that have a relatively low complexity and rely only on a single bit of information from each user. Our simulation results show that NOMA is still able to outperform OMA in many settings of interest including stochastic and even non-stationary (adversarial) ones.

Finally, Chapter 6 summarizes the thesis contributions and discusses some open issues and perspectives for future investigation.

1.3 List of publications and invited talks

The work conducted during this thesis has led to the following publications.

International Journals:

[J2sub] **H. El Hassani**, A. Savard, E. V. Belmega, and R. C. De Lamare, "Multi-user downlink NOMA systems aided by an ambient backscatter device: achievable rate region and energy-efficiency maximization," submitted to IEEE Transactions on Green Communications and Networking, Oct 2022.

[J1] **H. El Hassani**, A. Savard, and E. V. Belmega, "Adaptive NOMA in time-varying wireless networks with no CSIT/CDIT relying on a 1-bit feedback," IEEE Wireless Communications Letters, vol. 10, no. 4, pp. 750–754, 2021.

International conferences:

[C4] **H. El Hassani**, A. Savard, E. V. Belmega, and R. C. De Lamare, "Energy-Efficient Solutions in Two-user Downlink NOMA Systems Aided by Ambient Backscattering," in IEEE Global Communications Conference (GLOBECOM), Rio de Janeiro, Brazil, 2022.

[C3] **H. El Hassani**, A. Savard, E. V. Belmega, and R. C. De Lamare, "Energy-efficient cooperative backscattering closed-form solution for NOMA," in IEEE Global Communications Conference (GLOBECOM), Madrid, Spain, 2021, pp. 1–6.

[C2] **H. El Hassani**, A. Savard, and E. V. Belmega, "Energy-efficient 1-bit feedback NOMA in wireless networks with no CSIT/CDIT," in IEEE Statistical Signal Processing Workshop (SSP), Rio de Janeiro, Brazil, 2021, pp. 106–110.

[C1] **H. El Hassani**, A. Savard, and E. Veronica Belmega, "A closed-form solution for energy-efficiency optimization in multi-user downlink NOMA," in IEEE International Symposium on Personal, Indoor and Mobile Radio Communications (PIMRC), London, UK, 2020, pp. 1–5.

French national conferences:

[CF1] **H. El Hassani**, A. Savard, E. V. Belmega, and R. C. De Lamare, " Rétrodiffusion cooperative efficace en énergie pour un système multi-utilisateurs à accès multiple NOMA," in GRETSI 2022, Nancy, France.

Invited talks:

[S3] "Multi-user downlink NOMA systems aided by an ambient backscatter device: achievable rate region and energy-efficiency maximization", PUC-Rio, Rio de Janeiro, Brazil, 23/05/2022.

[S2] "Energy-Efficient Cooperative Backscattering Closed-Form Solution for NOMA", ELIOT Student Webinars, 13/12/2021 (Virtual).

[S1] "A closed-form solution for energy-efficiency optimization in multi-user downlink NOMA", ELIOT Student Webinars, 25/01/2021 (Virtual).

Chapter 2

Preliminaries and state of the art

Contents

In this chapter, we provide the technical background necessary for understanding the rest of the thesis. We first present a brief description of the Non-Orthogonal Multiple Access (NOMA) technique in both uplink and downlink transmissions. We then evaluate the performance of the former compared to the Orthogonal Multiple Access (OMA) technique where we focus on downlink transmissions for the rest of this thesis. We then introduce the Ambient Backscatter Communication (AmBC) systems and compare them with other cooperative technologies. We finally present different energy-efficiency metrics and different optimization tools for solving the resource allocation problems under investigation.

2.1 Non-Orthogonal Multiple Access

The previous generations of mobile systems have adopted OMA as the core technology for allowing simultaneous access of multiple users to the network. This access is performed in an orthogonal (non-interfering) manner where only one user is served on each resource block such as frequency band, time slot, etc. Although OMA techniques prevent interference between users and require simple receivers, they are limited by the number of available orthogonal resources. Recently, NOMA has emerged as a very promising technology to enable massive connectivity which is highly demanded in Beyond 5G (B5G) and Sixth Generation (6G) future networks [7, 14].

2.1.1 Power domain NOMA

In contrast to OMA, NOMA can support massive connectivity by superposing the messages of an arbitrary number of users on the same resource block [14, 27–32]. Hence, users can concurrently exploit scarce bandwidth resources in a more efficient manner. To overcome the multi-user interference caused by the superposed messages, Successive Interference Cancellation (SIC) decoding scheme is implemented at the receiver side [10, 33–36]. In the next subsections, we explain the principles behind NOMA by considering a simple two-user system in a downlink transmission with $|h_1|^2/\sigma_1^2 \geq |h_2|^2/\sigma_2^2$, and an uplink transmission with $|h_1|^2 \geq |h_2|^2$, where h_k, σ_k^2, $k \in \{1, 2\}$ denote the channel gain and the noise variance of user k respectively. The conditions on the channel gains differ in both transmissions depending on the normalization by the noise at the receiver end. We then focus on downlink NOMA and show the conditions under which it can outperform OMA.

Downlink NOMA

Basic principle: We consider a simple system, illustrated in Figure 2.1, composed of one base station (BS) and two users all equipped with a single antenna. The BS wishes to send a message $X_k, k \in \{1, 2\}$ to user k, such that $\mathbb{E}[|X_k|^2] = 1$ where $\mathbb{E}[.]$ is the expectation operator. The BS performs Superposition Coding (SC) [37] and broadcasts the message

$$X = \sqrt{p_1}X_1 + \sqrt{p_2}X_2, \tag{2.1}$$

to both users, where p_k, $k \in \{1, 2\}$ denotes the power allocated to user k and is restricted to the power budget $P_{\max}$ of the BS, i.e., $p_1 + p_2 \leq P_{\max}$. Unlike conventional water-filling, downlink NOMA adopts a power allocation policy depending on the quality of service (QoS) requirements of each user and the objective to be achieved. However, to compensate for the poor channel conditions and ensure a certain QoS or enhance user fairness, the

power is allocated following the reverse order of the users' channel gain, where high transmission powers are given to users with weak channel conditions and vice versa: in our example, this means that $p_2 \geq p_1$ [38].

At the receiver side, each user k receives the signal

$$Y_k = h_k(\sqrt{p_1}X_1 + \sqrt{p_2}X_2) + Z_k, \quad k \in \{1, 2\}, \tag{2.2}$$

where Z_k is the additive white Gaussian noise (AWGN) at user k with zero mean and variance σ_k^2.

To separate the superposed messages and recover the desired one, Successive Interference Cancellation (SIC) decoding is implemented following the order of the increasing channel gains normalized by the noise variance (i.e., $|h_k|^2/\sigma_k^2$). With this order, each user first decodes the messages of the users with poorer channel links, to eliminate their interference and then retrieves its desired message. Thus, when the decoding is performed at a particular user, the messages of users stronger than the former are treated as additional noise. The BS assigns the SIC order based on the channel state information (CSI) feedback received from users. As such, users update information on the SIC ordering from the BS.

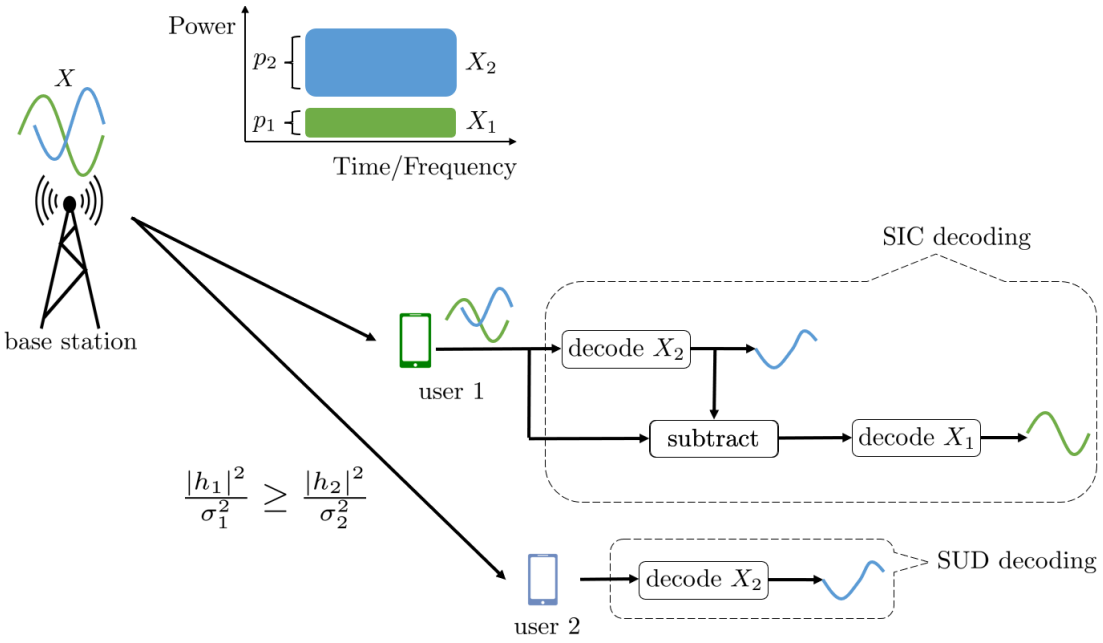

Figure 2.1: Downlink NOMA in a simple two-user system

More precisely, the user with the strong channel, i.e., user 1, employs SIC as follows: to extract the desired message X_1, user 1 first decodes the interfering message X_2 destined to user 2 and then subtracts it from the received signal Y_1. As such, user 1 decodes its own message free from interference. As for the user with the weak channel gain, i.e., user 2, employs Single User Detection (SUD) where the message X_2 is decoded directly by treating the other message X_1 as additional noise.

Capacity region: The theory behind NOMA has been around for many years [39, 40]. In fact, the concept of downlink NOMA is a special case of Superposition Coding (SC) and SIC for the broadcast channel and is equivalent to the degraded broadcast channel, where the strong and weak users are considered as least and most degraded respectively (i.e., $\mathbb{I}(X_2;Y_2) \leq \mathbb{I}(X_2;Y_1)$) [39, 40]. In this case, the capacity region is known and can be achieved in a single-input single-output channel [33, 39, 40]. For the setup illustrated in Figure 2.1, the capacity region for the discrete memoryless broadcast channel is given by [39, 40]

$$R_1 \leq \mathbb{I}(X_1;Y_1|X_2) \tag{2.3}$$
$$R_{2\to1} \leq \mathbb{I}\left(X_2;Y_1\right) \tag{2.4}$$
$$R_{2\to2} \leq \mathbb{I}\left(X_2;Y_2\right), \tag{2.5}$$

where $\mathbb{I}(.;.)$ denotes the mutual information, R_1 is the data rate of the message X_1 destined to user 1, and $R_{2\to k}, k \in \{1,2\}$ the data rate achieved by user k when decoding the message X_2.

Note that since the strong user (i.e., user 1) first decodes the message X_2, the achievable data rate of the message destined to user 2 must satisfy $R_2 \leq \min\left(R_{2\to1}, R_{2\to2}\right)$. However, since the channel is degraded (i.e., $\mathbb{I}(X_2;Y_2) \leq \mathbb{I}(X_2;Y_1)$), R_2 is reduced to the expression (2.5) and the achievable rate region writes as

$$R_1 \leq \mathbb{I}(X_1;Y_1|X_2) \tag{2.6}$$
$$R_2 \leq \mathbb{I}\left(X_2;Y_2\right). \tag{2.7}$$

In the case of a Gaussian broadcast channel

$$R_1 \leq \log_2\left(1+\frac{p_1|h_1|^2}{\sigma_1^2}\right) \tag{2.8}$$
$$R_{2\to1} \leq \log_2\left(1+\frac{p_2|h_1|^2}{p_1|h_1|^2+\sigma_1^2}\right) \tag{2.9}$$
$$R_{2\to2} \leq \log_2\left(1+\frac{p_2|h_2|^2}{p_1|h_2|^2+\sigma_2^2}\right). \tag{2.10}$$

Similarly, the achievable data rate of user 2 must satisfy $R_2 \leq \min\left(R_{2\to1}, R_{2\to2}\right)$. Since $|h_1|^2/\sigma_1^2 \geq |h_2|^2/\sigma_2^2$, R_2 is reduced to the expression (2.10) and the achievable rate region writes as

$$R_1 \leq \log_2\left(1+\frac{p_1|h_1|^2}{\sigma_1^2}\right) \tag{2.11}$$
$$R_2 \leq \log_2\left(1+\frac{p_2|h_2|^2}{p_1|h_2|^2+\sigma_2^2}\right). \tag{2.12}$$

Uplink NOMA

Basic principle: In the uplink, both users transmit their individual messages simultaneously over the same frequency band with either a maximum or controlled transmit power. The received signal at the BS is hence a superposition of X_1 and X_2

$$Y = h_1\sqrt{p_1}X_1 + h_2\sqrt{p_2}X_2 + Z, \tag{2.13}$$

where Z is the AWGN at the BS with zero mean and variance denoted by σ^2. The principle of NOMA in the uplink is illustrated in Figure 2.2.

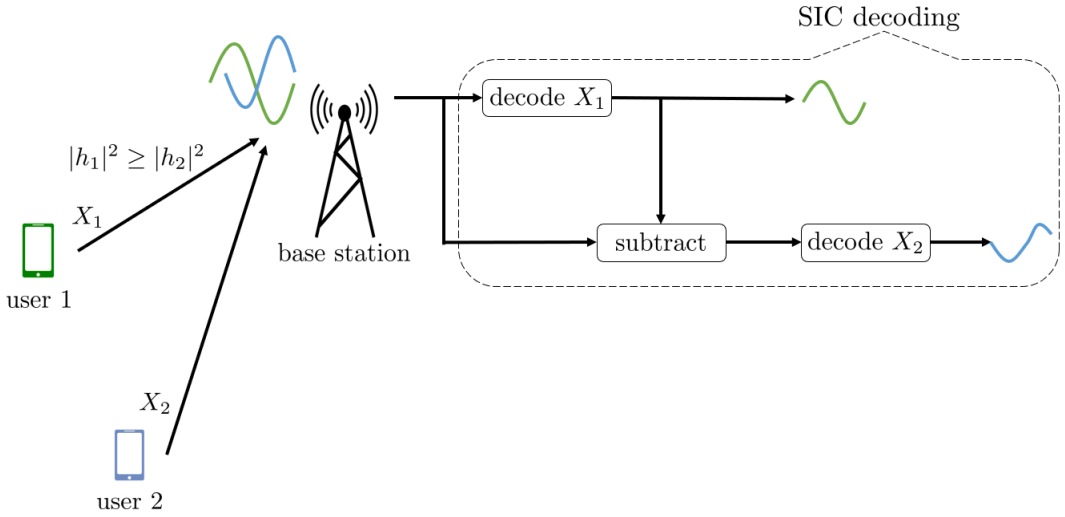

Figure 2.2: Uplink NOMA in a simple two-user system

Each signal at the BS experiences distinct channel gains and, unlike downlink NOMA, all received signals at the receiver are desired ones. The BS applies SIC and it successively decodes and cancels each message of the strong channel users prior to decoding the messages of the weak channel users. In our example, the BS first decodes the message of the user with the strong channel gain, i.e., user 1, while treating the message X_2 as additive noise, and then it decodes the message of the user with the weak channel gain, i.e., user 2, free of interference. In downlink NOMA, each user receives the superposed messages via the same channel and the difference in the received power between the superposed messages depends only on the power allocated to each message. On the contrary, in uplink NOMA, the BS receives the users superposed messages via their respective channels. Therefore, the difference in the received power between different messages depends on both the users' transmit powers and their different channel gains.

Capacity region: Uplink NOMA is modelled as a multiple access channel where both users concurrently transmit at the same time and frequency. Their signals are superposed and interfere with each other at the BS where SIC is applied to retrieve, successively, both

messages. The capacity region of the multiple access channel is achieved via NOMA and depends on the decoding order of the users. For example, if the message X_1 is decoded first, the capacity region for the case of discrete memoryless multiple access channel, is given by [39, 40]

$$R_1 \leq \mathbb{I}(X_1; Y) \tag{2.14}$$

$$R_2 \leq \mathbb{I}\left(X_2; Y | X_1\right), \tag{2.15}$$

and for the case of a Gaussian multiple access channel

$$R_1 \leq \log_2\left(1 + \frac{p_1|h_1|^2}{p_2|h_2|^2 + \sigma^2}\right) \tag{2.16}$$

$$R_2 \leq \log_2\left(1 + \frac{p_2|h_2|^2}{\sigma^2}\right). \tag{2.17}$$

If the message X_2 is decoded first, the achievable region is similar by simply changing the order of the two users.

In this thesis, we focus squarely on downlink NOMA systems. Even though there exist major concerns regarding the decoding complexity of NOMA for user terminals compared to the BS in uplink NOMA, recent advances in device processing capabilities have rendered the implementation of SIC at the user end practical [7, chapter 18], [41]. For example, a category of relatively advanced user terminals, known as network-assisted interference cancellation and suppression (NAICS) terminals, have recently been adopted in Third Generation Partnership Project (3GPP) LTE Advanced (LTE-A) [42–45]. In fact, the processing capabilities of user terminals have steadily improved throughout the years, where based on Moore's law, the processing power doubles approximately every two years [46]. Therefore, new generations of user terminals will be capable of performing SIC decoding.

As for the case of low-cost devices such as Internet of Things (IoT), the SIC process may still remain challenging. However, there exist some solutions such as IoT device pairing or applying NOMA between IoT devices paired with advanced user terminals, where SIC and SUD techniques are performed at the user terminal and the IoT device respectively [38].

2.1.2 Comparison with OMA

In this subsection, we analyze the performance gain of downlink NOMA compared with its OMA counterpart. By considering the same system model in Figure 2.1, where user 1 and user 2 perform SIC and SUD respectively. Here we focus on maximizing the achievable sum-rate, hence the entire power budget of the BS is consumed and the individual powers are such that $p_1 + p_2 = P_{\max}$. Their respective data rates in NOMA are

$$R_1^{\text{NOMA}} = \log_2\left(1 + \frac{p_1|h_1|^2}{\sigma_1^2}\right), \quad R_2^{\text{NOMA}} = \log_2\left(1 + \frac{p_2|h_2|^2}{p_1|h_2|^2 + \sigma_2^2}\right). \tag{2.18}$$

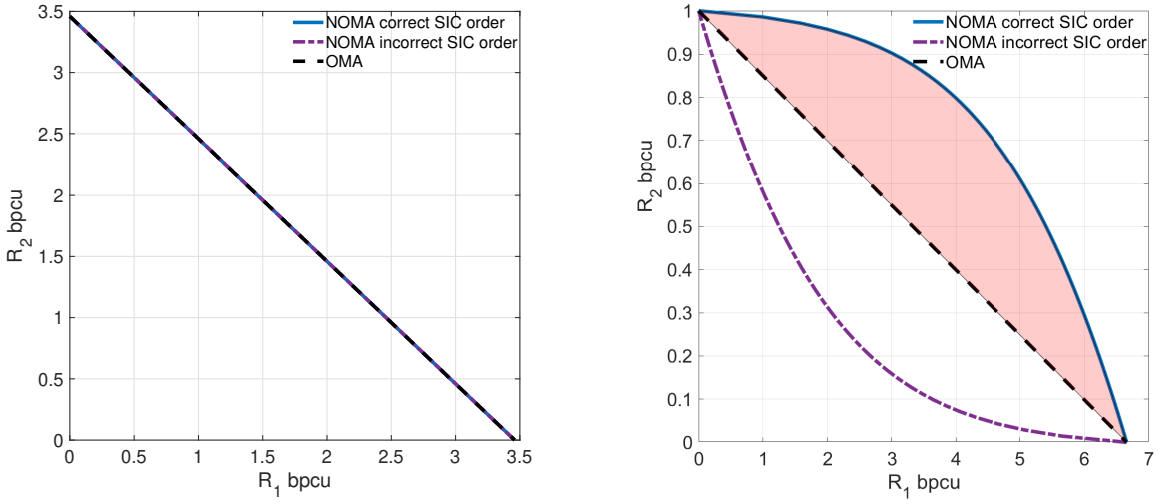

(a) Symmetric channel
$|h_1|^2/\sigma_1^2 = |h_2|^2/\sigma_2^2 = 10$ dB

(b) Asymmetric channel
$|h_1|^2/\sigma_1^2 = 20$ dB and $|h_2|^2/\sigma_2^2 = 0$ dB

Figure 2.3: The capacity regions of downlink NOMA and OMA.
NOMA can outperform OMA only in the case of asymmetric channels.

On the other hand, in downlink OMA, considering a fraction $\beta \in [0, 1]$ of time slot assigned to user 1 and the remaining $(1-\beta)$ assigned to user 2, the data rate of each user are

$$R_1^{\text{OMA}} = \beta \log_2 \left(1 + \frac{P_{\max}|h_1|^2}{\sigma_1^2}\right), \quad R_2^{\text{OMA}} = (1-\beta) \log_2 \left(1 + \frac{P_{\max}|h_2|^2}{\sigma_2^2}\right). \tag{2.19}$$

Figures 2.3(a) and 2.3(b) show the capacity regions of both OMA and NOMA for the cases of symmetric channels: $|h_1|^2/\sigma_1^2 = |h_2|^2/\sigma_2^2 = 10$ dB, and asymmetric channels: $|h_1|^2/\sigma_1^2 = 20$ dB and $|h_2|^2/\sigma_2^2 = 0$ dB. For NOMA two cases are considered: defined users' decoding order, i.e., in the order of increasing users' channels, and an alternative version of NOMA using a reversed order decoding at the users end. The NOMA curves are obtained by varying the allocated power p_1 and p_2 in (2.18), such that $P_{\max} = p_1 + p_2 = 1$ W. Similarly, the OMA curve is obtained by varying β between 0 and 1. In the case of symmetric channels, the rate region for OMA and NOMA are identical independently from the SIC decoding order. In the asymmetric case, the rate region of NOMA is greatly improved compared to OMA, as can be seen in the red highlighted area of Figure 2.3(b). Furthermore, the SIC decoding order must be carefully assigned as the data rates achieved by NOMA with a reversed order decrease and are even lower than those achieved by OMA. Therefore, NOMA systems can outperform OMA systems provided that the correct decoding order is known and when a difference between the channels of the multiplexed users exists.

In Chapter 4, we aim at investigating the performance of a NOMA system in the context of AmBC. In the next section, we provide an overview of this technology.

2.2 Ambient backscatter communication

Ambient backscatter communication (AmBC) has emerged as a promising solution for internet of things (IoT) where a passive backscatter device can send information by reflecting the ambient radio frequency (RF) signals without being power greedy [21, 22]. In this section, we briefly describe the principle of Ambient Backscatter Communication (AmBC) and compare it to other similar cooperative technologies.

2.2.1 Basic principle

Ambient backscatter communication (AmBC) is a low-power and low-cost technology enhancing green communications by alternately absorbing and reflecting existing RF signals in the environment without need of additional radio emissions, making IoT transmissions more energy-efficient [18, 19, 23, 47]. An ambient backscatter device, also called a tag, backscatters the RF signal generated by a source (e.g., BS, Wi-Fi hotspot, a smartphone, etc.) to transmit information in a passive way while also harvesting energy used for its circuit operation. This is achieved by tuning the load impedance due to which the impinging RF waves are reflected or absorbed by the ambient backscatter device.

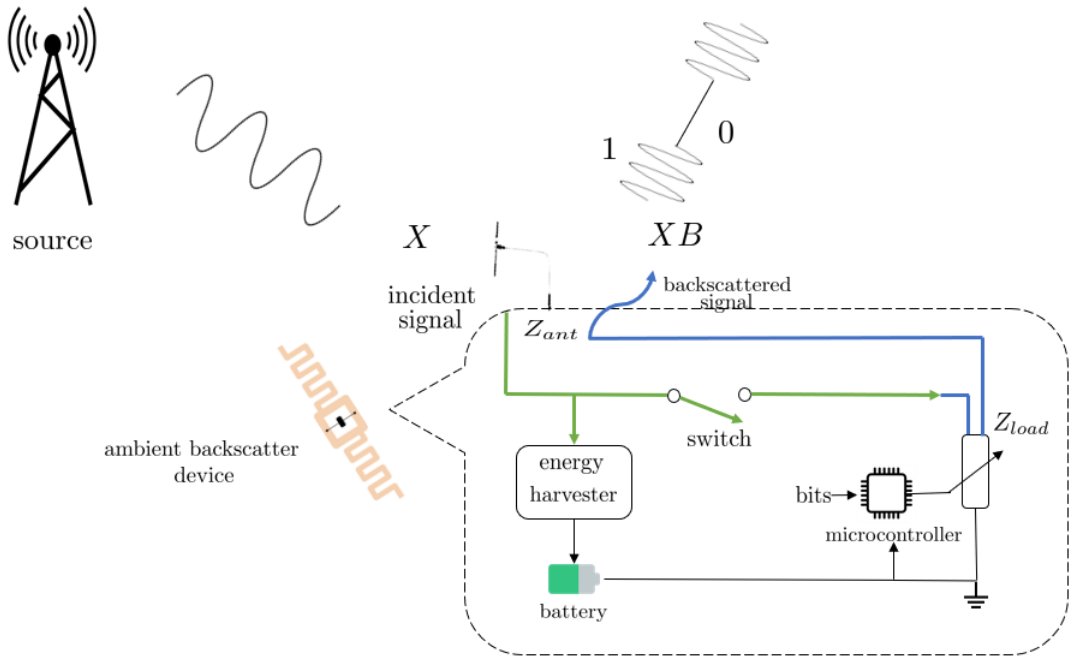

Figure 2.4: Ambient backscatter communication

More specifically, in its simplest implementation illustrated in Figure 2.4 the ambient backscatter device switches between two states resulting in an on-off keying (OOK) modulation. These states correspond to a backscattering state, in which the ambient signal is reflected (i.e., the message of the ambient backscatter device is B=1), and a

transparent state in which no signal is reflected but absorbed (i.e., the message is B=0). These two states represent the encoded bits $B \in \{0, 1\}$ that can be detected through variations in the received power via a simple energy detector [17, 22, 23].

In practice, this is realized by a switch consisting of a transistor connected to the two branches of the ambient backscatter device dipole antenna. The switch modulates the antenna impedance and triggers a variation in the amount of the energy reflected. Hence, the transistor is either off or in non-conductive stage (i.e., the transparent state) or in conductive stage where it shorts the two branches of the antenna (i.e., the backscattering state) [17].

The amount of reflected energy is linked to the antenna and the load impedances by

$$\Gamma_{\text{load}} = \frac{Z_{\text{load}} - Z_{\text{ant}}}{Z_{\text{load}} + Z_{\text{ant}}} \tag{2.20}$$

$$= \rho e^{j\phi}, \tag{2.21}$$

where Γ_{load} is the complex reflection coefficient, Z_{load} and Z_{ant} are the load and the antenna impedances respectively; $\phi \in [0, 2\pi)$ is the phase shift of the reflection coefficient and $\rho \in [0, 1]$ represents its squared magnitude accounting for the amount of the signal's energy that is reflected. Since the ambient backscatter device contains passive load circuit components such as resistors, capacitors and inductors, the incident signal is not amplified and can only be attenuated by the factor ρ. The other amount of energy $(1-\rho)$ is absorbed and harvested by the ambient backscatter device. Hence, by varying the load impedance Z_{load}, the ambient backscatter device achieves different reflection coefficients, and thus modulates its own information while controlling the amount of reflected and absorbed energy. Thus, the backscattered signal is express as

$$X_b = \sqrt{\rho}(h_{sb} X B), \tag{2.22}$$

where h_{sb} is the channel between the source and the ambient backscatter device and X is the message of the ambient source. Since $\rho \in [0, 1]$, the backscattered signal can be considered as an attenuation of the incident signal.

Note that the ambient backscatter device can generate higher-order modulation by selecting different load impedances resulting in a large number of reflection states [48].

2.2.2 Symbiotic Radio

In the general concept of AmBC, the ambient backscatter device uses the existing RF signals to transmit its own message B to the receiver. The ambient source unintentionally provides the ambient backscatter device with RF signals and the receiver is only interested in recovering the ambient backscatter device message B. However, due to the spectrum sharing nature of AmBC, and since the ambient signal X is unknown, a severe interference from the direct link may occur [49].

A novel technique called Symbiotic Radio was proposed, where the ambient backscatter device is integrated within a primary communication system and shares not only the same spectrum but the same receiver as well [50–53]. In this case, the source can be used to purposely support both the primary and the ambient backscatter device transmissions and the receiver jointly decodes both messages.

An interesting observation was made in [50], in the case when the ambient backscatter device symbol duration is much longer than that of the primary signal, the backscattered signal may even enhance the primary transmission. Therefore, it appears as a win-win situation for the AmBC, as a concept useful in IoT networks, to coexist with cellular communications using symbiotic radio technology.

2.2.3 Ambient backscattering vs. Relaying

At a first glance, AmBC seems to operate similarly to cooperative communications, where a relay node is willing to help a transmission between a source and its destination, by processing and forwarding some information. Various relaying schemes can be found in the literature [54, 55], but the closest to the behavior of AmBC is Amplify-and-Forward (AF) relaying.

In the AF protocol, the relay receives the signal

$$Y = h_{sr}X + Z, \tag{2.23}$$

where X is the message sent by the source, h_{sr} is the channel coefficient between the source and the relay and Z is the AWGN at the relay. The relay then amplifies the received signal and forwards [56]

$$X_r = G(h_{sr}X + Z), \tag{2.24}$$

where G is the amplification gain of the relay which can be seen as equivalent to the reflection coefficient ρ of the ambient backscatter device. The difference between the two technologies is that AmBC are more efficient in energy and in hardware complexity since relays need to be equipped with dedicated power source and active electronic components such as analog-to-digital converter, mixers, power amplifiers, etc. [57]. This results in an increase of the cost and the power consumption in the system.

Moreover, the presence of the active components results in an amplification of the noise Z at the relay end which is then forwarded to the users as shown in (2.24) which can affect its performance. Since the ambient backscatter device is passive, no noise is reflected as shown in (2.22).

At last, the relay is considered as an intermediate node between the source and the destination, whose only purpose is to extend the transmission range and to improve the communication without sending any message of its own. On the contrary, the ambient backscatter device utilizes the signal sent by the source to send its own information.

2.2.4 Ambient Backscatter Communication vs. Reconfigurable Intelligent Surfaces

To enhance the strength of the backscattered link, a large number N of reflective elements can be deployed, which leads to the concept of Reconfigurable Intelligent Surfaces (RIS) [58]. In general, RIS are simple and low-cost surfaces of electromagnetic material that can cover walls, buildings, etc., and have the ability to modify the phase or amplitude of the incident radio waves in a programmable and controllable way [59,60]. By intelligently tuning the phase shifts of the reflective elements, the angle of the reflection can be controlled in a way that the backscattered waves are added constructively (e.g., enhance the received signal power) or destructively (e.g., suppress the co-channel interference) in certain directions.

Each reflective element n backscatters the incident signal with a reflection coefficient given by

$$\Gamma_{n,\text{load}} = \rho_n e^{j\phi_n}, n \in \{1, \ldots, N\}. \tag{2.25}$$

In general, there exist two different assumptions for the reflection coefficient [58].

- ▷ *Constant amplitude and varying phase-shift* where only the phase-shift can be designed to improve the system performance. In this case, the squared modulus of the n-th reflection coefficient is maximized (i.e., $|\Gamma_{n,\text{load}}|^2 = \rho_n = 1$). This assumption is widely considered in existing works [61–64]. Here, the reflective elements are fully reflecting the signal and the main purpose of the RIS is to enhance the signal quality and assist the transmission of the existing system and no encoding is performed. The set of allowed phase-shifts is

$$\mathcal{F}_1 = \{\, \Gamma_{n,\text{load}} \,|\, \Gamma_{n,\text{load}} = e^{j\phi_n},\ \phi_n \in [0, 2\pi) \,\}, \tag{2.26}$$

- ▷ *Varying amplitude and phase-shift* where both the amplitude and the phase-shift can be designed to improve the system performance. In this case, the ambient backscatter device can be seen as a single reflective element of the RIS. The set of allowed amplitudes and phase-shifts is

$$\mathcal{F}_2 = \{\, \Gamma_{n,\text{load}} \,|\, \Gamma_{n,\text{load}} = \rho_n e^{j\phi_n},\ \rho_n \in [0, 1],\ \phi_n \in [0, 2\pi) \,\}. \tag{2.27}$$

In this thesis, the main focus is to develop energy-efficient resource allocation policies in NOMA systems. Since resource management plays a significant role in improving the systems performance, in the next section, we present various metrics of energy efficiency and describe the basic theoretical and algorithmic framework applied to solve our resource allocation problems.

2.3 Energy efficiency in wireless communication networks

The skyrocketing growth of the number of connected devices that wireless communications have been encountering poses serious sustainability concerns [15, 16]. Therefore, designing energy-aware systems have become ineluctable where the data rates must be increased and the corresponding incurred power consumption must be reduced. Energy-efficiency optimization has been widely investigated in the literature in the context of cognitive radio [65], multiple input multiple output channel [66], contention-based synchronization in orthogonal frequency division multiplexing access communication systems [67], etc., but for different system models and/or energy-efficiency metrics [68,69]. In this section, we provide various energy-efficiency metrics. We then introduce some convex optimization tools used for solving our resource allocation problems, in the case where the channels are static and perfectly known at the transmitter. We end by providing some elements of online and reinforcement learning, used in the case where the channels are arbitrarily varying in time and no information nor statistics of the channels are known at the transmitter side.

2.3.1 Energy-efficiency performance metrics

There exist two main approaches regarding energy efficiency: a difference-based approach, consisting in the difference between the sum rate and the consumed power of the system; and a fractional-based one, consisting in the ratio between the sum rate and the consumed power of the system [70]. Both approaches can be unified under the umbrella of bi-objective optimization introduced next.

2.3.1.1 Sum rate vs. power consumption trade-off

Following the theory of multi-objective optimization, the trade-off between increasing the sum rate and saving the power of the system can be captured by formulating mathematically a bi-criterion optimization problem [65, 71] in which the objectives are the sum rate R_{sum} and the negative overall power consumption, namely,

$$\underset{\mathbf{x} \in \mathcal{X}}{\text{maximize}} \quad \Big(R_{\text{sum}}(\mathbf{x});\ -P_{\text{total}}(\mathbf{x}) - P_c \Big), \tag{2.28}$$

where $\mathbf{x}$ is the vector of decision variables, for instance the power allocation vector, $\mathcal{X}$ is the feasible set, P_{total} and P_c are respectively the total transmit power and the constant circuit power consumption which includes the power dissipated in all other circuit blocks of both the transmitter and receivers. The two above objectives are contradictory: to maximize the sum rate, the system transmissions take place at full power, which obviously is not

energy-efficient; and to minimize the power consumption, there should be no transmission, which is neither rate- nor QoS-efficient.

Such a bi-criterion optimization problem can be solved by finding the Pareto-boundary of the feasible set of the rate-power pairs. This boundary contains all the Pareto-optimal solutions representing the rate-power feasible pairs that cannot be improved in both objectives simultaneously while remaining in the feasible set. If both objectives are convex, and $\mathcal{X}$ is a convex set (which is the case in power allocation), then finding the Pareto boundary reduces to maximizing the weighted sum of the two contrasting objectives [72], namely,

$$\underset{\mathbf{x} \in \mathcal{X}}{\text{maximize}} \quad R_{\text{sum}}(\mathbf{x}) - \alpha \left(P_{\text{total}}(\mathbf{x}) + P_c\right), \tag{2.29}$$

where $\alpha \geq 0$ is the parameter that trades off between the sum rate and the power consumption and sweeps the entire Pareto-boundary while weighting the priority given to the two opposing objectives. The rate-driven and power-driven objective functions are characterized by small and large values of α respectively.

2.3.1.2 Sum rate vs. overall power consumption ratio

Another well-established definition of the energy efficiency is the ratio between the sum rate and the overall power consumption [65, 70, 71, 73, 74] measured in bits per Joule of consumed energy

$$\xi_{\text{EE}}(\mathbf{x}) = \frac{R_{\text{sum}}(\mathbf{x})}{P_{\text{total}}(\mathbf{x}) + P_c}. \tag{2.30}$$

Maximizing this ratio is equivalent to maximizing the sum rate vs. overall power consumption for a specific choice of the weight α that yields a point on the Pareto-boundary of the bi-criterion problem (2.28) [75]. This point, which represents the best trade-off between the sum rate and the overall power consumption in terms of their ratio, can be obtained using Dinkelbach's iterative algorithm [70, 76, 77] described in Algorithm 1. Assuming that the numerator (i.e., the sum rate) is concave and the denominator (i.e., the overall power consumption) is affine, the maximization of the ratio in (2.30) is a concave-convex fractional problem and its solution is equivalent to finding the unique zero of the objective function given in (2.29) with respect to α [70].

2.3.2 Optimization tools

Resource allocation is an essential step towards improving the energy efficiency of wireless communication systems, where a suboptimal allocation of resources may have a crucial impact on the system's overall performance. In this thesis, we focus on maximizing the energy efficiency in NOMA systems in terms of different parameters such as power allocation (i.e., the power allocated to each message of the multiplexed users given a

Algorithm 1 Dinkelbach's algorithm

$\epsilon > 0$, $n = 0$, $\alpha_n = 0$
while $F(\alpha_n) > \epsilon$ **do**
  $\mathbf{x}_\mathbf{n}^* = \arg\max_{\mathbf{x}\in\mathcal{C}} \{R_{\text{sum}}(\mathbf{x}) - \alpha_n(P_{\text{total}}(\mathbf{x}) + P_c)\}$
  $F(\alpha_n) = R_{\text{sum}}(\mathbf{x}_\mathbf{n}^*) - \alpha_n(P_{\text{total}}(\mathbf{x}_\mathbf{n}^*) + P_c)$
  $\alpha_{n+1} = \frac{R_{\text{sum}}(\mathbf{x}_\mathbf{n}^*)}{P_{\text{total}}(\mathbf{x}_\mathbf{n}^*)+P_c}$
  $n = n + 1$
end while

limited power budget at the transmitter), decoding scheme (i.e., SIC or SUD while ensuring a successful decoding), etc. The resource optimization should be tackled in different ways depending on the system's conditions. In the following subsections, we introduce some of the most common mathematical tools to solve our resource allocation problem: the convex optimization method for the case of perfectly known channel state information at the transmitter (CSIT), and reinforcement learning in the case of unknown channel state information at the transmitter (CSIT).

2.3.2.1 Convex optimization

Let us consider a standard form for a convex problem [72, Chapter 5]

$$\begin{aligned} \min_{\mathbf{x}} \quad & f_0(\mathbf{x}) \\ \text{s.t.} \quad & f_i(\mathbf{x}) \leq 0, i \in \{1, \ldots, m\}, \end{aligned} \tag{2.31}$$

where the functions f_0 and $f_i, i \in \{1, \ldots, m\}$ are convex w.r.t $\mathbf{x}$. The problem in (2.31) describes finding an $\mathbf{x}$ that minimizes the objective function $f_0(\mathbf{x})$ under the inequality constraints $f_i(\mathbf{x}) \leq 0, i \in \{1, \ldots, m\}$. The Lagrangian function for the problem writes as

$$\mathcal{L}(\mathbf{x}, \lambda_1, \ldots, \lambda_m) = f_0(\mathbf{x}) + \sum_{i=1}^{m} \lambda_i f_i(\mathbf{x}), \tag{2.32}$$

where $\lambda_i, i \in \{1, \ldots, m\}$ refers to the Lagrange multiplier associated with the i-th inequality constraint. We can obtain a global optimal solution to the problem in (2.31) by satisfying the following Karush-Kuhn-Tucker (KKT) optimality conditions

- ▷ Stationarity: $\nabla\mathcal{L}(\mathbf{x}, \lambda_1, \ldots, \lambda_m) = 0$
- ▷ Complementary slackness: $\lambda_i f_i(\mathbf{x}) = 0, i \in \{1, \ldots, m\}$
- ▷ Feasibility constraints: $f_i(\mathbf{x}) \leq 0, \lambda_i \geq 0, i \in \{1, \ldots, m\}$,

where ∇ is the Nabla operator defining the first-order partial derivatives vector. The above KKT conditions are necessary and sufficient for optimality [72, page 243].

2.3.2.2 Online learning

Reinforcement learning is a branch of machine learning that learns through a trial-and-error process from the interaction with the environment by receiving positive or negative rewards as feedback for taking certain decisions or actions [78].

In this thesis, we focus on so-called Multi-Armed Bandit (MAB), a class of reinforcement learning where, at each iteration t, an agent selects an arm or action $\mathbf{a}^{(t)}$ among known actions $\mathcal{A}$, and receives a corresponding reward $u^{(t)}(\mathbf{a}^{(t)})$ generated by the environment in order to maximize the expected reward which is unknown. The agent faces a trade-off between data exploitation and exploration. On the one hand, the agent has to exploit actions that have been tried in the past and found to yield better payoffs. On the other hand, it has to explore other actions to obtain more information about the unexplored actions in order to make better decisions in the future [79]. The best trade-off between exploitation and exploration is obtained through action selection algorithms.

Regret as a performance metric: The notion of merit that allows one to assess the performance of a MAB algorithm is that of the pseudo-regret [80] defined as

$$\mathbb{E}[\mathrm{Reg}_T] = \mu^* - \frac{1}{T}\sum_{t=1}^{T}\mathbb{E}[u^{(t)}(\mathbf{a}^{(t)})], \tag{2.33}$$

in stochastic environments, where μ^* represents the maximal expected reward given as $\mu^* = \max_{\mathbf{a}\in\mathcal{A}} \mu(\mathbf{a})$, with $\mu(\mathbf{a}) = \mathbb{E}[u^{(t)}(\mathbf{a})]$ being the unknown expected reward of an arbitrary action $\mathbf{a} \in \mathcal{A}$. Intuitively, the pseudo-regret measures the gap between cumulative reward of the dynamic policy $\mathbf{a}^{(t)}, \forall t \in \{1, \ldots, T\}$, compared with the fixed optimal policy $\mathbf{a}^* = \arg\max_{\mathbf{a}\in\mathcal{A}} \mu(\mathbf{a})$ in hindsight. In non-stationary environments, the pseudo-regret definition is

$$\mathbb{E}[\mathrm{Reg}_T] = \max_{\mathbf{a}\in\mathcal{A}} \frac{1}{T}\sum_{t=1}^{T}\mathbb{E}[u^{(t)}(\mathbf{a}) - u^{(t)}(\mathbf{a}^{(t)})], \tag{2.34}$$

which represents the performance gap between the best *fixed* strategy over the horizon T and the online policy.

A dynamic policy $\mathbf{a}^{(t)}$ is said to have the *no-regret property* if $\limsup_{T\to\infty} \mathrm{Reg}_T \leq 0$. This means that a no-regret dynamic policy performs at least as good as the best fixed policy maximizing the expected reward when the time horizon T grows large. The objective of MABs is to design action selection policies that lead to no regret and at the best regret decay rate possible [79]. This objective is not straightforward since the environment is variable and these variations are completely arbitrary making the reward function encountered not known in advance.

Below, we briefly provide an overview of two of the most popular MAB algorithms, which will be exploited later on to design efficient resource allocation algorithms in the case of unknown CSIT.

Upper Confidence Bound: Upper Confidence Bound (UCB) is a deterministic no-regret algorithm designed specifically for stochastic environments, which enjoys an optimal decay rate of the pseudo-regret such that $\mathbb{E}[\mathrm{Reg}_T] = \mathcal{O}(\log T/T)$ [80], where the expectation is take over the stochastic environment. The updating policy rule is

$$\mathbf{a}^{(t+1)} = \arg\max_{\mathbf{a}\in\mathcal{A}} \left(\hat{\mu}_{\mathbf{a}}^{(t)} + \sqrt{\frac{\delta \log t}{2n_{\mathbf{a}}^{(t)}}} \right), \tag{2.35}$$

where $n_{\mathbf{a}}^{(t)}$ denotes the number of times arm $\mathbf{a}$ was selected up to iteration t, $\hat{\mu}_{\mathbf{a}}^{(t)}$ denotes the empirical mean reward of arm $\mathbf{a}$

$$\hat{\mu}_{\mathbf{a}}^{(t)} = \frac{\sum_{\tau=1}^{t} u^{(\tau)}(\mathbf{a}) \mathbb{1}[\mathbf{a}^{(\tau)} = \mathbf{a}]}{n_{\mathbf{a}}^{(t)}}, \tag{2.36}$$

where $\mathbb{1}[\cdot]$ is the indicator function and δ is the learning parameter that trade-offs between data exploration and exploitation.

Exponential-weights for Exploration and Exploitation: Exponential-weight algorithm for Exploration and Exploitation (EXP3) is a different and random no-regret algorithm designed for more general environments going beyond the stochastic case [81]. The regret decay rate of EXP3 is $\mathbb{E}[\mathrm{Reg}_T] = \mathcal{O}(1/\sqrt{T})$, where the expectation is taken with respect of the randomness within the EXP3 algorithm and any randomization employed by the adversary, hence slower than UCB in stochastic environments, but having the advantage of accounting for arbitrary dynamics that may even be adversary (in which UCB can be brought to a halt). The updated policy $\mathbf{a}^{(t+1)} \in \mathcal{A}$ is drawn randomly following a discrete distribution:

$$p^{(t)}(\mathbf{a}) = (1-\gamma)\frac{\exp(\eta G^{(t)}(\mathbf{a}))}{\sum_{b=1}^{|\mathcal{A}|}\exp(\eta G^{(t)}(b))} + \frac{\gamma}{|\mathcal{A}|}, \quad \forall \mathbf{a} \in \mathcal{A}, \tag{2.37}$$

where $|\mathcal{A}|$ is the number of arms, $G^{(t)}(\mathbf{a})$ is the cumulative estimated reward of an arbitrary arm $\mathbf{a}$ given as: $G^{(t)}(\mathbf{a}) = \sum_{\tau=1}^{t} \hat{u}^{(\tau)}(\mathbf{a}) \mathbb{1}[\mathbf{a}^{\tau} = \mathbf{a}]$, with $\hat{u}^{(t)}(\mathbf{a}) = u^{(t)}(\mathbf{a})/p^{(t)}(\mathbf{a})$ and γ, η are the learning parameters that trade-off between data exploration and exploitation.

Complexity discussion: Both UCB and EXP3 have a linear complexity $\mathcal{O}(|\mathcal{A}|)$ per learning iteration. EXP3 requires at most $\mathcal{O}(1/\epsilon^2)$ iterations to reach an pseudo-regret below $\epsilon > 0$ due to its $\mathcal{O}(1/\sqrt{T})$ regret decay rate; and since the regret decay of UCB is $\mathcal{O}(\log T/T)$ (much better than EXP3), UCB requires much less iterations compared to EXP3 [79].

Chapter 3

Energy efficiency in multi-user downlink NOMA with perfect CSI

Contents

3.1 Introduction

In this Chapter, we study the energy efficiency of a multi-user Non-Orthogonal Multiple Access (NOMA) downlink system, formulated as a bi-criterion convex optimization problem, similarly to [82], assuming perfect knowledge of the channel state information at the transmitter (CSIT). Aside from the power budget constraint, we also consider minimum quality of service (QoS) constraints for all links. Remarkably,

we provide the closed-form solution – known only in the special case of two users [7, 83] – for the general case of $K \geq 2$ users, as opposed to [73, 82], in which only iterative methods were proposed for the same problem. Our closed-form solution allows us to fully characterize the entire Pareto-optimal boundary of the rate vs. power trade-off points. Our numerical simulations show that NOMA outperforms Orthogonal Multiple Access (OMA) both in terms of achievable sum rate and of consumed power, irrespective from the trade-off parameter.

In [84] and [74], different closed-form power allocation solutions have been provided in multi-user downlink NOMA systems. In [84], the rate maximization problem was considered, in which the transmission always takes place at maximum power (which is not power-efficient). In [74], the energy efficiency defined as the ratio between the sum rate and the overall power consumption was studied. By using a skillful variable change, which lead to an intermediary closed-form solution to a multi-variate non-convex problem, finding the maximum energy efficiency in a multi-user setting was reduced to a univariate bisection method. Nevertheless, the solutions in [74, 84] provide only very specific points on the Pareto-optimal boundary, whereas our closed-form solution provides all rate vs. power optimal trade-offs.

In the following Section, we describe the multi-user NOMA downlink system and formulate the energy-efficiency optimization problem.

3.2 System model and problem formulation

In this Section, we define the system model and formulate the energy-efficiency optimization problem as a trade-off between the sum rate and the overall power consumption.

3.2.1 System model

The system under study is composed of a single transmitter (e.g., base station (BS), femtocell, access point, etc.) and K receivers (e.g., mobile phones, Internet of Things (IoT) devices, etc.), all equipped by a single antenna, as illustrated in Figure 3.1. The transmitter employs Superposition Coding (SC) technique and sends the message $X = \sum_{k=1}^{K} X_k$, where X_k, of average power $p_k \geq 0$, denotes the message intended for receiver k. The received signal at receiver k writes as

$$Y_k = h_k X + Z_k, \quad k \in \{1, \ldots, K\}, \tag{3.1}$$

where Z_k, of variance σ_k^2, is the additive white Gaussian noise (AWGN) at receiver k. We assume that perfect channel state information (CSI) is available at the transmitter and

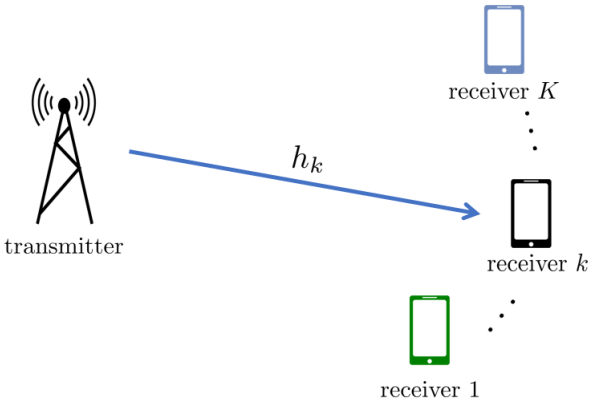

Figure 3.1: Multi-user downlink NOMA system

that the receivers are arranged on descending order of their channel gains normalized by the noise power such that

$$\frac{(h_1)^2}{\sigma_1^2} \geq \ldots \geq \frac{(h_K)^2}{\sigma_K^2}, \tag{3.2}$$

which means that the i-th strongest user with respect to the channel quality decodes first the signals of the weaker users $j \geq i+1$ using Successive Interference Cancellation (SIC), and only sees the interference coming from the stronger users $j \leq i-1$. We denote $H_{k|0} = \frac{(h_k)^2}{\sigma_k^2}$ as the channel gain of the link between the transmitter and user k normalized by the noise power at user k. This choice of notation will be useful to make a distinction between the channels resulting from the direct and the backscattered links introduced in Chapter 4, where the system model is extended to include ambient backscatter devices. Note that the following analysis is independent of the channel model and also applies for complex channels up to a multiplicative factor of 2. Hence, the achievable rate of the k-th user writes as

$$R_k(\mathbf{p}) = C\left(\gamma_k\right), \quad \forall k \ \in \{1, \ldots, K\}, \tag{3.3}$$

where $C(x) = \frac{1}{2}\log_2(1+x)$ represents Shannon capacity and γ_k is the signal-to-interference-plus-noise ratio (SINR) to decode the message destined to user k defined as

$$\gamma_k = \frac{H_{k|0}p_k}{H_{k|0}(p_1+\ldots+p_{k-1})+1}, \quad \forall k > 1, \tag{3.4}$$

and $\mathbf{p} = (p_1, \ldots, p_K)$ denotes the power allocation vector with

$$H_{1|0} \geq \ldots \geq H_{K|0}. \tag{3.5}$$

The system is constrained by an overall power budget at the transmitter such that $\sum_{k=1}^{K} p_k \leq P_{\max}$ as well as by individual minimum QoS constraints given as $R_k(\mathbf{p}) \geq R_{\min,k}\ \forall k$. These constraints define the set of feasible power allocation vectors given as

$$\mathcal{P} \triangleq \left\{ \mathbf{p} \in \mathbb{R}_+^K \;\middle|\; \sum_{k=1}^{K} p_k \leq P_{\max}, R_k(\mathbf{p}) \geq R_{\min,k},\ \forall k \right\}. \tag{3.6}$$

3.2.2 Problem formulation

We formulate the energy efficiency as a bi-criterion optimization problem [65, 70], which in our case writes as

$$\underset{\mathbf{p} \in \mathcal{P}}{\text{maximize}} \quad \left(\sum_{k=1}^{K} R_k(\mathbf{p}); \; -\sum_{k=1}^{K} p_k - P_c \right), \tag{3.7}$$

where P_c denotes the constant circuit power consumption. To solve such a bi-criterion optimization problem, we need to find the Pareto-boundary of the feasible set of the rate-power pairs. This boundary contains all the Pareto-optimal solutions, which represent the rate-power feasible pairs which cannot be improved in both objectives simultaneously while remaining in the feasible set. Under the channel order assumed, the sum rate is jointly concave w.r.t $\mathbf{p}$ as shown in [84]. Hence, the optimization problem (3.7) is convex and finding the Pareto-boundary reduces to maximizing the weighted sum of the two opposing objectives [72]

$$\underset{\mathbf{p} \in \mathcal{P}}{\text{maximize}} \quad \sum_{k=1}^{K} R_k(\mathbf{p}) - \alpha \left(\sum_{k=1}^{K} p_k + P_c \right), \tag{3.8}$$

where $\alpha \geq 0$ is the parameter that trades off between sum rate and power consumption and sweeps the entire Pareto-boundary. In what follows, we first provide the closed-form solution in Section 3.3 and then, in Section 3.4, exploit this solution in the maximization of the ratio between the sum rate and the overall power consumption.

3.3 Optimal power allocation

Because of the QoS constraints, the feasible set may be void. Indeed, depending on the channel conditions, the minimum rate requirements for all users may not be met under the available power budget. In [84], necessary and sufficient feasibility conditions were introduced.

3.3.1 Feasibility condition

Proposition 1. *[84] The optimization problem* (3.7) *is feasible if and only if the following condition on the system parameters holds*

$$P_{\max} \geq P_{\min} \triangleq \sum_{i=1}^{K} \frac{A_i - 1}{H_{i|0}} \prod_{j=i+1}^{K} A_j, \tag{3.9}$$

where $A_k = 2^{2R_{\min,k}}, \forall k \geq 1$. Intuitively, $P_{\min}$ denotes the overall minimum power required for all the QoS constraints to be met with equality.

3.3.2 Introducing a variable change

To simplify the mathematical derivations, we introduce the following variable $\theta_k(\mathbf{p}) = \sum_{i=1}^{k} p_i, \forall k \geq 1$. The optimization problem under study can be rewritten as

$$\max_{\mathbf{p}} \sum_{k=1}^{K} \frac{1}{2} \log_2 \left(\frac{1 + H_{k|0}\theta_k(\mathbf{p})}{1 + H_{k|0}\theta_{k-1}(\mathbf{p})} \right) - \alpha(\theta_K(\mathbf{p}) + P_{\mathrm{c}})$$

$$\begin{aligned} &\text{s.t. } \theta_K(\mathbf{p}) \leq P_{\max}, \\ &\qquad \theta_k(\mathbf{p}) \geq \ A_k\theta_{k-1}(\mathbf{p}) + \frac{(A_k - 1)}{H_{k|0}}, \ \forall k \in \{1, \ldots, K\}, \end{aligned} \tag{3.10}$$

which is a convex problem [84, 85] that we solve analytically and in closed-form using the Karush-Kuhn-Tucker (KKT) optimality conditions introduced in Chapter 2.

3.3.3 Closed-form solution

If the feasibility condition (3.9) is satisfied, and given that (3.10) is convex, we can apply the Lagrange multipliers to obtain the optimal expressions of $p_k^*, \forall k \geq 2$ as functions of p_1 by solving the KKT optimality conditions, which are necessary and sufficient. The multi-variable problem (3.10) is turned into a single variable optimization problem w.r.t p_1 that is proved to be convex. This leads to our main result below.

Theorem 1. *The optimal power allocation maximizing the energy efficiency in* (3.7) *for a downlink multi-user NOMA system is obtained in closed-form as follows*

$$\begin{aligned} p_k^*(\alpha) &= (A_k - 1)\left(\frac{1}{H_{k|0}} + p_1^*(\alpha) \prod_{i=2}^{k-1} A_i + \sum_{i=2}^{k-1} \frac{A_i - 1}{H_{i|0}} \prod_{j=i+1}^{k-1} A_j \right), \quad \forall\ k \geq 2, \\ p_1^*(\alpha) &= \max\left(\min\left(\overline{p_1}(\alpha); u\right); \ell\right), \end{aligned} \tag{3.11}$$

where ℓ, u and $\overline{p_1}(\alpha)$ are expressed below

$$\ell = \frac{A_1 - 1}{H_{1|0}}, \tag{3.12}$$

$$u = \frac{1}{\prod_{i=2}^{K} A_i} \left(P_{\max} - P_{\min} + \ell \prod_{j=2}^{K} A_j \right), \tag{3.13}$$

$$\overline{p_1}(\alpha) = \frac{1}{(2\ln 2)\ \alpha\ \prod_{i=2}^{K} A_i} - \frac{1}{H_{1|0}}. \tag{3.14}$$

The bounds ℓ and u represent the lower and upper bounds on p_1 respectively and $\overline{p_1}(\alpha)$ is the unique critical point of the single variable function w.r.t p_1. The complete proof is given in Appendix A.

Under the assumed order of the channels in (3.5), and as shown in the proof, all users except for the strongest one, i.e., user 1, should meet their QoS with equality in order to maximize the overall energy efficiency.

3.4 Ratio between the sum rate and power consumption

In this Section, we present the special case of maximizing the ratio sum rate vs. overall power consumption, as introduced in Section 2.3, and show that our solution reduces the complexity of the Dinkelbach procedure to a univariate bisection method.

3.4.1 Univariate bisection-based solution

We consider the energy efficiency defined as the ratio between the sum rate and the overall power consumption measured in bits per Joule of consumed energy

$$\xi_{\mathrm{EE}}(\mathbf{p}) = \frac{\sum_k R_k(\mathbf{p})}{\sum_k p_k + P_c}, \tag{3.15}$$

whose solution also lies on the Pareto-boundary of the bi-criterion problem (3.7).

In [74], the authors proposed a skillful variable change for the maximization of $\xi_{\mathrm{EE}}(\mathbf{p})$, leading to a closed-form intermediary solution where solving $\xi_{\mathrm{EE}}(\mathbf{p})$ reduces to a univariate bisection method.

Although our closed-form solution solves a different (more general) problem, it can also be exploited for the same purpose. Using fractional programming [71, 73] and our closed-form solution in Theorem 1, simplifies the optimization of (3.15) to finding the unique zero of the following function

$$F(\alpha) = \sum_{k=1}^{K} R_k(\mathbf{p}^*(\alpha)) - \alpha\left(\sum_{k=1}^{K} p_k^*(\alpha) + P_c\right). \tag{3.16}$$

Algorithm 2 $\xi_{\mathrm{EE}}(\mathbf{p})$ maximization using Dinkelbach

$\epsilon > 0$, $n = 0$, $\alpha_n = 0$
while $F(\alpha_n) > \epsilon$ **do**
  Compute $\mathbf{p}^*$ via eq. (3.11)
  Update $F(\alpha)$
  Update $\alpha \leftarrow \xi_{\mathrm{EE}}(\mathbf{p}^*)$
  $n = n + 1$
end while

3.4.2 Complexity analysis

Thanks to our closed-form expression of the optimal power allocation $\mathbf{p}^*$, the complexity of the operations inside the repeat-loop of our Algorithm 2 scales as $\mathcal{O}(K)$. The optimal solution is reached after few iterations of the loop, due to the super-linear convergence rate of the Dinkelbach's procedure [86].

3.5 Numerical results

In this Section, we compare the performance of NOMA and OMA in terms of both achievable sum rate and power consumption by considering the following setup, which is common in the literature [82, 87]: $K = 3$ users, $P_{\max} = 10$ W available transmit power, $P_c = 1$ W circuit power consumption, $R_{\min,k} = 1$ bps, $\forall k$, i.e., all users have the same minimum rate requirement. We also assume that the noise variances are such that $\sigma_k^2 = 0.1, \forall k$ and that the channel gains are such that $h_k \sim \mathcal{N}(0, 5), \forall k$. The curves are averaged over 10^5 independent channel realizations.

We note that the numerical values obtained in the figures below depend on the setting and the input parameters. However, our main conclusions are general and carry over many other settings.

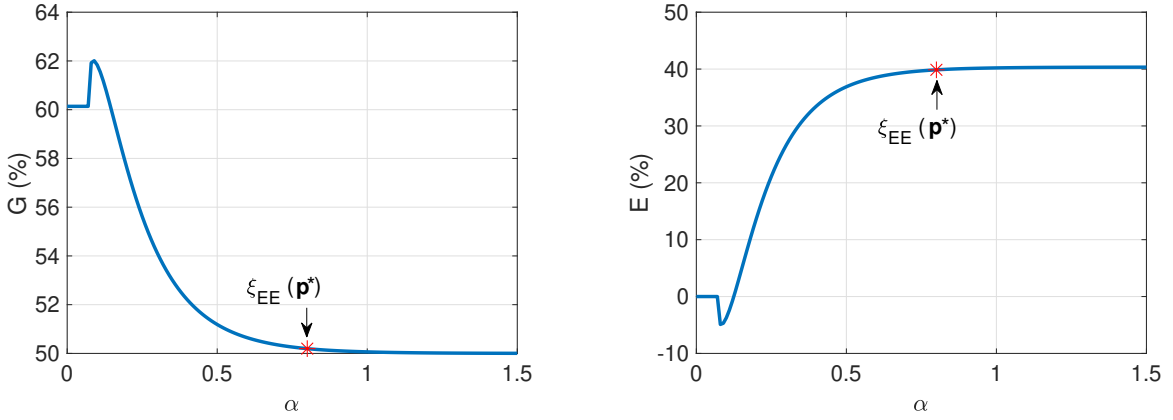

(a) Relative sum-rate gain of NOMA vs. OMA

(b) Relative power consumption excess of OMA vs. NOMA

Figure 3.2: NOMA vs. OMA as a function of the parameter α that tradeoffs between sum rate and power consumption in the energy-efficiency bi-objective optimization for $P_{\max} = 10\,W$. NOMA outperforms OMA in terms of sum rate for any α. In terms of power consumption, for rate-driven objectives (small values of α) OMA may consume less power (down to 5%) than NOMA. At the opposite, for power-efficient objectives (large values of α) OMA consumes more power (up to 40%) than NOMA.

Under OMA, the transmitter serves the K users by performing time sharing with equal time slots. Each user k is allocated a power $q_k \in [0, P_{\max}]$ and can thus achieve the rate $R_k^{\text{OMA}}(\mathbf{q}) = \frac{1}{2K} \log_2 \left(1 + H_{k|0} q_k\right)$. Note that under OMA, the total amount of consumed power writes as $\frac{1}{K} \sum_k q_k + P_c$. For a fair comparison with NOMA, the same individual QoS constraints $\{R_{\min,k}\}_k$ are imposed in addition to the power budget $P_{\max}$ to compute the optimal power allocation under OMA, denoted by $\mathbf{q}^*(\alpha)$.

In Figure 3.2(a) and Figure 3.2(b), we illustrate the relative sum-rate gain, $G(\alpha)$, of NOMA vs. OMA and the relative power consumption excess, $E(\alpha)$, of OMA vs. NOMA

respectively, as a function of α, the parameter that trades off between rate and power consumption. To be precise, the two-performance metrics $G(\alpha)$ and $E(\alpha)$ are defined as

$$G(\alpha) \triangleq \frac{\sum_k \left[R_k^{\mathrm{NOMA}}(\mathbf{p}^*(\alpha)) - R_k^{\mathrm{OMA}}(\mathbf{q}^*(\alpha))\right]}{\sum_k R_k^{\mathrm{OMA}}(\mathbf{q}^*(\alpha))}, \tag{3.17}$$

$$E(\alpha) \triangleq \frac{\sum_k \left[\frac{1}{K} q_k^*(\alpha) - p_k^*(\alpha)\right]}{\sum_k p_k^*(\alpha) + P_c}. \tag{3.18}$$

In Figure 3.2, notice that the gain G is always non-negative, which means that NOMA cannot decrease the achievable sum rate compared to OMA and, for low values of α (when the sum rate dominates the power consumption in the objective) the relative sum-rate gain goes up to 62%. Furthermore, for very small α, both NOMA and OMA consume the entire available power budget in order to maximize their sum rate, resulting in $E = 0$. Then, NOMA first starts by consuming more power than OMA (for relatively small values of α when the objective is rate-driven), yielding a negative power excess E. Finally for larger α (power-efficient objectives), OMA consumes up to 40% more power than NOMA. Although for small values of α, NOMA consumes more power than OMA, it achieves higher sum rates, which is the target goal.

It is also worth mentioning that the two metrics $G(\alpha)$ and $E(\alpha)$ exhibit opposite behavior. Specifically, the sum-rate gain of NOMA vs. OMA is larger for small values of α, whereas the power excess of OMA vs. NOMA is larger for larger values of α. This means that, when the sum rate is the critical or dominant objective (small α), NOMA clearly outperforms OMA in terms of sum rate, but can consume more power. On the other hand, when the power consumption is the most critical objective (large α), NOMA clearly outperforms OMA in terms of power consumption but the gain in terms of sum rate drops.

We also highlight the specific point $\alpha = \xi_{\mathrm{EE}}(\mathbf{p}^*)$, obtained by Algorithm 2, which represents the optimal energy-efficiency ratio defined in (3.15).

In Figure 3.3, we present the relative sum-rate gain G and the relative power consumption excess E as a function of the base station power budget $P_{\max}$ for five different values of $\alpha \in \{0;\ 0.1;\ 0.2;\ 0.5;\ 1\}$.

First, in Figure 3.3(a) we note that NOMA always outperforms OMA in terms of sum rate for all values of α and power budget $P_{\max}$. The largest gaps in the sum rate are achieved for small α, i.e., when the objective reduces to maximizing the sum rate, with little or no power consumption consideration. For $\alpha > 0$, the optimal solution tradeoffs between sum rate and power consumption.

For large values of α, a decrease in the relative sum-rate gain can be observed as the objective becomes more power efficient. Nevertheless, NOMA still achieves a higher sum rate where the gain approaches 50%, irrespective from $P_{\max}$.

With respect to the power consumption, NOMA does not always outperform OMA. Indeed, in Figure 3.3(b), we see that for small values of α and large values of $P_{\max}$, NOMA

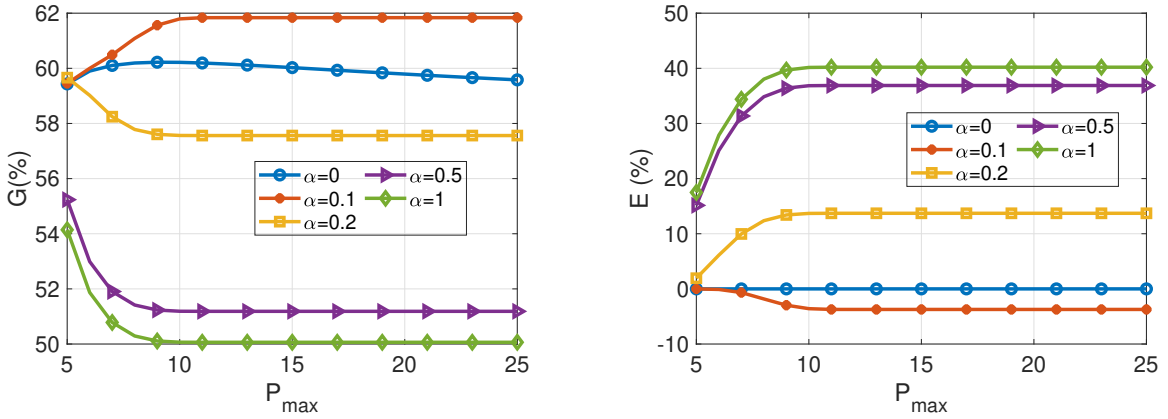

(a) Relative sum-rate gain of NOMA vs. OMA

(b) Relative power consumption excess of OMA vs. NOMA

Figure 3.3: NOMA vs. OMA as a function of the maximum power $P_{\max}$ for different values of α. NOMA always outperforms OMA in terms of sum rate and the gap between them decreases with α. In terms of power consumption, for rate-driven objectives (small values of α) OMA may consume less power (down to 4%) than NOMA. At the opposite, for power-efficient objectives (large values of α) OMA consumes more power (up to 40%) than NOMA.

consumes more power than OMA, resulting into negatives of the excess E. Nevertheless, for these values of α, the objective is sum-rate driven with little or no consideration of the power consumption. When α increases and the objective becomes more power efficient, it can be seen that OMA is outperformed by NOMA and may require up to 40% more power to achieve nearly half the sum rate of NOMA ($\alpha = 1$).

In general, we can conclude that when the emphasis in the objective function is on the sum rate (small α), NOMA is more rate-efficient than OMA. Similarly, when the emphasis in the objective function is on reducing the power consumption (large α) again NOMA is more power-efficient than OMA.

3.6 Summary

In this Chapter, we provided a closed-form solution to the energy efficiency maximization, defined as a bi-criterion problem, in a multi-user downlink NOMA system. We showed that our solution is also quite useful when maximizing the ratio between the sum rate and overall power consumption.

In the next Chapter, we extend the system model to include Ambient Backscatter Communication (AmBC) where the optimal power allocation policy derived in this Chapter would be exploited.

Chapter 4

Downlink NOMA aided by ambient backscattering

Contents

4.1 Introduction

In this Chapter, we extend the system model considered in Chapter 3 to incorporate Ambient Backscatter Communication (AmBC). The objective is to investigate the energy-efficiency maximization in a multi-user downlink Non-Orthogonal Multiple Access (NOMA) system aided by an ambient backscatter device that modulates its own information by reflecting the incident signal coming from the NOMA transmitter.

Several optimization problems were investigated in the context of backscatter communications [88–90]. In [88], the ergodic capacity maximization of backscatter-receiver link was investigated by jointly optimizing the transmit power of the source and the reflection coefficient of the backscatter device. In [89], an energy-efficient resource allocation scheme was proposed in terms of the optimal time allocation for the sleep vs. harvesting energy states of the backscatter device, its reflection coefficient, and the power of the RF source. Similarly, the throughput maximization problem has been investigated in [90].

In the last years, a great research interest focused on investigating NOMA in the context of backscatter communications. In [91], a backscatter cooperation scheme was proposed for a two users NOMA downlink system, where one of the users backscatters the surplus power of the received signal to enhance the reception of the other user. The ergodic rate and the outage performance were analyzed. The optimal reflection coefficient and the optimal power allocation at the base station (BS) were derived, under outage constraints for NOMA. In [92], an iterative algorithm for the optimal reflection coefficient and the power allocation policy was proposed to maximize the energy efficiency of a two-user downlink NOMA system aided by an ambient backscatter device. The authors in [93] considered the same model to enhance the sum rate of the system under imperfect SIC decoding. The same authors investigated the energy-efficiency maximization problem for a NOMA system aided by AmBC in a vehicular scenario under imperfect SIC decoding [94].

To sum up, the above relevant literature on NOMA systems aided by AmBC has covered both experimental and theoretical aspects. However, most of the existing works consider either the simple backscattering state where the backscatter device always reflects the ambient signal and acts as a passive relay, or that the backscattered signal, which contains a multiplicative term of the ambient signal and the backscatter device message, has a Gaussian distribution, both cases leading to conventional Shannon capacity when deriving the achievable rates [88–90, 92–95]. To the best of our knowledge, a rigorous investigation of the information-theoretic achievable rate region of NOMA in the context of AmBC is still lacking. In this Chapter, we aim at filling this gap by deriving the achievable rate region and only then developing resource allocation techniques to optimize the energy efficiency of the system.

First, we investigate the special case of a fixed backscattering state where the backscatter device does not transmit any information of its own and acts as a passive

relay. We derive a closed-form solution for an arbitrary number of users. We first show that the expression of the optimal reflection coefficient can be obtained in closed form, resulting in a reformulated optimization with respect to the power allocation that is convex and has been solved in the previous Chapter in closed-form. Our novel contributions are two-fold: we solve the energy-efficiency maximization problem for an arbitrary number of users $K \geq 2$ as opposed to the particular case of only $K = 2$ users in [92]; we propose a low-complexity algorithm to solve the maximization of the overall rate vs. power ratio based on our previous closed-form solution as opposed to the iterative sub-gradient algorithm in [92].

We further extend this investigation to multiple ambient backscattering devices. We provide analytical closed-form expressions of the optimal reflection coefficients and the optimal power allocation for the case of two backscatter devices. The problem becomes difficult for more than two backscatter devices and our methodology cannot be extended easily. Nevertheless, we evaluate the performance of NOMA aided by several (up to four) backscatter devices via numerical simulations.

We then tackle the general case, in which the ambient backscatter device transmits information and is not always in fixed backscattering state. First, we derive the information-theoretic achievable rate regions, we then propose a joint optimization framework to maximize the energy efficiency of the system.

4.2 System model and problem formulation

In this Section, we introduce the system model extended from Section 3.2 and the corresponding energy-efficiency optimization problem.

4.2.1 Ambient backscatter NOMA system

We extend the system model of Chapter 3 by including an ambient backscatter device, as depicted in Figure 4.1, that can backscatter the radio frequency (RF) signal coming from the transmitter, also called a source, to send information and harvest energy. Some applications for this are smart home or smart healthcare. For example, in the smart home scenario, a Wi-Fi access point communicates with a smart phone while an IoT sensor in the home transmits its own signal to the smart phone by riding on the Wi-Fi signals.

The source sends the message M_i of codeword X_i intended for each receiver $i \in \{1, \ldots, K\}$ with power p_i via Superposition Coding (SC) and broadcasts $X = \sum_{i=1}^{K} X_i$, which contains all the superimposed encoded messages. We assume that the backscatter device sends a common information to all receivers. The binary code B sent by the backscatter device to all receivers is encoded by modulating the amplitude of the direct signal with two distinct scattering states: an active backscattering state, in which the

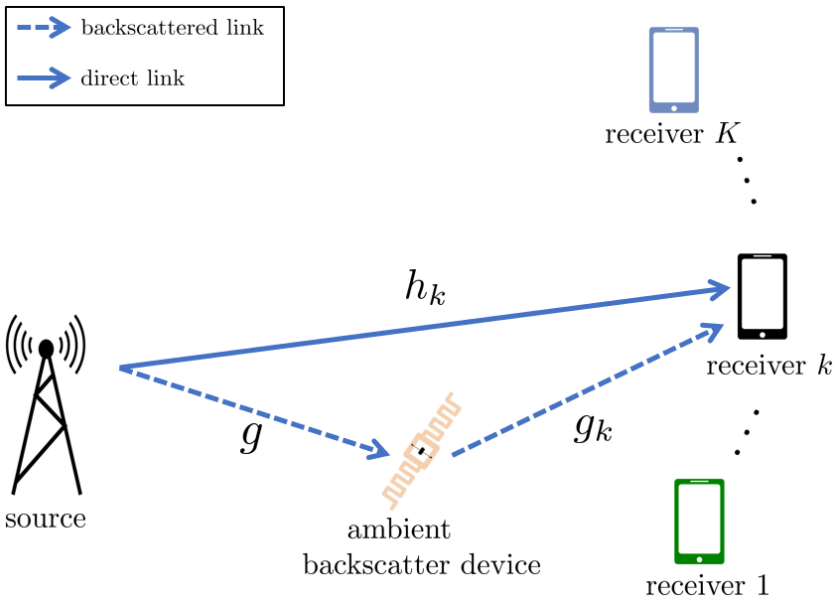

Figure 4.1: Multi-user downlink NOMA system aided by an ambient backscatter device

ambient signals are reflected and $B = 1$; and a transparent state, in which the backscatter device does not reflect the incoming signals and $B = 0$. Thus, the backscatter device can send information by switching between backscattering and transparent states, which is referred to as on-off keying (OOK) [18, 21, 96].

4.2.2 Received signals model

The received signal Y_k at user k is composed of the direct signal coming from the source and the backscattered signal, which is given by

$$Y_k = \underbrace{h_k X}_{\text{direct signal}} + \underbrace{\sqrt{\rho}\, g\, g_k B X}_{\text{backscattered signal}} + Z_k, \quad \forall k \in \{1, \ldots, K\}, \tag{4.1}$$

where h_k, g and g_k[1] are the channel gains between the source and receiver k, the source and the backscatter device and the backscatter device and receiver k, respectively, $Z_k \sim \mathcal{N}(0, \sigma_k^2)$ is the additive white Gaussian noise (AWGN), and the parameter ρ is the reflection coefficient.

The users are arranged on the same order of $H_{k|0} = \frac{(h_k)^2}{\sigma_k^2}$, $k \in \{1, \ldots, K\}$, as in Chapter 3, where

$$H_{1|0} \geq \ldots \geq H_{K|0}. \tag{4.2}$$

Note that the source decides the SIC ordering only based on the direct link to the users without accounting for the backscattered link. Indeed, since the backscatter device is

[1] For the purpose of mathematical derivation, we assume that the source has full knowledge of h_k and g^d which can be obtained through pilot-based channel estimation, and g_k^d which can be backscattered to the source.

inherently opportunistic when sending its own message, the source has no control over its backscattering state.

4.2.3 Problem formulation in the general case

Our aim is to maximize the energy efficiency of the multi-user NOMA system aided by the ambient backscatter device defined as the trade-off between the sum of achievable rates of the users and the power consumption given as [65, 70]

$$(\mathbf{EE0}) \quad \max_{(\rho,\mathbf{p})\in\mathcal{P}} \sum_{k=1}^{K} R_k(\rho,\mathbf{p}) - \alpha\left(\sum_{k=1}^{K} p_k + P_c\right).$$

The set $\mathcal{P}$ contains all admissible reflection coefficients ρ and transmit power allocation policies $\mathbf{p} = (p_1, \ldots, p_K)$ defined as

$$\mathcal{P} \triangleq \Bigg\{(\rho,\mathbf{p}) \in [0,1]\times\mathbb{R}_+^K \;\Bigg|\; 0\le\rho\le 1, \sum_{j=1}^{K} p_j \le P_{\max}, R_k(\rho,\mathbf{p}) \ge R_{\min,k}, \\ R_{k\to i}(\rho,\mathbf{p}) \ge R_{k\to k}(\rho,\mathbf{p}),\ \forall 1\le k\le K, \forall i\le k\Big\}. \tag{4.3}$$

Before delving into a detailed analysis of this problem, in the following Section, we first investigate the special case of a fixed backscattering state.

4.3 Special case: fixed backscattering state

In the transparent state, the ambient backscatter device does not reflect the ambient signal and is fully harvesting energy. In this case, $B = 0$ and the system corresponds to the one that has been already investigated in the previous Chapter.

Here, we focus on the fixed backscattering state where the ambient backscatter device is reflecting the signal coming from the source. In this case, $B = 1$ and the received signal writes as

$$Y_k = (h_k + \sqrt{\rho}\ g\ g_k)X + Z_k, \quad \forall k \in \{1,\ldots,K\}. \tag{4.4}$$

The achievable rate of user k is [28, 39, 40]

$$R_k(\rho,\mathbf{p}) = C\Big(\min_i(\gamma_{k\to i})\Big), \quad \forall k\ \ge 2,\ \forall i\le k, \tag{4.5}$$

where $C(x) = \frac{1}{2}\log_2(1+x)$ represents Shannon capacity and $\gamma_{k\to i}$ is the SINR to decode the message destined to user k at receiver i defined as

$$\gamma_{k\to i} = \frac{(h_i + \sqrt{\rho}gg_i)^2 p_k}{(h_i+\sqrt{\rho}gg_i)^2(p_1+\ldots+p_{k-1})+\sigma_i^2}, \quad \forall k>1, \forall i<k. \tag{4.6}$$

To ensure the SIC decoding order described in (4.2), the SINR needs to meet the following constraints

$$\gamma_{k\to i} \geq \gamma_{k\to k}, \quad \forall k > 1, \forall i < k, \tag{4.7}$$

In this case, the achievable rate of user k simplifies to

$$R_k(\rho, \mathbf{p}) = C(\gamma_{k\to k}) = \frac{1}{2}\log_2\left(1+\frac{H_{k|1}(\rho)p_k}{H_{k|1}(\rho)(p_1+\ldots+p_{k-1})+1}\right), \quad \forall k \in \{1,\ldots,K\}, \tag{4.8}$$

where $H_{k|1}(\rho) = \frac{(h_k+\sqrt{\rho}gg_k)^2}{\sigma_k^2}$ for simplicity. Using the same notations $\theta_k(\mathbf{p}) = \sum_{i=1}^{k} p_i$, $\forall k \geq 1$ with $\theta_0(\mathbf{p}) = 0$ and $A_k = 2^{2R_{\min,k}}$ introduced in Chapter 3, the energy-efficiency maximization problem (**EE0**) is cast as

$$(\mathbf{EE1}) \quad \max_{\rho,\mathbf{p}} \sum_{k=1}^{K} \frac{1}{2}\log_2\left(\frac{1+H_{k|1}(\rho)\theta_k(\mathbf{p})}{1+H_{k|1}(\rho)\theta_{k-1}(\mathbf{p})}\right) - \alpha(\theta_K(\mathbf{p})+P_c)$$

$$\begin{aligned}
\text{s.t.} \quad & (C1) \quad \theta_K(\mathbf{p}) \leq P_{\max}, \\
& (C2) \quad \theta_k(\mathbf{p}) \geq A_k\theta_{k-1}(\mathbf{p}) + \frac{(A_k-1)}{H_{k|1}(\rho)}, \quad \forall k \in \{1,\ldots,K\}, \\
& (C3) \quad \gamma_{k\to i} \geq \gamma_{k\to k}, \quad \forall k \geq 2, \ \forall i \leq k-1, \\
& (C4) \quad 0 \leq \rho \leq 1,
\end{aligned}$$

where $(C1)$ is the total power constraint, $(C2)$ are the K individual minimum rate constraints, $(C3)$ is the SINR SIC ordering constraints and $(C4)$ is the ambient backscatter reflection coefficient constraint.

4.3.1 Optimal reflection coefficient and power allocation policy

The resulting optimization problem (**EE1**) is non-convex because of the coupling between ρ and $\mathbf{p}$ as also discussed in [92] for the special two-user case $K = 2$. In [92], an iterative algorithm based on duality and sub-gradient descent is proposed. Here, we show that this problem can be solved in closed form and in the general multi-user case $K \geq 2$, without the need for an iterative procedure.

4.3.1.1 Decoupling the optimization problem

The optimization problem (**EE1**) can be solved by decoupling it into two sub-problems without loss of optimality. We first optimize ρ for an arbitrary power allocation vector $\mathbf{p}$, then we optimize $\mathbf{p}$ with the fixed optimal reflection coefficient ρ^*.

Optimal reflection coefficient

We start by optimizing ρ while considering a fixed arbitrary power allocation $\mathbf{p} \in \mathcal{P}$ and solve the optimization problem (**EE1**) w.r.t the reflection coefficient ρ. The objective function in (**EE1**) is increasing w.r.t ρ and it turns out that the optimal reflection coefficient is independent of $\mathbf{p}$ and can be obtained in closed-form as shown in the following Theorem.

Theorem 2. *The optimal reflection coefficient ρ^* for a fixed power allocation vector $\mathbf{p}$ is given by*

$$\rho^* = \begin{cases} \min\left(1, \min \mathcal{R}\right), & if\ \mathcal{R} \neq \emptyset \\ 1, & if\ \mathcal{R} = \emptyset, \end{cases} \tag{4.9}$$

where $\mathcal{R} \triangleq \left\{ \left(\frac{h_k}{\sigma_k} - \frac{h_{k+1}}{\sigma_{k+1}}\right)^2 \Big/ \left(g(\frac{g_{k+1}}{\sigma_{k+1}} - \frac{g_k}{\sigma_k})\right)^2 \;\middle|\; 2 \leq k \leq K \ s.t.\ g_{k+1} > g_k \right\}.$

The detailed proof is provided in Appendix B. The optimal ρ^* above is independent from $\mathbf{p}$, which means that decoupling the optimization problem with respect to ρ and $\mathbf{p}$ does not incur any optimality loss. Also, under ρ^* the constraint (C3) is satisfied and, as proven in Appendix B, the channels are ordered as

$$H_{1|1}(\rho^*) \geq H_{2|1}(\rho^*) \geq ... \geq H_{K|1}(\rho^*), \tag{4.10}$$

which will be put to great use to find the optimal power allocation vector $\mathbf{p}^*$.

Optimal power allocation

Given the optimal ρ^* and exploiting the resulting channel order in (4.10), we can prove that the optimization problem (**EE1**) is equivalent to the simpler problem below.

$$(\mathbf{EE2}) \quad \max_{\mathbf{p}} \ \sum_{k=1}^{K} \frac{1}{2} \log_2 \left(\frac{1 + H_{k|1}(\rho^*)\theta_k(\mathbf{p})}{1 + H_{k|1}(\rho^*)\theta_{k-1}(\mathbf{p})} \right) - \alpha(\theta_K(\mathbf{p}) + P_{\mathrm{c}})$$

$$\text{s.t.} \quad (C1) \quad \theta_K(\mathbf{p}) \leq P_{\max},$$
$$(C2a) \quad \theta_k(\mathbf{p}) \geq A_k\theta_{k-1}(\mathbf{p}) + \frac{(A_k - 1)}{H_{k|1}(\rho^*)}, \quad \forall 1 \leq k \leq K.$$

The resulting problem is convex w.r.t $\mathbf{p}$ and is similar to the optimization problem already investigated in the previous Chapter. For the sake of completeness, we provide the optimal power allocation policy expressed below

Corollary 1 (Chapter 3, Proposition 1, Theorem 1)**.** *The optimization problem* (**EE2**) *is feasible if and only if the following condition holds* $P_{\max} \geq P_{\min} \triangleq \sum_{i=1}^{K} \frac{A_i - 1}{H_{i|1}(\rho^*)} \prod_{j=i+1}^{K} A_j$.

When (**EE2**) *is feasible, the optimal power allocation is obtained in closed-form as follows*

$$\begin{aligned} p_k^*(\alpha) &= (A_k - 1)\left(\frac{1}{H_{k|1}(\rho^*)} + p_1^*(\alpha) \prod_{i=2}^{k-1} A_i + \sum_{i=2}^{k-1} \frac{A_i - 1}{H_{i|1}(\rho^*)} \prod_{j=i+1}^{k-1} A_j\right), \quad \forall\ k \geq 2, \\ p_1^*(\alpha) &= \max\left(\min\left(\overline{p_1}(\alpha); u\right); \ell\right), \end{aligned} \tag{4.11}$$

where $\ell = \frac{A_1 - 1}{H_{1|1}(\rho^*)}$, $u = \dfrac{\left(P_{\max} - P_{\min} + \ell \prod_{j=2}^{K} A_j\right)}{\prod_{i=2}^{K} A_i}$ *and* $\overline{p_1}(\alpha) = \dfrac{1}{(2 \ln 2)\ \alpha \prod_{i=2}^{K} A_i} - \frac{1}{H_{1|1}(\rho^*)}$.

4.3.1.2 Sum rate vs. power consumption ratio

Our optimal closed-form solution can be used to maximize the energy efficiency defined by the ratio between the achievable sum rate and the total power consumption given by

$$\xi_{\mathrm{EE}}(\rho, \mathbf{p}) = \frac{\sum_k R_k(\rho, \mathbf{p})}{\sum_k p_k + P_{\mathrm{c}}}. \tag{4.12}$$

Since only the numerator, i.e., the sum rate, depends on the reflection coefficient ρ, it follows that ρ^* maximizing the objective (**EE1**) also maximizes $\xi_{\mathrm{EE}}(\rho, \mathbf{p})$ for all $\mathbf{p}$, and decoupling the problem's variables does not incur any optimality loss.

In order to find the optimal power allocation policy, we need to maximize $\xi_{\mathrm{EE}}(\rho^*, \mathbf{p})$ with respect to $\mathbf{p}$, which is a fractional program since the sum rate $\sum_k R_k(\rho^*, \mathbf{p})$ is a concave function with respect to $\mathbf{p}$.

Using fractional programming discussed in Section 2.3, maximizing $\xi_{\mathrm{EE}}(\rho^*, \mathbf{p})$ reduces to searching the unique zero point of the function $F(\alpha) = \sum_k R_k(\rho^*, \mathbf{p}^*) - \alpha\left(\sum_k p_k^* + P_{\mathrm{c}}\right)$. Similar to the previous Chapter, this search is performed via a Dinkelbach's procedure, given in Algorithm 3, that is reduced to a simple line-search thanks to our closed-form solution.

In what follows, we extend our investigation to the case of multiple ambient backscatter devices.

4.3.2 Extension to multiple ambient backscattering devices

In this Section, we extend our investigation to a NOMA system assisted by several ambient backscatter devices. We first tackle the case of two-user two-backscatter device

Algorithm 3 $\xi_{\text{EE}}(\rho, \mathbf{p})$ maximization using Dinkelbach

$\epsilon > 0$, $n = 0$, $\alpha_n = 0$
Compute ρ^* via eq. (4.9)
while $F(\alpha_n) > \epsilon$ **do**
  Compute $\mathbf{p}^*$ via eq. (4.11)
  Update $F(\alpha)$
  Update $\alpha \leftarrow \xi_{\text{EE}}(\rho^*, \mathbf{p}^*)$
  $n = n + 1$
end while

where the solution is obtained in analytical closed-form. We then discuss the case of multi-user multi-backscatter device where the closed-form solution cannot be extended.

4.3.2.1 Two-user two-backscatter device case

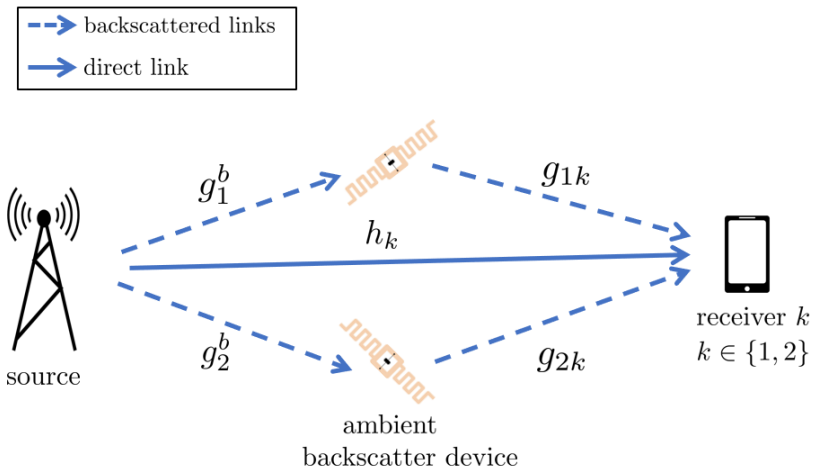

Figure 4.2: Two-backscatter two-user downlink NOMA system

We first study the case of a two-user downlink NOMA system, i.e., $K = 2$, where the transmission is assisted by two backscatter devices as depicted in Figure 4.2. The received signal at each user k writes as

$$Y_k = \left(h_k + \sqrt{\rho_1} g_1^b g_{1k} + \sqrt{\rho_2} g_2^b g_{2k}\right) X + Z_k, \quad \forall k \in \{1, 2\}, \tag{4.13}$$

where g_j^b and g_{jk} denote the channel gains between the source and ambient backscatter device j and between ambient backscatter device j and receiver k, respectively. ρ_j denotes the reflection coefficient of the ambient backscatter device j.

The achievable rate of each user $k \in \{1, 2\}$ is expressed as in (4.5) with

$$\gamma_{k \to i} = \frac{(h_i + \sqrt{\rho_1} g_1^b g_{1i} + \sqrt{\rho_2} g_2^b g_{2i})^2 p_k}{(h_i + \sqrt{\rho_1} g_1^b g_{1i} + \sqrt{\rho_2} g_2^b g_{2i})^2 (p_1 + \ldots + p_{k-1}) + \sigma_i^2}. \tag{4.14}$$

To ensure a successful SIC decoding following the order described in (4.2), the constraints $\gamma_{k\to i} \geq \gamma_{k\to k}$, $\forall k > 1, \forall i \leq k$ needs to be satisfied. In this case, the achievable rate of user k simplifies to

$$R_k(\boldsymbol{\rho}, \mathbf{p}) = C(\gamma_{k\to k}) = \frac{1}{2}\log_2\left(\frac{1 + H_{k|1,1}(\boldsymbol{\rho})\theta_k(\mathbf{p})}{1 + H_{k|1,1}(\boldsymbol{\rho})\theta_{k-1}(\mathbf{p})}\right), \quad \forall k \in \{1, 2\}, \tag{4.15}$$

where $\boldsymbol{\rho} = (\rho_1, \rho_2)$ denotes the reflection coefficient vector and $H_{k|1,1}(\boldsymbol{\rho}) = \frac{(h_k + \sqrt{\rho_1} g_1^b g_{1k} + \sqrt{\rho_2} g_2^b g_{2k})^2}{\sigma_k^2}$ the normalized channel gain when both backscatter devices reflect the signal. The resulting optimization problem can be written as follows

$$(\mathbf{EE3}) \quad \max_{\boldsymbol{\rho}, \mathbf{p}} \sum_{k=1}^{2} \frac{1}{2}\log_2\left(\frac{1 + H_{k|1,1}(\boldsymbol{\rho})\theta_k(\mathbf{p})}{1 + H_{k|1,1}(\boldsymbol{\rho})\theta_{k-1}(\mathbf{p})}\right) - \alpha(\theta_2(\mathbf{p}) + P_{\mathrm{c}})$$

$$\begin{aligned}
\text{s.t.} \quad & (C1) \quad \theta_2(\mathbf{p}) \leq P_{\max}, \\
& (C2) \quad \theta_k(\mathbf{p}) \geq A_k\theta_{k-1}(\mathbf{p}) + \frac{(A_k - 1)}{H_{k|1,1}(\boldsymbol{\rho})}, \quad \forall k \in \{1, 2\}, \\
& (C3) \quad \gamma_{2\to 1} \geq \gamma_{2\to 2}, \\
& (C4) \quad 0 \leq \rho_1, \rho_2 \leq 1.
\end{aligned}$$

The problem (**EE3**) is not convex due to the joint optimization of the reflection coefficient vector $\boldsymbol{\rho} = (\rho_1, \rho_2)$ and the allocated power vector $\mathbf{p} = (p_1, p_2)$. Nevertheless, we can exploit a similar approach to the problem (**EE1**) and decouple it into two sub-problems without loss of optimality. For ease of presentation and simplicity, we consider the following notation

$$G_k = \frac{h_k}{\sigma_k}; \quad G_{1k} = \frac{g_1^b g_{1k}}{\sigma_k}; \quad G_{2k} = \frac{g_2^b g_{2k}}{\sigma_k}, \quad \forall k \in \{1, 2\}. \tag{4.16}$$

Optimal reflection coefficients

Since the objective function in (**EE3**) is increasing w.r.t ρ_1 and ρ_2 unilaterally, the optimal values ρ_1^* and ρ_2^* lie on the Pareto boundary of the feasible set and are expressed in the following Theorem.

Theorem 3. *For any feasible power allocation policy (p_1, p_2), the optimal values of the reflection coefficients ρ_1^* and ρ_2^* of* (**EE3**) *can be found in closed form as follows. Let*

$$\overline{\rho_1} = \left(\frac{G_1 - G_2}{G_{12} - G_{11}}\right)^2, \quad \widetilde{\rho_1} = \left(\frac{G_1 - G_2 - (G_{22} - G_{21})}{G_{12} - G_{11}}\right)^2$$
$$\overline{\rho_2} = \left(\frac{G_1 - G_2}{G_{22} - G_{21}}\right)^2, \quad \widetilde{\rho_2} = \left(\frac{G_1 - G_2 - (G_{12} - G_{11})}{G_{22} - G_{21}}\right)^2.$$

[H1] If $(G_{12}-G_{11})\leq 0$ ***and*** $(G_{22}-G_{21})\leq 0$, *then* $\rho_1^*=\rho_2^*=1$.
[H2] If $(G_{12}-G_{11})\leq 0$ ***and*** $(G_{22}-G_{21})>0$, *then* $\rho_1^*=1;\rho_2^*=\min\{1,\widetilde{\rho_2}\}$.
[H3] If $(G_{12}-G_{11})>0$ ***and*** $(G_{22}-G_{21})\leq 0$, *then* $\rho_1^*=\min\{1,\widetilde{\rho_1}\};\rho_2^*=1$.
[H4] If $(G_{12}-G_{11})>0$ ***and*** $(G_{22}-G_{21})>0$, *then*
i) If $G_{22}G_{11}-G_{12}G_{21}\geq 0$*:* $\rho_1^*=\min\{1,\overline{\rho_1}\};\rho_2^*=\min\{1,\max\{0,\widetilde{\rho_2}\}\}$;
ii) If $G_{22}G_{11}-G_{12}G_{21}<0$*:* $\rho_1^*=\min\{1,\max\{0,\widetilde{\rho_1}\}\};\rho_2^*=\min\{1,\overline{\rho_2}\}$.

The expressions of the optimal reflection coefficients above are independent from the power allocation policy, and given that the larger the reflection coefficients are, the smaller the minimum power required to fulfill each QoS constraint in $(C2)$ is. Thus, choosing $\boldsymbol{\rho}^*=(\rho_1^*,\rho_2^*)$ as in Theorem 3 does not incur an optimality loss. The detailed proof is provided in Appendix C.

Optimal power allocation

For $\boldsymbol{\rho}^*$ in Theorem 3, we have the channel order $H_{1|1,1}(\boldsymbol{\rho}^*)\geq H_{2|1,1}(\boldsymbol{\rho}^*)$, and the optimization problem (**EE3**) reduces to

$$(\mathbf{EE4})\quad \max_{\mathbf{p}}\ \sum_{k=1}^{2}\frac{1}{2}\log_2\left(\frac{1+H_{k|1,1}(\boldsymbol{\rho}^*)\theta_k(\mathbf{p})}{1+H_{k|1,1}(\boldsymbol{\rho}^*)\theta_{k-1}(\mathbf{p})}\right)-\alpha(\theta_2(\mathbf{p})+P_{\mathrm{c}})$$

$$\text{s.t.}\quad (C1)\quad \theta_2(\mathbf{p})\leq P_{\max},$$
$$(C2a)\quad \theta_k(\mathbf{p})\geq\ A_k\theta_{k-1}(\mathbf{p})+\frac{(A_k-1)}{H_{k|1,1}(\boldsymbol{\rho}^*)},\quad \forall k\in\{1,2\},$$

which has already been solved in the previous Chapter for an arbitrary number of users. The optimal power allocation policy is obtained similar to (4.11) where the normalized channel gain $H_{k|1}(\rho^*)$ is replaced by the normalized channel gain $H_{k|1,1}(\boldsymbol{\rho}^*)$ obtained from the two backscattered links.

4.3.2.2 Multi-user multi-backscatter device case

In the case of $K>2$ users and two ambient backscatter devices, since the successful SIC constraint $(C3)$ becomes $H_{(k-1)|1,1}(\boldsymbol{\rho})\geq H_{k|1,1}(\boldsymbol{\rho}),\forall k\in\{1,\ldots,K\}$, the optimization problem (**EE3**) becomes hard to solve w.r.t the reflection coefficients pair (ρ_1,ρ_2).

In this case, according to Theorem 3, six cases need to be discussed for each pair $H_{(k-1)|1,1}(\boldsymbol{\rho})\geq H_{k|1,1}(\boldsymbol{\rho})$. Since the obtained ρ_1^* and ρ_2^* are coupled, one has to find the feasibility region defined by the set of all $(K-1)$ successful SIC constraints, which is

obtained through a nested six cases loop. Thus, generalizing our solution to the multi-user case is not trivial.

In the case of multi-backscatter devices, the graphical method by which we have obtained Pareto boundary of the feasible reflection coefficients is very limited, since no physical image of the feasible set is possible beyond two helping devices. The constraint $(C3)$ becomes a multi-variable inequality, and, hence it is necessary to exploit a more general (algorithmic) method to solve the problem. Moreover, the number of cases discussed in Theorem 3 will grow exponentially with the number of backscatter devices, which further complicates the extension of our closed-form solution.

4.3.3 Numerical results

In this section, we evaluate the performance of our energy-efficient solution for NOMA and OMA with and without backscattering. Since the coverage area of ambient backscatter communication systems is relatively small, we assume that communication links have a strong line-of-sight and fading-free pathloss channels of the type $h = d^{-\eta}$ [91,97,98], where d is distance between different nodes and η is the path loss exponent. All the results are averaged over 10^3 independent channel realizations satisfying the feasibility condition. The users are randomly located within a cell of radius 15 m. The maximum distance between the backscatter devices and the base station is 3 m. The pathloss exponent is $\eta = 2.5$. The system parameters are $P_{max} = 60$ dBm, $P_{\mathrm{c}} = 30$ dBm, $\sigma_k^2 = \sigma^2 = -20$ dBm and $R_{\min,k} = R_{\min}, k \in \{1, 2\}$.

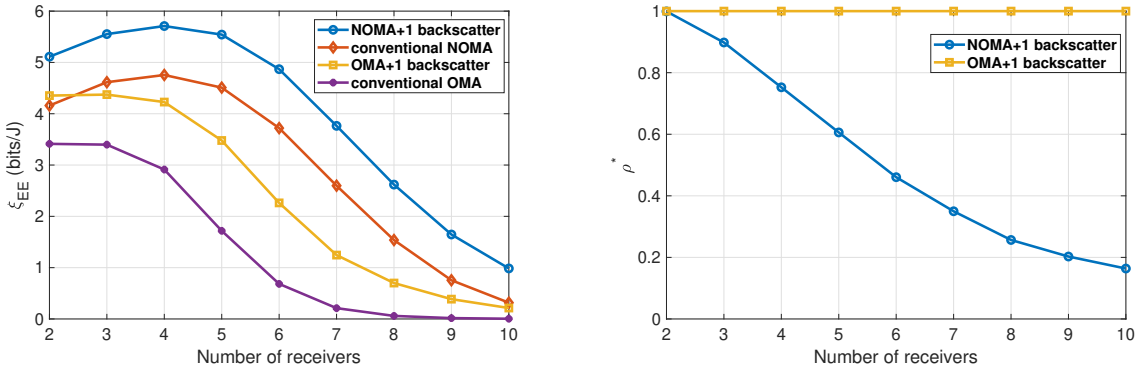

(a) Energy efficiency as a function of the number of users K.

(b) Optimal reflection coefficient ρ^* as a function of the number of users K.

Figure 4.3: Energy efficiency and optimal reflection coefficient as a function of the number of receivers. Backscattering always improves the energy efficiency of both NOMA and OMA irrespective from the number of users K. When K grows large the backscattering advantage decreases.

Figure 4.3(a) plots the energy efficiency of NOMA and OMA with and without the help of an ambient backscatter device as a function of the number of users K for

$R_{\min} = 1$ bit/s. First, NOMA aided by an ambient backscatter device always outperforms OMA (with or without backscattering) and conventional NOMA irrespective from the number of receivers K. Moreover, we see that for a large number of receivers, NOMA with backscattering outperforms the other schemes in terms of energy efficiency. We can also notice that backscattering does not decrease the energy efficiency under NOMA or OMA.

Furthermore, we see that when the number of receivers increases, the energy efficiency of NOMA with backscattering decreases. The intuition behind this follows from the expression of the optimal reflection coefficient in (4.9), which depends on the smallest difference between the channel gains: the larger the number of users K, the smaller the channel gap. When K increases, ρ^* eventually reaches zero, cancelling the backscatter effect and leading to a conventional NOMA.

This can also be observed in Figure 4.3(b), in which the optimal reflection coefficient ρ^* is illustrated as a function of the number of users K, under both NOMA and OMA. Note that, under OMA, all users' rates are increasing functions of ρ, leading to a constant optimal value: $\rho^* = 1$. This means that the backscatter device reflects the entire ambient incident signal. With NOMA, only a fraction of the ambient incident signal is reflected ($\rho^* < 1$), which decreases with the number of users K. Nevertheless, this enables energy harvesting at the backscatter device, which can then be used for its circuit operation.

For the case of multiple ambient backscatter devices, we compare our proposed solution with three benchmarks: OMA with two backscatter devices, NOMA with one backscatter device as well as conventional NOMA (without backscattering). More importantly, we also analyze here the more general case of three and four backscatter-aided NOMA schemes, whose solutions are obtained via exhaustive search, and investigate the energy efficiency as a function of the number of cooperative backscatter devices.

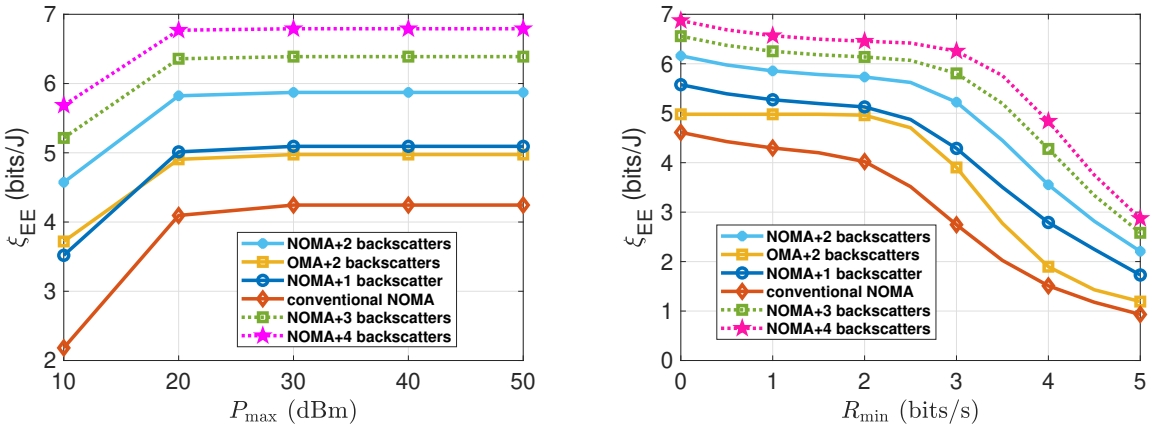

(a) Energy efficiency as a function of $P_{\max}$.

(b) Energy efficiency as a function of $R_{\min}$.

Figure 4.4: Energy efficiency as a function of $P_{\max}$ and $R_{\min}$. Two backscatters-aided NOMA always outperforms other benchmark schemes and the energy efficiency increases with the number of backscatter devices.

Figure 4.4(a) depicts the energy efficiency (ξ_{EE}) as a function of $P_{\max}$. We see that our proposed scheme outperforms all other benchmarks irrespective from $P_{\max}$. Furthermore, ξ_{EE} increases with the number of cooperative backscatter devices and with $P_{\max}$ until it reaches a flat level, beyond which increasing the power has no longer effect on the $P_{\max}$.

Figure 4.4(b) depicts ξ_{EE} as a function of $R_{\min}$. We see that NOMA with two backscatter devices outperforms NOMA with a single backscatter device, which outperforms OMA with two backscatter devices. For larger minimum QoS levels, the energy efficiency decreases since more power is consumed to meet the users' minimum rate constraints. At last, we see that ξ_{EE} increases with the number of cooperative backscatter devices.

In the following Section, we will tackle the general case where the ambient backscatter device transmits information and is not always in a fixed backscattering state.

4.4 Information-theoretic achievable rate regions

Most of the existing works [88–90,92–95,99] consider either the simple backscattering state, or that the backscattered signal composed of the product $B\ X$ follows a Gaussian distribution where Shannon's information capacity expression $C(\cdot)$ is used to approximate the maximum achievable rate, without investigating the achievable rates when taking into account the ambient backscatter device's message B. These assumptions may not be realistic in practice, since the backscatter device usually has its own information to transmit besides harvesting energy for its circuit operation. In the following, we take into account explicitly the message of the backscatter device, which clearly sets our work apart from the existing literature.

Because of the form of the backscattered signal $B\ X$ in the received signal Y_k expressed in (4.1), where both X and B are random variables, the Shannon's capacity function $C(\cdot)$ cannot be used to derive the achievable rates expressions. Hence, we start by deriving the information-theoretic achievable rate region, before delving into resource optimization problems of the ambient backscatter NOMA system.

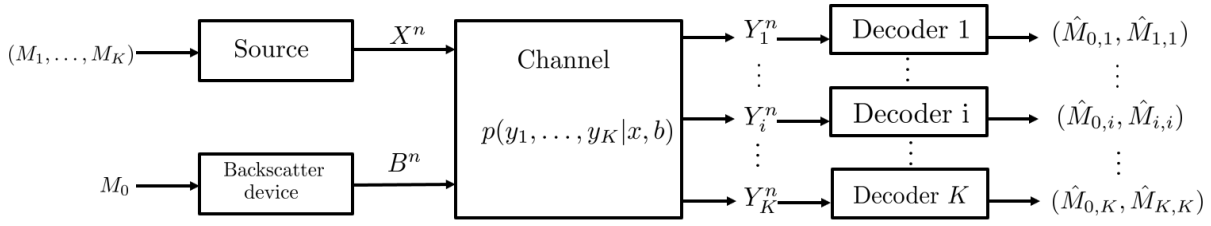

Figure 4.5: Source-backscatter device to K-receivers discrete channel model

4.4.1 Discrete memoryless channel

We start with the discrete memoryless channel case of the joint multiple access and broadcast communication system depicted in Figure 4.5, and then derive the achievable rate region for the Gaussian channel described in our predefined model.

Both the source and the ambient backscatter device wish to communicate independent messages reliably to K receivers. The backscatter device encodes its common message M_0 into a codeword B^n and transmits it over the shared channel. The source uses a superposition coding technique to encode each private message M_i destined to receiver i in a layered manner and broadcasts the codeword X^n consisting of all merged encoded messages $M_1, \ldots, M_K$. Upon receiving the sequence Y_i^n, receiver $i \in \{1, \ldots, K\}$ computes an estimate $\hat{M}_{0\to i}$ of the message M_0 and uses SIC to obtain an estimate $\hat{M}_{i\to i}$ of the message M_i, by first computing the estimates $\hat{M}_{j\to i}$ of the messages M_j, for all $j \in \{K, K-1, \ldots i+1\}$ following this precise successive order.

Using elements from information theory [39, 40], we first describe the codebook generation for both messages X, using the superposition coding technique, and B. We introduce the auxiliary random variables $U_j,\ j \in \{2, \ldots, K\}$ serving as "cloud centers" representing the messages M_j that can be distinguished by receivers $i \leq j$. By defining the error events of unsuccessful decoding of X and B and by using information-theoretic typicality arguments, we derive the achievable rates for which the receivers can reliably decode X and B (i.e., when the average probability of error $\mathbb{P}(\varepsilon_i)$ of each receiver i tends to 0). Complete details can be found in Appendix D. The resulting achievable rate region of the ambient backscatter NOMA system is given in the following Theorem.

Theorem 4. *The achievable rate region of the discrete memoryless source-backscatter device to K receivers channel is given by the set of rate tuples $(R_0, R_1, \ldots, R_K)$ defined below:*

$$R_0 \leq \min_{1\leq i\leq K} \mathbb{I}(B; Y_i|U_K), \tag{4.17}$$

$$R_K \leq \min_{1\leq i\leq K} \mathbb{I}(U_K; Y_i|B), \tag{4.18}$$

$$R_0 + R_K \leq \min_{1\leq i\leq K} \mathbb{I}(U_K, B; Y_i), \tag{4.19}$$

$$R_j \leq \min_{i\leq j} \mathbb{I}(U_j; Y_i|B, U_K, \ldots, U_{j+1}),\ \forall\ 1 \leq j \leq K-1, \tag{4.20}$$

where U_i are auxiliary randoms variables accounting for X_i for all $2 \leq i \leq K$.

In practice, the data rate of the backscatter device is significantly lower than that of the source because of its design simplicity and power limitations as argued in [17, 18, 95, 96, 100–102]. Assuming that $R_0 << R_K$ in particular, the expressions in (4.18) and (4.19) in Theorem 4 can be simplified to

$$R_K \leq \min\left(\min_{1\leq i\leq K} \mathbb{I}(U_K; Y_i|B), \min_{1\leq i\leq K} \mathbb{I}(U_K, B; Y_i)\right) \overset{(a)}{=} \min_{1\leq i\leq K} \mathbb{I}(U_K; Y_i|B), \tag{4.21}$$

where (a) follows from the chain rule and the positivity of the mutual information. This yields the achievable rate region given in the following Lemma.

Lemma 1. *Assuming that the ambient backscatter device has a very low data rate compared to that of the source, $R_0 << R_K$, the achievable rate region in Theorem 4 simplifies to*

$$R_0 \leq \min_{1\leq i\leq K} \mathbb{I}(B;Y_i|U_K), \tag{4.22}$$

$$R_K \leq \min_{1\leq i\leq K} \mathbb{I}(U_K;Y_i|B), \tag{4.23}$$

$$R_j \leq \min_{i\leq j} \mathbb{I}(U_j;Y_i|B,U_K,\ldots,U_{j+1}),\ \forall\ 1\leq j\leq K-1. \tag{4.24}$$

4.4.2 Gaussian channel

Having obtained the achievable rate region in the discrete memoryless case given in Lemma 1, we now derive the achievable rate region for the AWGN model described in Section 4.2 and, more specifically, for the received signal Y_k observed at each receiver k.

We assume that the message of the ambient backscatter device B follows the Bernoulli distribution $B \sim \text{Bern}(q)$, where $q = Pr[B=1]$ is the probability of the backscattering state and $(1-q) = Pr[B=0]$ is the probability of the transparent state. By assuming that $V \sim \mathcal{N}(0,p_1)$ and $U_i \sim \mathcal{N}(0,p_i), \forall i \in \{2,\ldots,K\}$, which stands in our case for X_1 and $X_i, \forall i \in \{2,\ldots,K\}$, respectively, that are most commonly used in the literature when describing the codeword $X = \sum_{k=i}^{K} X_i$ sent using NOMA, we can compute the achievable rate region for the Gaussian case which is given in the following Theorem.

Theorem 5. *The achievable rate region of the AWGN source-backscatter device to K-receiver channel is the set of rate tuples $(R_0,R_1,\ldots,R_K)$, such that*

$$R_0 \leq \min_{1\leq i\leq K} \mathbb{H}(Y_i|U_K) - \frac{q}{2}\log_2\left(2\pi e\sigma_i^2\left(H_{i|1}(\rho)\sum_{k=1}^{K-1}p_k+1\right)\right) - \frac{1-q}{2}\log_2\left(2\pi e\sigma_i^2\left(H_{i|0}\sum_{k=1}^{K-1}p_k+1\right)\right) \tag{4.25}$$

$$R_k \leq qC\left(\min_{i\leq k}(\gamma_{k\to i|1})\right) + (1-q)C\left(\min_{i\leq k}(\gamma_{k\to i|0})\right), \quad \forall\ 1\leq k\leq K, \tag{4.26}$$

where $H_{i|0} = (h_i)^2/\sigma_i^2$, $H_{i|1}(\rho) = (h_i+\sqrt{\rho}gg_i)^2/\sigma_i^2$ represent the normalized channel gains when the backscatter device is in the transparent state ($B=0$) and in the backscattering state ($B=1$), respectively, and $\gamma_{k\to i|0} = \frac{H_{i|0}p_k}{1+H_{i|0}(p_1+\ldots+p_{k-1})}$ and $\gamma_{k\to i|1} = \frac{H_{i|1}(\rho)p_k}{1+H_{i|1}(\rho)(p_1+\ldots+p_{k-1})}$ are the corresponding SINR when receiver i decodes the message intended for receiver k.

The proof follows information-theoretic techniques where the continuous random variables $V \sim \mathcal{N}(0,p_1)$ and $U_k \sim \mathcal{N}(0,p_k)$ are quantized to extend the expressions of mutual information in discrete memoryless channel given in Lemma 1 to the Gaussian

channel [39, 40]. The Gaussian distribution is chosen such that it maximizes the mutual information expressions in (4.23) and (4.24) [2] and leads to Shannon capacity given in Theorem 5. The complete details are provided in Appendix D.

At last, note that the conditional entropy $\mathbb{H}(Y_i|U_K)$ in Theorem 5 is very difficult to compute in closed-form because of the non-trivial sum of two dependent variables X and B X in the received signal Y_k, where $B \sim \text{Bern(p)}$ and $X \sim \mathcal{N}(0, \sum_{i=1}^{K} p_i)$, and is left open for future investigation.

Having derived the achievable rate region for the system model described in Section 4.2, we now investigate the resource allocation problem and, in particular, the system's energy-efficiency maximization.

Since by assumption we have $R_0 << R_K$ and knowing that the ambient backscatter device is a low-power device which performs energy harvesting for its own circuit operations, we only focus on maximizing the energy efficiency of the downlink NOMA system (enhanced by ambient backscattering) alone.

4.5 Energy-efficiency maximization

In this Section, we maximize the energy efficiency defined as the trade-off between the sum of achievable rates of the users and the power consumption given in (**EE0**). The achievable rate of receiver k follows from Theorem 5 and is expressed as

$$R_k(\rho, \mathbf{p}) = qC\left(\min_{i\leq k}(\gamma_{k\to i|1})\right) + (1-q)C\left(\min_{i\leq k}(\gamma_{k\to i|0})\right), \quad \forall\ 1 \leq k \leq K, \tag{4.27}$$

which can be seen as an expected value of the achievable rate of receiver k over the message B, i.e., the ergodic achievable rate over the fading channel $h_k + \sqrt{\rho} g g_k B,\ B \in \{0, 1\}$.

We notice that when either $q = 0$ or $q = 1$, i.e., either pure transparent or pure backscattering state, the optimization problem (**EE0**) is equivalent to the optimization problem solved in the previous Chapter and in (**EE1**) respectively.

The feasible set $\mathcal{P}$ accounts for all the constraints: the maximum power budget of the source, the receivers targeted QoS expressed as $R_k(\rho, \mathbf{p}) \geq R_{\min,k}$, the successful SIC process expressed as $qC\left(\gamma_{k\to i|1}\right) + (1-q)C\left(\gamma_{k\to i|0}\right) \geq qC\left(\gamma_{k\to k|1}\right) + (1-q)C\left(\gamma_{k\to k|0}\right)$ to avoid having an error when receiver i, $\forall i \leq k-1$, performs SIC and decodes the message destined to receiver k and the range of the reflection coefficient, respectively.

Furthermore, since SIC decoding is a key component for NOMA [7, 9, 12, 35, 103], it has to be performed successfully and independently from the backscatter device's state in order to avoid error propagation that may affect the performance of the system (e.g.,

[2] Note that the Gaussian assumption is optimal for the source assuming $R_0 \ll R_K$, but may not be optimal in general.

the targeted quality of service). To ensure successful SIC, we impose a minimum rate constraint in terms of the minimum SINR level for each state of the backscatter device: $\gamma_{k\to i|1} \geq \gamma_{k\to k|1}$ and $\gamma_{k\to i|0} \geq \gamma_{k\to k|0}$, $\forall k \in \{1,\ldots,K\}$ and $i \leq k$. All the above leads to the feasible set

$$\mathcal{P} \triangleq \Bigg\{ (\rho,\mathbf{p}) \in [0,1]\times\mathbb{R}_+^K \;\Bigg|\; 0\leq\rho\leq 1, \sum_{j=1}^{K} p_j \leq P_{\max}, R_k(\rho,\mathbf{p}) \geq R_{\min,k}, \\ \gamma_{k\to i|0} \geq \gamma_{k\to k|0}, \gamma_{k\to i|1} \geq \gamma_{k\to k|1},\ \forall 1\leq k\leq K, \forall i\leq k \Big\}. \tag{4.28}$$

The successful SIC decoding constraint in the transparent state, given as $\gamma_{k\to i|0} \geq \gamma_{k\to k|0}$, is equivalent to $\frac{p_k}{\frac{1}{H_{i|0}}+(p_1+\ldots+p_{k-1})} \geq \frac{p_k}{\frac{1}{H_{k|0}}+(p_1+\ldots+p_{k-1})}$, which is readily satisfied due to the assumed channels ordering in (4.2) (i.e., $H_{i|0} \geq H_{k|0}$, $\forall k \geq 2, i \leq k-1$), and can hence be removed altogether. Second, since the successful SIC constraint in the transparent state $\gamma_{k\to i|0} \geq \gamma_{k\to k|0}$ is readily satisfied, and by ensuring that $\gamma_{k\to i|1} \geq \gamma_{k\to k|1}$ is met in the optimization problem (**EE0**), the achievable rate of receiver k in (4.27) reduces to

$$R_k(\rho,\mathbf{p}) = qC(\gamma_{k\to k|1}) + (1-q)C(\gamma_{k\to k|0}), \quad \forall\ 1\leq k\leq K. \tag{4.29}$$

By introducing the variable $\theta_k(\mathbf{p}) = \sum_{i=1}^{k} p_i$, $\forall k \geq 1$ with $\theta_0(\mathbf{p}) = 0$, the optimization problem is equivalent to

$$(\mathbf{EE5}) \quad \max_{\rho,\mathbf{p}} \sum_{k=1}^{K} R_k(\rho,\mathbf{p}) - \alpha(\theta_K(\mathbf{p}) + P_{\mathrm{c}})$$

$$\begin{aligned} \text{s.t. } & (C1) \quad \theta_K(\mathbf{p}) \leq P_{\max}, \\ & (C2) \quad R_k(\rho,\mathbf{p}) \geq R_{\min,k}, \quad \forall 1\leq k\leq K, \\ & (C3) \quad \gamma_{k\to i|1}(\rho,\mathbf{p}) \geq \gamma_{k\to k|1}(\rho,\mathbf{p}), \quad \forall 2\leq k\leq K, \forall i\leq k-1, \\ & (C4) \quad 0\leq\rho\leq 1. \end{aligned}$$

A major issue in the above optimization problem is the minimum rate constraint $(C2)$ which makes (**EE5**) non convex. Indeed, the rate $R_k(\rho,\mathbf{p})$ is not concave w.r.t $\mathbf{p}$ since $R_k(\rho,\mathbf{p})$ is expressed as a weighted sum of the capacity in the backscattering state $C(\gamma_{k\to k|1})$ and the capacity in the transparent state $C(\gamma_{k\to k|0})$. In what follows we propose a modification that will simplify the problem.

4.5.1 Constraints modification

We introduce a modification to the constraint $(C2)$ such that, instead of having $R_k(\rho,\mathbf{p}) \geq R_{\min,k}$, we require each of the averaged terms in (4.29) to be bounded:

$C(\gamma_{k\to k|0}) \geq R_{\min,k}$ and $C(\gamma_{k\to k|1}) \geq R_{\min,k}$. This means that the minimum rate constraint needs to be satisfied in the transparent state and in the backscattering state individually. This modification restricts the original feasible set leading to a potential optimality loss. Our intuition is that any incurred optimality loss will be limited in practice, given that the rate of the backscatter device is much lower than that of the source ($R_0 << R_K$). After some mathematical manipulations, we replace the constraint $(C2)$ by

$$\theta_k(\mathbf{p}) \geq \; A_k\theta_{k-1}(\mathbf{p}) + \frac{A_k - 1}{H_{k|0}}, \quad \forall\; 2 \leq k \leq K, \forall i \leq k-1, \tag{4.30}$$

$$\theta_k(\mathbf{p}) \geq \; A_k\theta_{k-1}(\mathbf{p}) + \frac{A_k - 1}{H_{k|1}(\rho)}, \quad \forall\; 2 \leq k \leq K, \forall i \leq k-1, \tag{4.31}$$

where $A_k = 2^{2R_{min,k}}$. The main advantage of this modification is that it leads to the following simpler non-convex optimization problem, which we show that can be solved analytically.

$$(\mathbf{EE6}) \quad \max_{\rho,\mathbf{p}} \; \sum_{k=1}^{K} R_k(\rho,\mathbf{p}) - \alpha(\theta_K(\mathbf{p}) + P_{\mathrm{c}})$$

$$\begin{aligned}
\text{s.t.} \quad & (C1) \quad \theta_K(\mathbf{p}) \leq P_{\max}, \\
& (C2a) \quad \theta_k(\mathbf{p}) \geq \; A_k\theta_{k-1}(\mathbf{p}) + \frac{A_k - 1}{H_{k|0}}, \quad \forall 2 \leq k \leq K, \forall i \leq k-1, \\
& (C2b) \quad \theta_k(\mathbf{p}) \geq \; A_k\theta_{k-1}(\mathbf{p}) + \frac{A_k - 1}{H_{k|1}(\rho)}, \quad \forall 2 \leq k \leq K, \forall i \leq k-1, \\
& (C3) \quad \frac{p_k}{\frac{1}{H_{i|1}(\rho)} + \theta_{k-1}(\mathbf{p})} \geq \frac{p_k}{\frac{1}{H_{k|1}(\rho)} + \theta_{k-1}(\mathbf{p})}, \quad \forall 2 \leq k \leq K, \forall i \leq k-1, \\
& (C4) \quad 0 \leq \rho \leq 1,
\end{aligned}$$

where $(C2a)$ and $(C2b)$ are the modified minimum rate constraints for the transparent and backscattering states, respectively, and all other constraints remain unchanged. Note that since $H_{k|1}(\rho) \geq H_{k|0}$, the constraint $(C2b)$ will be omitted since satisfying $(C2a)$ is sufficient.

Even though we restricted $(C2)$ to simplify the problem (**EE5**), the resulting optimization problem (**EE6**) remains non convex due to the joint optimization of the reflection coefficient ρ and the vector of allocated powers $\mathbf{p}$. Nevertheless, following a similar approach to Section 4.3 (in which the backscatter device was assumed always in the backscattering state and, hence, a simpler energy-efficiency problem was solved), (**EE6**) can be solved by decoupling it into two sub-problems without loss of optimality.

4.5.2 Problem solution

Following a similar approach to Section 4.3, we first optimize ρ for an arbitrary power allocation $\mathbf{p}$, then optimize $\mathbf{p}$ with the fixed optimal reflection coefficient ρ^*.

Optimal reflection coefficient

We consider a fixed arbitrary power allocation $\mathbf{p} \in \mathcal{P}$ and solve the optimization problem (**EE6**) w.r.t the reflection coefficient ρ. It turns out that the optimal reflection coefficient can be expressed as in (4.9) where the proof follows similarly as in Appendix B.

Given the optimal reflection coefficient ρ^* in (4.9), the constraints $(C3)$ and $(C4)$ are readily satisfied. Also, as proven in Appendix B, it leads to $H_{1|1}(\rho^*) \geq \ldots \geq H_{K|1}(\rho^*)$, which will be very useful when deriving the optimal power allocation vector $\mathbf{p}^*$.

Following the same argument as in Section 4.3, decoupling the optimization problem by first optimizing over the reflection coefficient and then over the power allocation policy does not induce any optimality loss.

Optimal power allocation

We can thus fix $\rho = \rho^*$ and solve the remaining problem below in terms of the power allocation policy $\mathbf{p}$ with no optimality loss.

$$(\mathbf{EE7}) \quad \max_{\mathbf{p}} \ \eta_{EE}(\mathbf{p}) \triangleq \sum_{k=1}^{K} R_k(\rho^*, \mathbf{p}) - \alpha(\theta_K(\mathbf{p}) + P_{\mathrm{c}})$$

$$\text{s.t.} \quad (C1) \quad \theta_K(\mathbf{p}) \leq P_{\max},$$
$$(C2a) \quad \theta_k(\mathbf{p}) \geq A_k \theta_{k-1}(\mathbf{p}) + \frac{A_k - 1}{H_{k|0}}, \quad \forall\ 1 \leq k \leq K.$$

The remaining problem above is a convex optimization one since the objective function is concave w.r.t $\mathbf{p}$, as shown in Appendix E, and the constraints $(C1)$ and $(C2a)$ are affine.

Feasibility condition: Because of the minimum rate requirements of each receiver, the convex optimization problem (**EE7**) may not be feasible. Indeed, the power budget at the source $P_{\max}$ has to be greater or equal to the minimum power needed for satisfying the receiver's minimum rate constraints in $(C2a)$, expressed as $P_{\min} \triangleq \sum_{i=1}^{K} \frac{(A_i - 1)}{H_{i|0}} \prod_{j=i+1}^{K} A_j \leq P_{\max}$, which follows similarly as in Chapter 3 on optimal power allocation policies for K-receivers downlink NOMA without the ambient backscatter device.

If the aforementioned feasibility condition is met, and given that (**EE7**) is convex, we can apply the Lagrange multipliers method to obtain the optimal expressions of $p_k^*,\ \forall k \geq 2$ as functions of p_1 by solving the Karush-Kuhn-Tucker (KKT) optimality conditions, which are necessary and sufficient [72]. Hence, the multi-variable problem (**EE7**) is turned into a single variable optimization problem w.r.t p_1 which is proved to be convex, leading to the main result below.

Theorem 6. *If the optimization problem* (**EE7**) *is feasible, the optimal power allocation* $\mathbf{p}$ *is given analytically as follows*

$$\begin{aligned} p_k^* &= (A_k - 1)\left(\frac{1}{H_{k|0}} + p_1^* \prod_{i=2}^{k-1} A_i + \sum_{i=2}^{k-1} \frac{(A_i - 1)}{H_{i|0}} \prod_{j=i+1}^{k-1} A_j\right), \quad \forall\ k \geq 2, \\ p_1^* &= \max\left(\min\left(\overline{p_1}; u\right); \ell\right), \end{aligned} \tag{4.32}$$

where $\ell = \frac{(A_1-1)}{H_{1|0}}$, $u = \left(P_{\max} - P_{\min} + \ell \prod_{j=2}^{K} A_j\right) \Big/ \prod_{i=2}^{K} A_i$ *and* $\overline{p_1}$ *represents the unique critical point of the single variable function* $f_1(p_1) \triangleq \eta_{EE}(p_1, p_2^*, \ldots, p_K^*)$ *w.r.t* p_1.

Unlike Chapter 3 and the fixed backscattering state investigated in Section 4.3, the resulting achievable rate expressions are more complex and lead to a more technically involved solution. The proof is detailed in Appendix E.

Energy efficiency as the ratio sum rate vs. overall consumed power:

Similar to Section 4.3, the energy-efficiency ratio ξ_{EE} can be maximized by exploiting our optimal solution $(\rho^*, \mathbf{p}^*)$ to (**EE0**) using Dinkelbach's method expressed in Algorithm 3, which reduces to finding the solution to the following equation w.r.t α

$$F(\alpha) \triangleq \sum_{k=1}^{K} R_k(\rho^*, \mathbf{p}^*) - \alpha \left(\sum_{k=1}^{K} p_k^* + P_c\right) = 0, \tag{4.33}$$

and where $\mathbf{p}^*$ is given in Theorem 6.

4.5.3 Numerical results

In this section, we present and discuss numerical results to evaluate the performance of our energy-efficient solution. The positions of the users are uniformly drawn in a disk of radius 20 m around the source. Similarly, the backscatter device position is drawn in a disk of radius 4 m surrounding the source. We consider the same system parameters as in Section 4.3 unless stated otherwise. The simulation results are averaged over 10^3 random draws of the nodes positions satisfying the feasibility condition in (3.9).

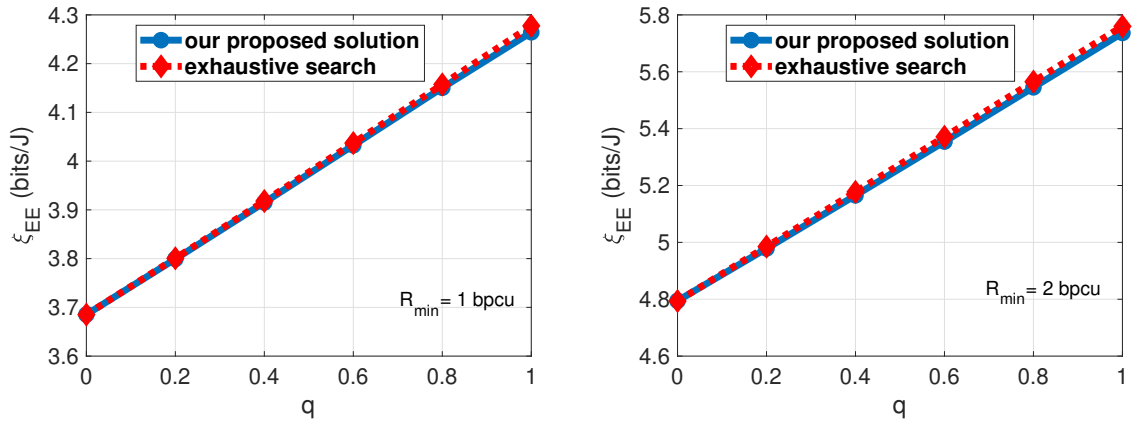

Figure 4.6: Energy efficiency (ξ_{EE}) sub-optimality comparison for different values of q and $R_{\min}$.

Impact of our modified constraints: In Figure 4.6, we compare the energy efficiency of the optimal solution to the original problem (**EE0**), obtained via exhaustive search, and our analytical solution to the modified problem (**EE6**) as a function of $q \in [0, 1]$ and for $R_{\min} \in \{1, 2\}$ bpcu. We see that the sub-optimality gap becomes smaller when q decreases. Indeed, the case $q = 0$ corresponds to conventional NOMA, without backscattering, for which the two solutions are identical (as the optimization problem (**EE0**) becomes equivalent to the one investigated in Chapter 3). The sub-optimality gap increases with $R_{\min}$, but remains negligible, which validates our intuition and highlights the interest of our analytical solution.

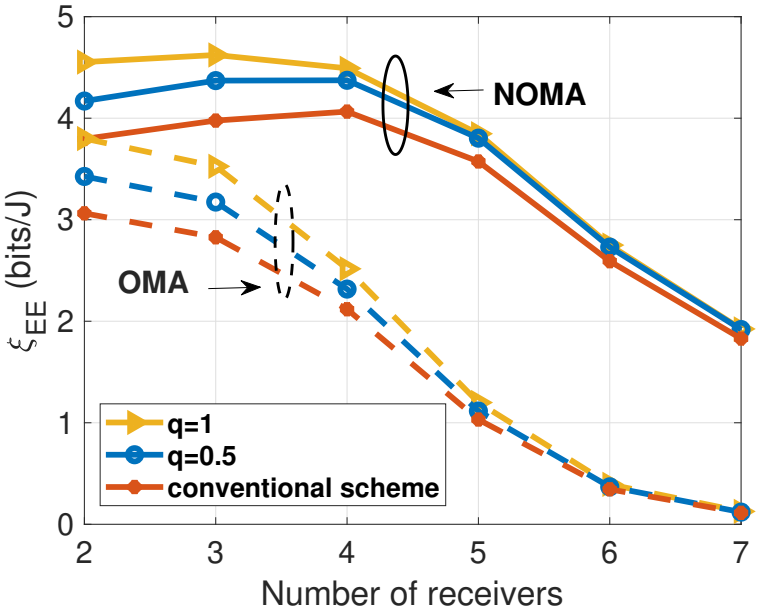

Figure 4.7: Energy efficiency (ξ_{EE}) as a function of the number of receivers K for different values of q.

NOMA vs. OMA evaluation: In Figure 4.7, we plot the energy efficiency ξ_{EE} of ambient backscatter-aided NOMA and OMA (as benchmark), as a function of the number of receivers for different values of $q \in \{0, 0.5, 1\}$ with $P_{\max} = 60$ dBm and $R_{\min} = 1$ bpcu. First, we see that NOMA with backscattering always outperforms its OMA counterpart irrespective from q. Moreover, we observe that the energy efficiency decreases with the number of receivers. Similar to our previous discussion in Section 4.3, the intuition comes from the expression of the optimal reflection coefficient that depends on the smallest difference between the channel gains. The larger the number of receivers K, the smaller the channel gap. When K increases, ρ^* tends to zero, vanishing the backscattering effect and leading to the conventional scheme without backscattering ($q = 0$).

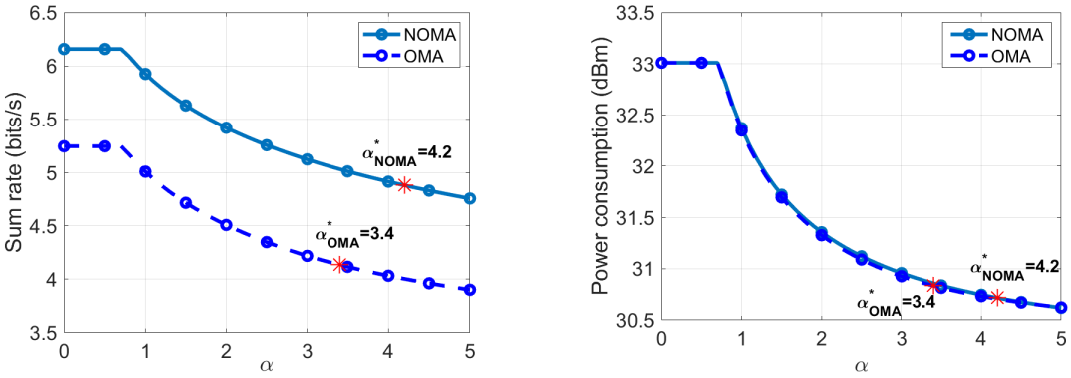

(a) Achievable sum rate. (b) Overall power consumption.

Figure 4.8: Achievable sum rate and overall power consumption as functions of the trade-off parameter α for an ambient backscatter-aided NOMA system with $K = 2$, $q = 0.5$ and $R_{min} = 1$ bpcu.

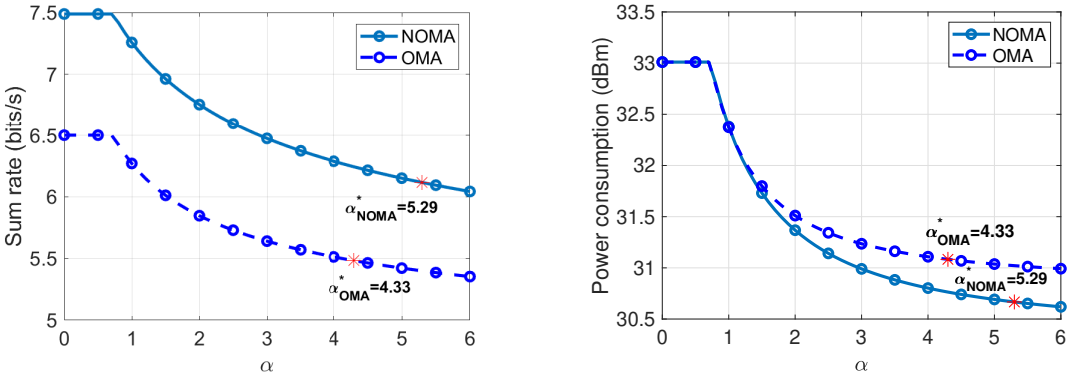

(a) Achievable sum rate. (b) Overall power consumption.

Figure 4.9: Achievable sum rate and overall power consumption as functions of the trade-off parameter α for an ambient backscatter-aided NOMA system with $K = 2$, $q = 0.5$ and $R_{min} = 2$ bpcu.

In Figure 4.8 and Figure 4.9 we plot the achievable sum rate and overall power consumption as functions of the trade-off parameter α where $q = 0.5$ and $R_{\min} = 1$ bpcu

and $R_{\min} = 2$ bpcu respectively. We see that NOMA achieves higher sum rate while consuming, at most, as much power as OMA, irrespective from α. Moreover, both the sum rate and power consumption decrease as α grows larger. Indeed, for very small values of α, the sum rate and power consumption are constant where the maximum power is used to achieve the maximum sum rate. As α grows larger, both the sum rate and power consumption decrease since the power minimization is given more importance which decreases the sum rate. Nevertheless, NOMA still outperforms OMA both in terms of sum rate and power consumption where it consumes as much power as OMA for $R_{\min} = 1$ bpcu and less power than OMA for $R_{\min} = 2$ bpcu. These observations validates our general conclusions made in Section 3.5 which state that NOMA is more rate-efficient or more power-efficient than OMA when the emphasis in the objective function is on the sum rate or on reducing the power consumption respectively. We also highlight the two points α^*_{NOMA} and α^*_{OMA} referring to the respective solutions of $F(\alpha) = 0$ in (4.33) providing the achievable sum rate and overall power consumption that are optimal in the sense of the energy efficiency ratio ξ_{EE}.

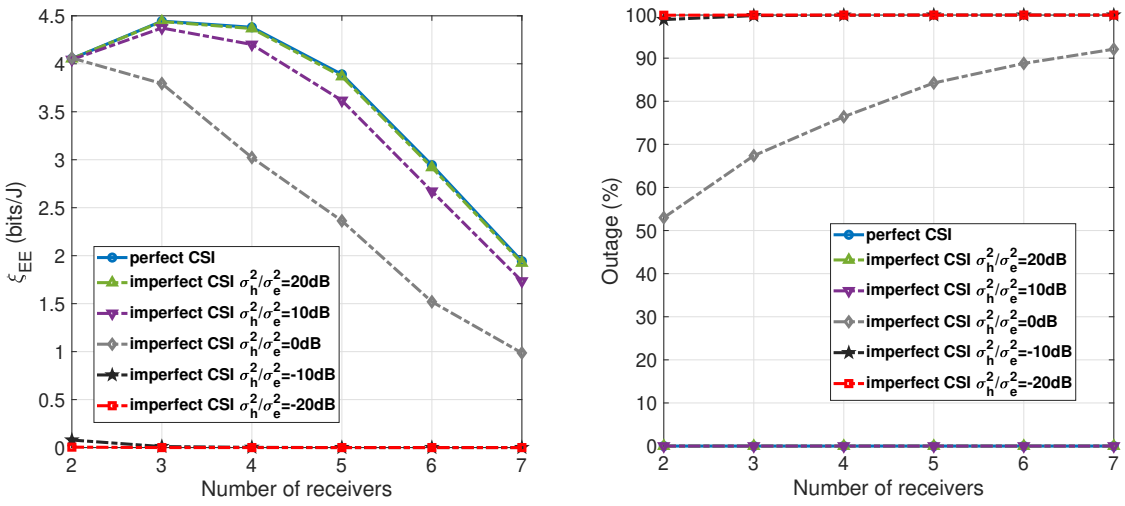

(a) Energy efficiency for different values of σ_e^2.

(b) Outage performance for different values of σ_e^2.

Figure 4.10: Impact of imperfect CSI on the energy efficiency (ξ_{EE}) and outage performance of NOMA as a function of the number of receivers K for different values of the error variance σ_e^2.

Impact of imperfect CSI: At last, we investigate the impact of imperfect CSI on our solution. We assume that only channel gain estimates $\hat{h}$ are available at the transmitter side such that $\hat{h} = h - e$, where $e \sim \mathcal{N}(0, \sigma_e^2)$ represents the estimation error of variance σ_e^2 for any channel link h. The power allocation policy is computed based on the estimated channel gains $\hat{h}$ and the system performance is obtained with the true channel gains h. Imperfect CSI may result in violating the user minimum rate constraints or the SIC constraints in (4.28), leading to an outage event. Hence, we plot both the energy efficiency

when the system is not in outage and the outage probability in Figure 4.10 for $q = 0.5$.

As expected, the performance is impacted by the quality of the channel estimation. For $\sigma_h^2/\sigma_e^2 \in \{-10, -20\}$ dB (poor estimation), the system is almost always in outage. For $\sigma_h^2/\sigma_e^2 = 20$ dB (excellent estimation) the imperfect CSI curves are superposed to the perfect CSI ones. When $\sigma_h^2/\sigma_e^2 = 10$ dB (good estimation), the outage is negligible and the energy efficiency is impacted but not critically so (the loss is below 11% for any K). When the error variance is as high as the channel variance ($\sigma_h^2/\sigma_e^2 = 0$ dB), the outage is very high: above 50% for $K = 2$ and reaches up to 90% for $K = 7$. Except for $K = 2$, the energy efficiency is also highly impacted in this case, the loss reaching up to 49% for $K = 7$ users. Hence, our solution relies on high quality CSI estimation. When this is unavailable, the impact of CSI errors has to be taken into account in the problem formulation and the solution design.

4.6 Summary

In this Chapter we investigated the energy-efficiency maximization problem of a downlink NOMA system in the presence of an ambient backscatter device which modulates its own binary information. We first investigated the special case of a fixed backscattering state, extended to multiple ambient backscattering devices, where the resource allocation policies were obtained in closed-form. We then derived the information-theoretic achievable rate region for the general case and obtained the optimal reflection coefficient and power allocation policy analytically. We also investigated the impact of imperfect CSIT and highlighted that when the channel estimation is sufficiently high, our solution is still relevant. In highly dynamic systems or whenever the channel estimation is too poor, other solutions have to be investigated based on robust optimization or adaptive machine learning techniques.

In the next Chapter, we will investigate a downlink NOMA system in the worst-case scenario where the knowledge on the channel state or distribution at the transmitter is not available.

Chapter 5

Resource allocation policies in downlink NOMA with no CSIT/CDIT

Contents

5.1 Introduction

In this Chapter, we investigate the performance of the system described in Chapter 3 with a two-user pairing strategy[1] and without assuming any knowledge on the channel

[1] Our analysis and results in this work carry over the more general case of multiple receivers that have been paired and assigned to orthogonal frequency bands. Pairing is a common operation in NOMA

state or distribution at the transmitter. As shown in previous Chapters, the power allocation is crucial in Non-Orthogonal Multiple Access (NOMA) and can be performed with known channel state information at the transmitter (CSIT).

The majority of works investigating NOMA [28, 84, 87, 105–108] rely on strong assumptions regarding the channel knowledge at the transmitter side. NOMA is shown to outperform OMA in terms of data rate or energy efficiency [82, 84, 87, 105, 106] when the CSIT is available, as well as in terms of outage probability [28, 107–111] when the channel distribution information at the transmitter (CDIT) is available.

Under perfect CSIT [82, 84, 87, 105, 106], the order under which the messages are decoded by SIC is based on the quality of the channels. When the transmitter does not have access to CSIT but to CDIT, NOMA can still improve both the achievable rate and the outage probability compared to OMA, by carefully allocating power to each of the served users and using a SIC ordering that is either based on the channel statistical characteristics [28, 107–109, 111] or on the CDIT and a 1-bit feedback mechanism related to the channel state known at the receiver end [110].

However, perfect CSIT is hard to obtain due to the large propagation delay, fast channel time variation, and imperfect channel estimation. Moreover, it may not be realistic because of the extensive overhead and computational cost and feedback, which is especially problematic in IoT networks composed of low-cost devices with low power and computational capabilities. For instance, in dense IoT networks, when taking into account the users' heterogeneity, mobility and connectivity patterns, the network may vary too quickly to reasonably assume perfect CSIT and may vary in a completely arbitrary way, even non-stationary, to assume CDIT.

Hence, we investigate a NOMA system with no CSIT and no CDIT. More precisely, we consider a time-varying downlink NOMA system, in which a transmitter serves two users over wireless channels with no access to CSIT or CDIT. Our main contribution lies in the design of a novel adaptive NOMA scheme that jointly allocates the overall power of the transmitter to the two users and decide which user performs SIC decoding to minimize the overall system outage probability and the outage-based energy efficiency. To circumvent the lack of channel knowledge at the transmitter, our novel scheme exploits reinforcement learning techniques, more precisely the so-called Multi-Armed Bandit (MAB) framework [78], that allows us to develop algorithms that have relatively low complexity and rely only on a single bit of information from each user. Our numerical simulations illustrate the enormous potential of our adaptive NOMA scheme outperforming its OMA counterpart in many settings of interest, including the presence of a malicious jammer.

MAB have recently been used in NOMA systems in [112, 113]. However, these works investigate the uplink NOMA setting, in which SIC decoding is performed at the unique

systems to reduce the complexity of the SIC decoding, which is relevant for IoT devices with limited power and computational resources [38, 104, 105].

receiver (having access to perfect channel state information and, hence, can order the users depending on their link quality) and is less complex compared to our downlink case. Moreover, the problems in [112, 113] are quite different and consist in data-rate and energy-efficiency maximization problems (assuming perfect CSIT) respectively, as opposed to our outage probability and outage-based energy-efficiency minimization problems with no CSIT/CDIT.

5.2 Arbitrarily varying wireless channels

In this Section, we describe the system model and focus on the case in which neither perfect CSIT nor CDIT is available.

5.2.1 System model

We consider a NOMA downlink network composed of a single-antenna transmitter, which can be an IoT access point or cellular access point etc., and two single-antenna receivers, e.g., IoT nodes or cellular users.

At each time instant t, the transmitter sends a signal to both users via superposition coding. The received signal at each user $k \in \{1, 2\}$ at time t writes as

$$y_k^{(t)} = h_k^{(t)} \left(\sqrt{p_1^{(t)}} x_1^{(t)} + \sqrt{p_2^{(t)}} x_2^{(t)} \right) + z_k^{(t)}. \tag{5.1}$$

We consider a stochastic channel model that varies at each time instant t. The noise term $z_k^{(t)}$ follows the complex Gaussian distribution $n_k^{(t)} \sim \mathcal{CN}(0, \sigma_k^2)$, similarly to $x_k^{(t)} \sim \mathcal{CN}(0, 1)$, the instantaneous message intended for user k. The variable $p_k^{(t)}$ denotes the power allocated by the transmitter to receiver k at time instant t. The instantaneous channel gain $h_k^{(t)}$ is unknown to the transmitter. Each user k needs to meet some QoS requirement given as the minimum or target rate $R_{\min,k}$.

We assume that both receivers have perfect knowledge of their own channel, which can be obtained through pilot-based channel estimation for instance, but that no CSIT nor CDIT is available at the transmitter side.

5.2.2 Unknown channels CSIT/CDIT

Under perfect CSIT, NOMA is performed as follows (for complete details the reader is referred to Chapter 3). The user i who encounters better channel condition $|h_i|/\sigma_i^2 > |h_j|/\sigma_j^2,\ j \in \{1, 2\} \setminus \{i\}$ carries out SIC decoding, whereas the weakest user j performs Single User Detection (SUD). Hence, the strongest user i first detects the message of the weakest user j, cancels it out and then decodes his own signal without interference.

The weakest user j decodes his own message directly by treating the interference as noise. Usually, more power is allocated by the transmitter to the weakest user for fairness reasons and to minimize the overall outage of the system.

However, when the transmitter does not have access to perfect CSIT, which is the working assumption in this Chapter, it cannot decide without error which user encounters better channel conditions, the users' decoding schemes (SIC or SUD) and its own optimal power allocation, which inevitably leads to outage events [28, 107, 108].

In what follows, we define outage-based probability metrics and propose a new adaptive NOMA scheme, in which the users' decoding choice and the power allocation at the transmitter are jointly tuned. The CSIT as well as CDIT will be considered unknown.

5.3 One-bit feedback and outage probability metrics

In this Section, we introduce the outage probability and the outage-based energy efficiency metrics. We reserve the indices i and j to denote the user performing SIC and the user performing SUD, respectively.

5.3.1 Achievable data rates

At each time step t, user i starts by decoding the message intended for user j, which requires the rate

$$R_{j\to i}^{(t)} = \log_2\left(1+\gamma_{j\to i}^{(t)}\right), \tag{5.2}$$

where $\gamma_{j\to i}^{(t)} = \frac{|h_i^{(t)}|^2 p_j^{(t)}}{|h_i^{(t)}|^2 p_i^{(t)}+\sigma_i^2}$ denotes the instantaneous signal-to-interference-plus-noise ratio (SINR) at user i when decoding the message destined to user j.

The achievable data rate of user i and j to detect their own message are respectively

$$R_i^{(t)} = \log_2(1+\gamma_i^{(t)}) \tag{5.3}$$

$$R_{j\to j}^{(t)} = \log_2(1+\gamma_{j\to j}^{(t)}), \tag{5.4}$$

where $\gamma_i^{(t)} = \frac{|h_i^{(t)}|^2 p_i^{(t)}}{\sigma_i^2}$ and $\gamma_{j\to j}^{(t)} = \frac{|h_j^{(t)}|^2 p_j^{(t)}}{|h_j^{(t)}|^2 p_i^{(t)}+\sigma_j^2}$ denote the instantaneous signal-to-noise ratio (SNR) at user i after removing the interference signal, and the SINR at user j respectively.

Since user i is chosen to carry out SIC, it will be allocated less power to ensure that the weakest user j does not suffer from outage too often, which would have a negative impact on the system's outage.

5.3.2 Outage probability

The system is considered in outage if both users cannot meet their QoS requirement. Thus, the system's outage probability is defined as

$$\begin{aligned}\mathbb{P}_{\text{out}}(i,\mathbf{p}) &\triangleq \mathbb{P}\Big[R_i^{(t)} \leq R_{\min,i} \ \cup \ \min(R_{j\to j}^{(t)}, R_{j\to i}^{(t)}) \leq R_{\min,j}\Big] \\ &= \mathbb{P}\Big[\gamma_i^{(t)} \leq \gamma_{\min,i} \ \cup \ \min(\gamma_{j\to j}^{(t)}, \gamma_{j\to i}^{(t)}) \leq \gamma_{\min,j}\Big], \end{aligned} \tag{5.5}$$

with $\gamma_{\min,i} \triangleq 2^{R_{\min,i}} - 1$, $\gamma_{\min,j} \triangleq 2^{R_{\min,j}} - 1$ and $\mathbf{p} = (p_i, p_j)$.

Since the aim here is to minimize the outage probability, the total power budget $P_{\max}$ is fully exploited such that $p_1^{(t)} + p_2^{(t)} = P_{\max}$ as in [28, 105, 114]. Hence, the feasible set is given as

$$\mathcal{P}_o = \{(i,\mathbf{p}) \mid i \in \{1,2\}, p_i \geq 0, p_j \geq 0, p_i + p_j = P_{\max}\}. \tag{5.6}$$

Because the transmitter is assumed to transmit at full power $P_{\max}$, we can write the allocated power to user i and j respectively as $p_i^{(t)} = \beta_o^{(t)} P_{\max}$ and $p_j^{(t)} = (1 - \beta_o^{(t)}) P_{\max}$, with $\beta_o^{(t)} \in (0, \frac{1}{2})$.

5.3.3 Outage-based energy efficiency

An energy efficient measure in the stochastic small-scale fading channels is defined as follows [115, 116]

$$\xi_{EE}(i,\mathbf{p}) = \frac{(R_{\min,1} + R_{\min,2})(1 - \mathbb{P}_{\text{out}}(i,\mathbf{p}))}{p_i + p_j + P_c}, \tag{5.7}$$

where P_c denotes the circuit power and $(1 - \mathbb{P}_{\text{out}}(i,\mathbf{p}))$ is the success probability or the probability that the QoS constraints are met. The expression of $\mathbb{P}_{\text{out}}(i,\mathbf{p})$ is given in (5.5).

The energy-efficiency measure in (5.7) is relevant in small-scale fading channels as the numerator $(R_{\min,1}+R_{\min,2})(1-\mathbb{P}_{\text{out}}(i,\mathbf{p}))$ represents the long-term average sum rate of the system. Also, $\xi_{EE}(i,\mathbf{p})$ incorporates the QoS constraint in the objective, simplifying the feasible set of the problem. Note that for the energy-efficiency maximization, transmitting at full power is no longer optimal leading to a feasible set different from (5.6) expressed as follows

$$\mathcal{P}_e = \{(i,\mathbf{p}) \mid i \in \{1,2\}, p_i \geq 0, p_j \geq 0, p_i + p_j \leq P_{\max}\}. \tag{5.8}$$

We note that when CDIT is available, the analytical expressions of the outage probability can be obtained under the assumption of stochastic Rayleigh channels. Hence finding the optimal policy $(i^*, \mathbf{p}^*)$ minimizing the outage $\mathbb{P}_{\text{out}}(i,\mathbf{p})$ or maximizing the energy efficiency $\xi_{EE}(i,\mathbf{p})$ reduces to solving two continuous optimization problems, one for each value of i, w.r.t $\mathbf{p}$ and then choosing the best value of i.

In the absence of CDIT, we exploit reinforcement learning techniques to propose a new adaptive NOMA scheme, in which the users' decoding choice and the power

allocation at the transmitter are jointly tuned based on past transmissions and relying on a single bit of feedback from each user. The feedback information is of acknowledgment (ACK)-type and conveys whether the users' QoS constraints have been met during the past transmission.

In the following Section, we introduce the MAB-based adaptive NOMA scheme for optimizing the predefined outage-based metrics.

5.4 Multi-armed bandits adaptive policies

In this Section, we exploit the MAB framework to learn and design iterative policies $\mathbf{a}^{(t)} \triangleq (i^{(t)}, \mathbf{p}^{(t)})$ that minimize the outage probability and the outage-based energy efficiency of a downlink NOMA system in the absence of CSIT and CDIT.

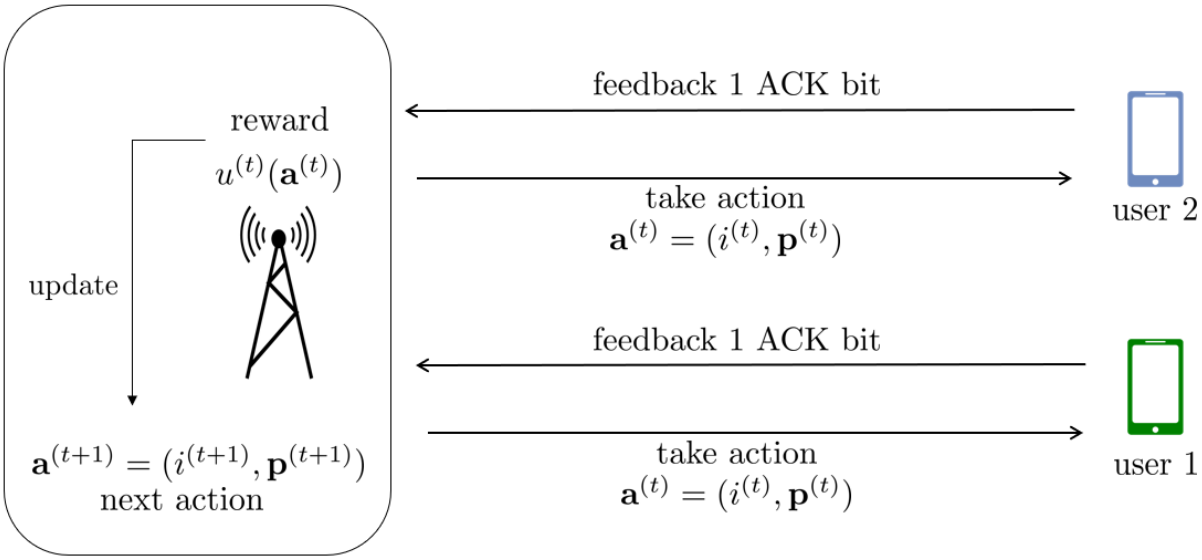

Figure 5.1: Multi-armed bandits adaptive policy.

As described in Figure 5.1, the learning is done in a sequential way, trial-and-error fashion where, by taking an action $\mathbf{a}^{(t)} = (i^{(t)}, \mathbf{p}^{(t)})$ at each time instant t and receiving the single bit feedback from each of the two users indicating whether their QoS requirements were met, the transmitter is able to compute the obtained past reward of the taken action $\mathbf{a}^{(t)}$ and update its policy accordingly. A possible action or arm at the transmitter is defined by the pair $\mathbf{a} \triangleq (i, \mathbf{p})$ which dictates both the decoding schemes of the two users via the index of the user performing SIC i and the transmit power allocation policy $\mathbf{p}$.

In order to exploit the basic MAB framework, we first need to quantize only the feasible set of each optimization problem, i.e., $\mathcal{P}_o$ and $\mathcal{P}_e$. Since $i \in \{1, 2\}$ we need to quantize the power allocation policy $\mathbf{p}$ which will obviously induce an optimality loss compared with the continuous power allocation. This will be evaluated in details via numerical simulations in Section 5.5

5.4.1 Policy quantization and binary reward

In what follows, we will define the set of arms or policies representing the possible choices of the joint optimization variable $\mathbf{a} \triangleq (i, \mathbf{p})$ for each outage-based metric.

A. Outage probability

Policy quantization: As already mentioned, the full power $P_{\max}$ is exploited to minimize the outage probability where $p_i = \beta_o P_{\max}$ and $p_j = (1-\beta_o)P_{\max}$ with $\beta_o \in (0, \frac{1}{2})$. Hence, the transmit power allocation policy will be dictated by β_o and each action is given as $\mathbf{a} \triangleq (i, \beta_o)$. We assume a discrete set: $\mathcal{B}_o = \{\beta_{o,1}, \beta_{o,2}, \ldots, \beta_{o,M_o}\}$ of choices for the power allocation variable β_o. We then denote by $\mathcal{A}_o = \{1, 2\} \times \mathcal{B}_o$ the set of arms or policies representing the possible choices of the joint optimization variable $\mathbf{a} \triangleq (i, \beta_o)$.

Binary reward: The instantaneous reward in this case is given as

$$u^{(t)}(\mathbf{a}^{(t)}) = \begin{cases} 1, & \text{if } \gamma_i^{(t)} \geq \gamma_{\min,i} \cap \min(\gamma_{j\to j}^{(t)}, \gamma_{j\to i}^{(t)}) \geq \gamma_{\min,j} \\ 0, & \text{otherwise,} \end{cases} \tag{5.9}$$

and conveys that, if either of the users' feedback bits equals 0, the system is in outage and $u^{(t)}(\mathbf{a}^{(t)}) = 0$, whereas, if both of the users' feedback equal 1 then $u^{(t)}(\mathbf{a}^{(t)}) = 1$. This reward is specifically chosen such that its expectation equals the probability of success since $\mu(\mathbf{a}) = \mathbb{E}[u^{(t)}(\mathbf{a})] = 1 - \mathbb{P}_{\text{out}}$. Therefore, minimizing the outage probability is equivalent to maximizing the expected reward given as

$$\mu^* \triangleq \max_{\mathbf{a}\in\mathcal{A}_o} \mathbb{E}[u^{(t)}(\mathbf{a})] \equiv \min_{i\in\{1,2\}, \beta_o \in \mathcal{B}_o} \mathbb{P}_{\text{out}}(i, \mathbf{p}_{\beta_o}), \tag{5.10}$$

where $\mathbf{p}_{\beta_o} = (\beta_o P_{\max}, (1-\beta_o)P_{\max})$ assuming stochastic channels.

B. Outage-based energy efficiency

Policy quantization: When maximizing the energy efficiency, transmitting at full power as in the previous case is not energy-efficient in general. Hence, we consider that only a fraction of the maximum budget $P_{\max}$ is exploited with $\beta_e \in \mathcal{B}_e \subset [0, 1]$ such that $\mathcal{B}_e = \{\beta_{e,1}, \beta_{e,2}, \ldots, \beta_{e,M_e}\}$ is discrete. In order to maintain fairness among users and to keep the overall number of possible choices low[2], user i carrying out SIC is allocated less power than user j where $p_i \in (0, \frac{1}{2}) \times P_{\max}$ and $p_j \in (\frac{1}{2}, 1) \times P_{\max}$. In [28], a power split of $\frac{1}{5} - \frac{4}{5}$ was considered to evaluate the outage performance of NOMA in the case of two users. Here, we consider a $\frac{1}{4} - \frac{3}{4}$ power split by taking the midpoint of each interval

[2] The complexity of MAB algorithms depends on the number of possible actions or arms, when the number of actions grows high, more exploration needs to be performed to discover which ones are optimal.

(i.e., $(0, \frac{1}{2})$ and $(\frac{1}{2}, 1)$) and we focus on the special choice of power allocation policy $\mathbf{p}_{\beta_e} = (\frac{1}{4}\beta_e P_{\max}, \frac{3}{4}\beta_e P_{\max})$. Of course, the $\frac{1}{4} - \frac{3}{4}$ power split between the two users will incur an optimality loss which will be evaluated and analyzed thoroughly via numerical simulations.

In this case, the action or arm is defined by the pair $\mathbf{a} \triangleq (i, \beta_e) \in \mathcal{A}_e = \{1, 2\} \times \mathcal{B}_e$ where the transmit power allocation policy $\mathbf{p}_{\beta_e}$ is defined via β_e as described above.

Binary reward: The energy-efficient instantaneous reward is given by

$$u^{(t)}(\mathbf{a}) = \begin{cases} \frac{R_{\min,1}+R_{\min,2}}{p_{i,\beta_e}+p_{j,\beta_e}+P_c}, & \text{if } \gamma_i^{(t)} \geq \gamma_{\min,i} \cap \min(\gamma_{j\to j}^{(t)}, \gamma_{j\to i}^{(t)}) \geq \gamma_{\min,j} \\ 0, & \text{otherwise,} \end{cases} \tag{5.11}$$

chosen such that its expectation equals precisely the energy-efficiency measure in (5.7), $\mu(\mathbf{a}) = \mathbb{E}[u^{(t)}(\mathbf{a})] = \xi_{EE}(i, \mathbf{p}_{\beta_e})$. Note that if either of the users' feedback bits equals 0 then the reward equals 0 and, if both users' feedback bits equal 1 then the reward equals $\frac{R_{\min,1}+R_{\min,2}}{p_{i,\beta_e}+p_{j,\beta_e}+P_c}$. Therefore, maximizing the energy efficiency amounts to maximizing the expectation of the reward

$$\mu^* \triangleq \max_{\mathbf{a}\in\mathcal{A}} \mathbb{E}[u^{(t)}(\mathbf{a})] \equiv \max_{i\in\{1,2\}, \beta_e \in \mathcal{B}_e} \xi_{EE}(i, \mathbf{p}_{\beta_e}). \tag{5.12}$$

We are now ready to describe our online adaptive NOMA approach.

5.4.2 Adaptive NOMA scheme

A generic dynamic policy for adaptive NOMA in this framework can be described as follows: at each time instant t, the decision maker or the transmitter selects an arm $\mathbf{a}^{(t)} = (i^{(t)}, \mathbf{p}^{(t)})$. Then it informs both users of their decoding techniques dictated by $i^{(t)}$ via one-bit broadcast (e.g., 1 if $i^{(t)} = 1$, and 0 otherwise) and it transmits the superimposed signal using the $\mathbf{p}^{(t)}$ power allocation policy dictated by either $\beta_o^{(t)}$ or $\beta_e^{(t)}$ to minimize either the outage probability or the outage-based energy efficiency. After the transmission, each user decodes his message following the policy assigned by the transmitter (either SIC or SUD) and feeds back a single bit indicating whether his QoS requirement was met or not. Based on the two feedback bits, the transmitter computes its reward defined in either (5.9) or (5.11), depending on the objective to optimize, and updates the choice of the next arm $\mathbf{a}^{(t+1)}$. This online process is summarized in Algorithm 4.

Notice that our low-power feedback mechanism is especially relevant for IoT networks connecting low-power wireless sensors. Moreover, via this simple online process, the transmitter is capable of learning the best decoding scheme (SIC/SUD) for each user jointly with the best power allocation in the quantized set without requiring CSIT nor CDIT and only a 1-bit feedback.

Algorithm 4 Adaptive NOMA via MAB with no CSIT or CDIT

Initialize: $t = 1$, $\mathbf{a}^{(1)} = (1, 0.5)$ arbitrarily

repeat

- choose policy $\mathbf{a}^{(t)} = (i^{(t)}, \mathbf{p}^{(t)})$: inform users of their decoding schemes ($i^{(t)}$) and transmit with power policy

  outage probability : $\mathbf{p}^{(t)} = \mathbf{p}_{\beta_o}^{(t)} = (\beta_o^{(t)}\ P_{\max},\ (1 - \beta_o^{(t)})\ P_{\max})$

  outage-based energy efficiency : $\mathbf{p}^{(t)} = \mathbf{p}_{\beta_e}^{(t)} = (\frac{1}{4}\ \beta_e^{(t)}\ P_{\max},\ \frac{3}{4}\ \beta_e^{(t)}\ P_{\max})$
- receive 1-bit ACK feedback from each user
- compute reward $u^{(t)}(\mathbf{a}^{(t)})$ given in

  outage probability : (5.9)

  outage-based energy efficiency : (5.11)
- update policy $\mathbf{a}^{(t+1)} \leftarrow \mathbf{a}^{(t)}$
- $t \leftarrow t + 1$

until end of transmission

In stochastic environments, the main idea of such iterative scheme is to learn the best policy or arm that obtains maximal expected reward, without knowing the statistics of the rewards of each arm in advance and based only on past observations as explained in Section 2.3. The performance of such an online learning algorithm is measured by the pseudo-regret defined in (2.33) as

$$\mathbb{E}[\mathrm{Reg}_T] = \mu^* - \frac{1}{T}\sum_{t=1}^{T}\mathbb{E}[u^{(t)}(\mathbf{a}^{(t)})], \tag{5.13}$$

which represents the gap between the optimal outage probability $\mathbb{P}_{\mathrm{out}}(i^*, \mathbf{p}_{\beta_o}^*)$ or the optimal energy efficiency $\xi_{EE}(i^*, \mathbf{p}_{\beta_e}^*)$ and the overall performance of the online algorithm over a fixed horizon of time T. In non-stationary and possibly adversarial environments, the pseudo-regret definition is defined in (2.34) as

$$\mathbb{E}[\mathrm{Reg}_T] = \max_{\mathbf{a}\in\mathcal{A}}\frac{1}{T}\sum_{t=1}^{T}\mathbb{E}[u^{(t)}(\mathbf{a}) - u^{(t)}(\mathbf{a}^{(t)})], \tag{5.14}$$

which represents the performance gap between the best fixed strategy over the horizon T and the online policy. A desirable property is that of no regret, i.e., $\limsup_{T\to\infty}\mathrm{Reg}(T) \leq 0$, which implies that the online algorithm has to perform at least as good as the optimal arm minimizing the outage probability or maximizing the energy efficiency.

In what follows, we focus on two well-known MAB algorithms for choosing the policy $\mathbf{a}^{(t)} = (i^{(t)}, \mathbf{p}^{(t)})$ that have the property of no regret by specifying the updating rule of the policy in our Algorithm 4 ($\mathbf{a}^{(t+1)} \leftarrow \mathbf{a}^{(t)}$). Namely, Upper Confidence Bound (UCB) and Exponential-weight algorithm for Exploration and Exploitation (EXP3) are investigated because they optimally trade-off between data exploration and exploitation to reach the best regret decay rates in the stochastic and adversarial MAB environments, respectively.

The updating policy rules for UCB and EXP3 have already been introduced in Section 2.3 and their expressions are given in (2.35) and (2.37) respectively.

5.5 Numerical results

In this section, we investigate the outage and energy-efficiency performance of our proposed adaptive NOMA schemes when no CSIT/CDIT is available at the transmitter.

Outage performance

First, we investigate the outage performance. Four cases depending on the resolution of the power allocation interval quantization $(0, \frac{1}{2})$ are considered: a) $M_o = 1$ or 2 arms; b) $M_o = 3$ or 6 arms; c) $M_o = 7$ or 14 arms; and d) $M_o = 15$ or 30 arms. The quantization is uniform and obtained by dichotomy such that for $M_o = 1$ (2 arms), we have $\mathcal{A}_o = \{1, 2\} \times \{0.25\}$; for $M_o = 3$ (6 arms), we have $\mathcal{A}_o = \{1, 2\} \times \{0.125, 0.25, 0.375\}$; etc.

As a comparison benchmark, we consider a conventional OMA system where the transmitter serves both users by time sharing. The achievable rate at user $k \in \{1, 2\}$ thus write as $R_k^{(t),\mathrm{OMA}} = \frac{1}{2} \log\left(1 + \gamma_k^{(t),\mathrm{OMA}}\right)$, where $\gamma_k^{(t)} = \frac{|h_k^{(t)}|^2 P_{\max}}{\sigma_k^2}$ denotes the instantaneous SNR at user k. Note that under OMA, the outage probability writes as $\mathbb{P}_{\mathrm{out}}^{\mathrm{OMA}} \triangleq \mathbb{P}\left[R_1^{(t),\mathrm{OMA}} \leq R_{\min,1} \cup R_2^{(t),\mathrm{OMA}} \leq R_{\min,2}\right]$.

We evaluate our schemes in a common downlink NOMA setup [52] assuming stochastic Rayleigh channels $h_k^{(t)} \sim \mathcal{CN}(0, \sigma_{h_k}^2)$, and setting the network parameters as: $P_{\max}/\sigma_k^2 = 20$ dB for $k \in \{1, 2\}$, $\sigma_{h_1}^2 = 1, \sigma_{h_2}^2 = 0.1$, $\gamma_{\min,1} = 1$ ($R_{\min,1} = 1$ bpcu), $\gamma_{\min,2} = 3$ ($R_{\min,2} = 2$ bpcu), unless otherwise specified. Both algorithms are run over a $T = 10^4$ time horizon and the provided results are averaged over $N = 10^3$ random runs.

Tunning the learning parameters: the parameters δ given in (2.35) and γ, η given in (2.37), that trade-off between data exploration and exploitation for UCB and EXP3 algorithms respectively, can lead to very poor performance if badly chosen. From a theoretical perspective, they should be chosen such that $\delta^* > 2$, $\eta^* = \frac{\gamma}{|\mathcal{A}_o|}$ and $\gamma^* = \sqrt{\frac{|\mathcal{A}_o| \ln |\mathcal{A}_o|}{(e-1)T}}$ in order to reach the optimal regret decay rate by minimizing the regret's upper bound [80, 81]. In practice, these values can be further improved to obtain better performance [117–119]. Based on numerical experiments, the following values were chosen: $\delta = 1$ instead of $\delta^* > 2$ (for UCB in Figure 5.2 and Figure 5.4), $\gamma = \gamma^* = 0.0464$ and $\eta = 0.02$ instead of $\eta^* = 0.0033$ (for EXP3 in Figure 5.2).

In Figure 5.2, we compare the outage performance obtained with UCB and EXP3 using a set of 14 arms ($M_o = 7$) with the fixed optimal arm $\mathbf{a}^*$ (computed offline and requiring CDIT) using a set of 14 arms ($M_o = 7$) as well as with OMA. Notice that

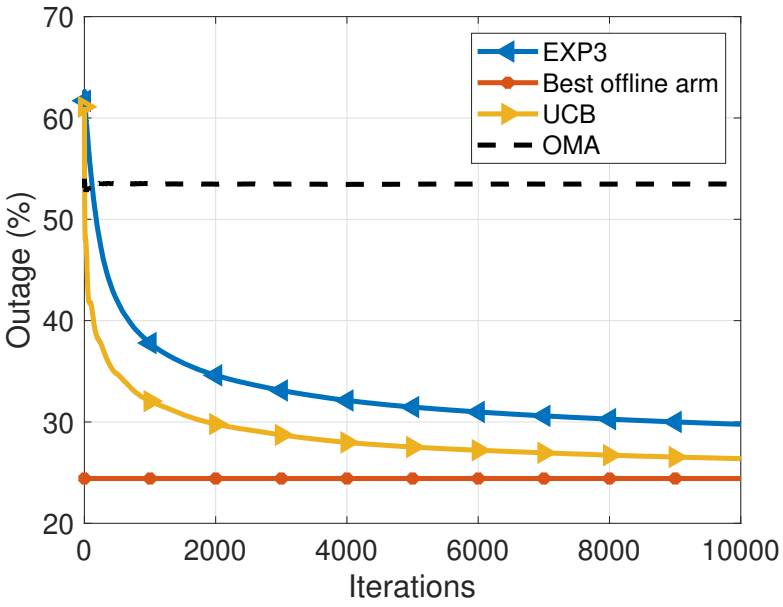

Figure 5.2: Outage of adaptive NOMA (via UCB or EXP3) relying on a 1-bit feedback compared to OMA and the best offline policy. Our schemes greatly outperform OMA in terms of outage probability.

both algorithms converge towards $\mathbf{a}^*$, the best offline solution by exploiting only 1-bit of feedback from the users as opposed to perfect CSIT or CDIT. Surprisingly, our proposed adaptive NOMA schemes quickly outperform OMA (after less than 100 iterations). Finally, UCB performs better than EXP3 as expected in stochastic environments.

Figure 5.3 depicts the outage performance of our adaptive NOMA schemes for different number of arms and $M_o \in \{1, 3, 7, 15\}$ as a function of the QoS requirement $\gamma_{\text{min},2}$ of user 2. Here, aside from the OMA benchmark, we also include the optimal outage probability obtained over a continuous power allocation policy $\beta_o \in (0, \frac{1}{2})$, to assess the optimality loss of our adaptive NOMA schemes based on quantization.

First, we remark that our adaptive NOMA schemes cannot decrease the outage performance compared to OMA and that the gap between both access techniques is maximized for moderate QoS requirement, and can go up to 48% in the case of 30 arms. Another important observation is that the performance gain of NOMA over OMA fades when the target data rates of the two users are the same. Therefore, NOMA cannot only take advantage of the users asymmetric channel conditions but also other users asymmetries such as their QoS requirements [7, 14, 120, 121] .

Also, we can see that increasing the number of arms, which increases the resolution of our power allocation quantization, allows to reduce the gap with the continuous optimal NOMA transmission scheme. At last, for low QoS requirements two arms are sufficient for outage optimality; however, as the QoS requirement increases, the number of arms has to increase.

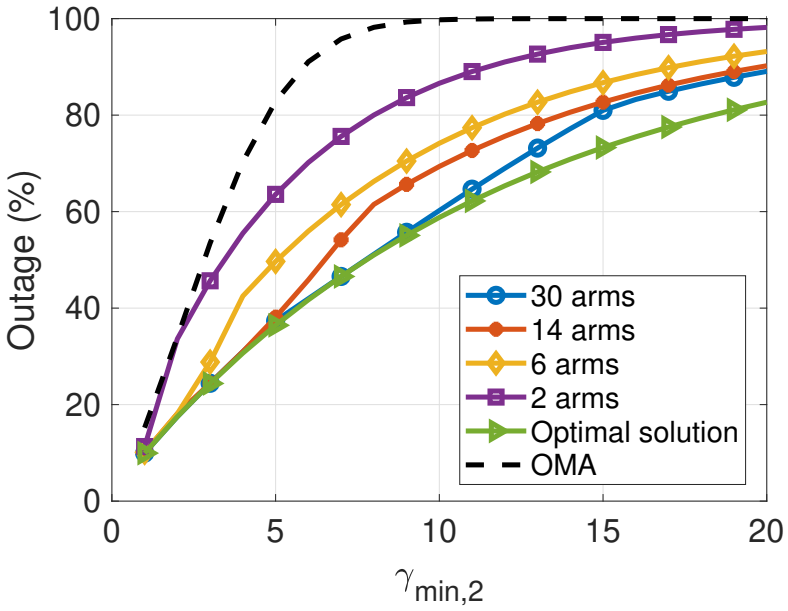

Figure 5.3: Impact of the number of arms on the outage probability. The outage decays with the number of arms. The quantization incurred optimality loss becomes negligible when choosing carefully the number of arms.

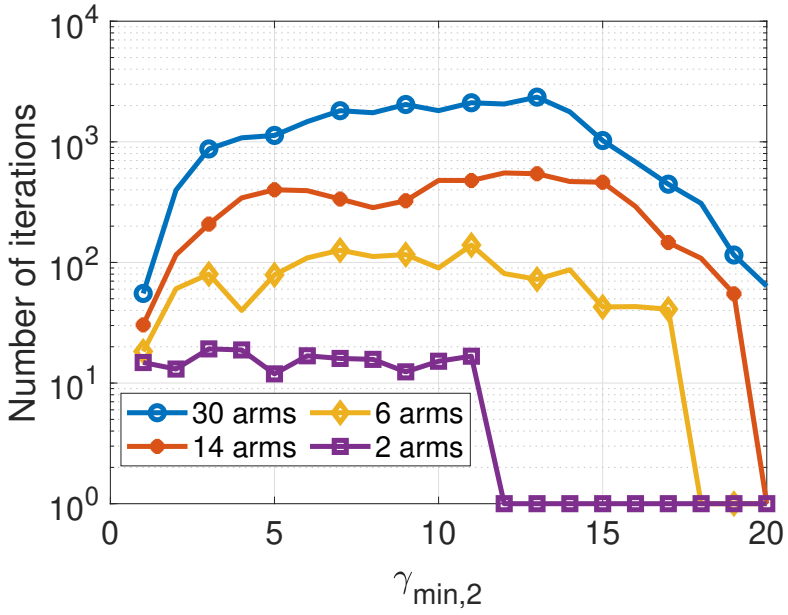

Figure 5.4: Impact of the number of arms on the speed of the adaptive NOMA scheme with UCB (iterations required to reach 10% regret). The exploration search increases with the number of arms.

So far, we have compared NOMA and OMA from an outage probability perspective. Since our adaptive NOMA approach relies on an iterative procedure, we also consider here the convergence speed. In Figure 5.4, we compare the number of iterations required

for adaptive NOMA with UCB to reach a regret of 10% for $M_o \in \{1, 3, 7, 15\}$. When the number of arms is increased, the longer it takes until UCB reaches the 10% level of regret. This can be explained by the fact that, when increasing the number of possible arms or policies, the duration of the exploration search for the best arm naturally increases.

To sum up, Figure 5.5 and Figure 5.4 highlight an important trade-off between outage optimality and latency of our adaptive NOMA schemes based on MAB. Indeed, the number of arms needs to be large enough to reduce the optimality loss caused by our quantization, but not too large to insure fast convergence. Hence, the best trade-off and number of arms will depend on the specific application and its requirements.

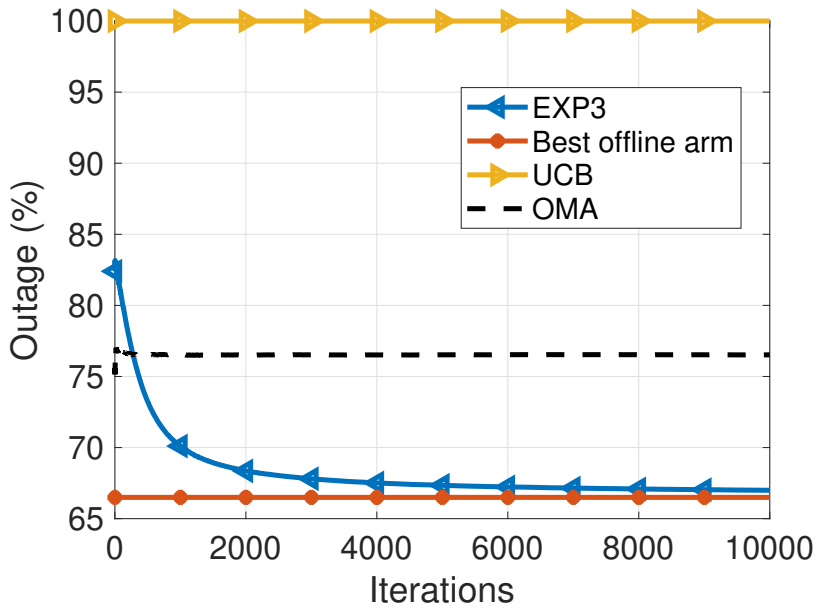

Figure 5.5: Outage of adaptive NOMA (via UCB or EXP3) relying on a 1-bit feedback compared to OMA and the best offline policy in the presence of a malicious jammer. UCB is always in outage, while EXP3 outperforms OMA and reaches the best offline policy.

Let us now consider a non-stationary and adversarial environment containing the presence of a malicious jammer whose aim is to put the system systematically in outage. For simplicity, we assume $\mathcal{A}_o = \{1, 2\} \times \{0.4\}$ (only two arms) and set $\delta = 1$ for UCB, $\gamma = \gamma^* = 0.009$, $\eta = 0.02$ for EXP3. The jammer is assumed to have knowledge of the system, more precisely, it knows the set of actions and the adaptive NOMA algorithm used at the transmitter. Since UCB is a purely deterministic algorithm, the jammer can anticipate precisely the arm or action chosen by the transmitter and is able to adjust its jamming power such that the system is systematically put in outage. This leads to a non-vanishing linear regret. The jammer cannot impact the system to such an extent when the transmitter is using EXP3. Indeed, with EXP3 the arm is randomly chosen following a probability distribution and cannot be perfectly anticipated even is such worst-case adversarial settings.

The outage performance of our adaptive NOMA schemes in the presence of a malicious jammer are depicted in Figure 5.5. We can see that UCB is always in outage, as expected; and that EXP3 can still reach the best offline policy.

Energy-efficiency performance

We now investigate the outage-based energy efficiency of our proposed adaptive NOMA scheme. Three cases based on the quantization set $\mathcal{B}_e$ are considered: a) 5-element $\mathcal{B}_{e,1} = \{0.2, 0.4, \dots 1\}$; b) 10-element $\mathcal{B}_{e,2} = \{0.1, 0.2, \dots, 1\}$; and c) 20-element $\mathcal{B}_{e,3} = \{0.05, 0.1, \dots, 1\}$ such that $\mathcal{B}_{e,1} \subset \mathcal{B}_{e,2} \subset \mathcal{B}_{e,3}$. The considered arm sets are thus given as $\mathcal{A}_{e,i} = \{1, 2\} \times \mathcal{B}_{e,i}$ of 10, 20 and 40 arms respectively.

We consider the same previous channel model and the following system parameters: $P_{\max}/\sigma_k^2 = 30$ dB for $k \in \{1, 2\}$, $\gamma_{\min,1} = 1$ ($R_{\min,1} = 1$ bpcu), $\gamma_{\min,2} = 10$ ($R_{\min,2} \simeq 3.5$ bpcu), $P_c = 1$ W (unless stated otherwise). The time horizon is set to $T = 5000$ for both UCB and EXP3 algorithms and the illustrated curves are averaged over 10^3 horizon realizations. The learning parameters were carefully tuned in order to provide the best performance and were set as $\delta = 0.1$, $\gamma = \gamma^* = 0.1311$ and $\eta = 0.08$.

Similarly, we compare the performance of our proposed adaptive NOMA scheme with OMA where the energy efficiency of user k write as: $\xi_{EE}^{\text{OMA}}(\beta_e) = \frac{(R_{\min,1}+R_{\min,2})(1-\mathbb{P}_{\text{out}}^{\text{OMA}}(\beta_e))}{\beta_e P_{\max}+P_c}$. The optimal $\beta_e^{*,\text{OMA}}$ is obtained offline with the help of CDIT.

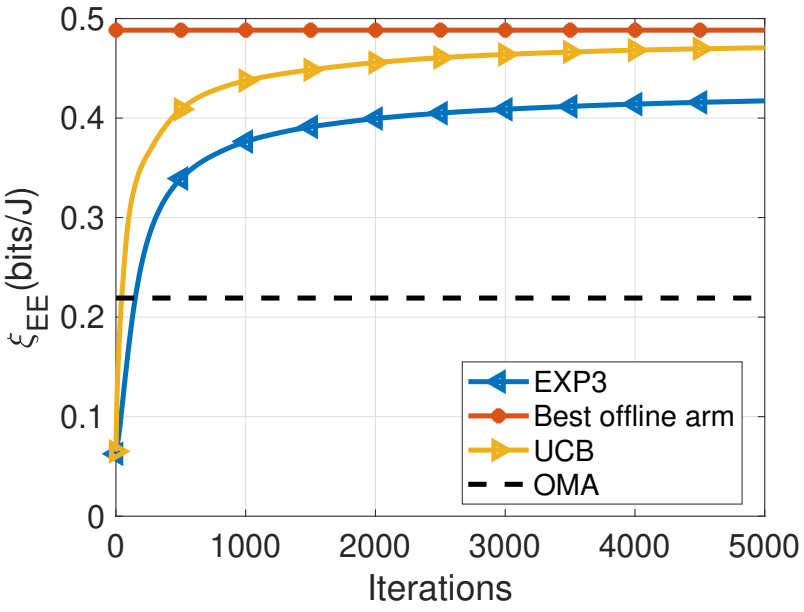

Figure 5.6: Energy efficiency of our adaptive NOMA (via UCB or EXP3) compared to the best offline arm and OMA.

In Figure 5.6, we compare the energy efficiency of our NOMA scheme with UCB and EXP3 using $\mathcal{A}_{e,3}$ (40 arms), with the fixed optimal arm $\mathbf{a}^*$ computed offline with the use

of CDIT. Note that both algorithms reach the energy efficiency of $\mathbf{a}^*$, the best fixed offline policy, by requiring only one-bit of feedback and no CSIT/CDIT. Further, our proposed NOMA scheme significantly outperforms OMA after a few iterations. UCB outperforms EXP3 in the stochastic case [122].

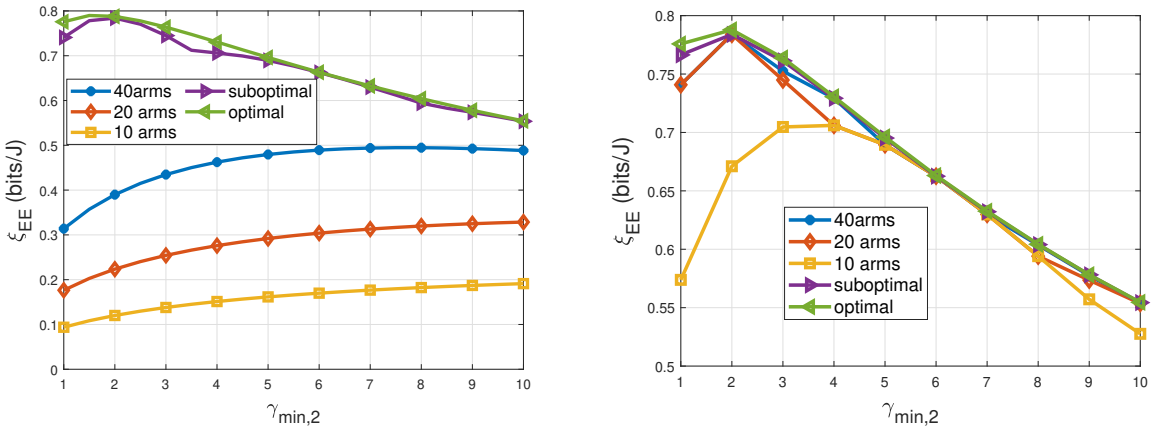

(a) Impact of the number of arms on the ξ_{EE} for $P_{\max} = 100$ W.

(b) Impact of the number of arms on the ξ_{EE} for $P_{\max} = 10$ W.

Figure 5.7: Impact of the number of arms on the ξ_{EE}. Trade-off performance vs. available information.

In Figure 5.7 we investigate the impact of the number of arms and the sub-optimality caused by the quantization $\mathcal{B}_e$ and the split $\frac{1}{4} - \frac{3}{4}$ for two scenarios: $P_{\max} = 100$ W and $P_{\max} = 10$ W, respectively. For this, we include the following benchmarks: **a)** sub-optimal energy efficiency obtained with the user power split $\frac{1}{4} - \frac{3}{4}$, but for an optimal choice of β_e; **b)** the optimal energy efficiency obtained over the entire set $\mathcal{P}_e$.

Both figures show a vanishing gap between the above sub-optimal and optimal schemes, showing hence the efficiency of our heuristic $\frac{1}{4} - \frac{3}{4}$ power split between the two users. In the large transmit power regime of Figure 5.7(a), the optimality loss of our adaptive NOMA scheme decreases with the number of arms. However, the gap remains large (more than 50% at low $\gamma_{\min,2}$), highlighting the trade-off between energy efficiency and available feedback. On the other hand, in the low power regime of Figure 5.7(b), the optimality gap is negligible for 20 arms.

In Figure 5.8, we study how the number of arms affects the regret performance of our adaptive NOMA. We focus only on UCB, since it is known to have a better decay rate than EXP3 in the stochastic case, and plot the number of iterations required to reach a regret level of 10%. We see that the larger the number of arms, the more iterations are needed. Hence, even if a better energy-efficiency performance can be achieved by increasing the number of arms, additional time is needed to explore and exploit all arms. This highlights another fundamental trade-off between energy efficiency and complexity and a larger amount of time is required to reach better performance.

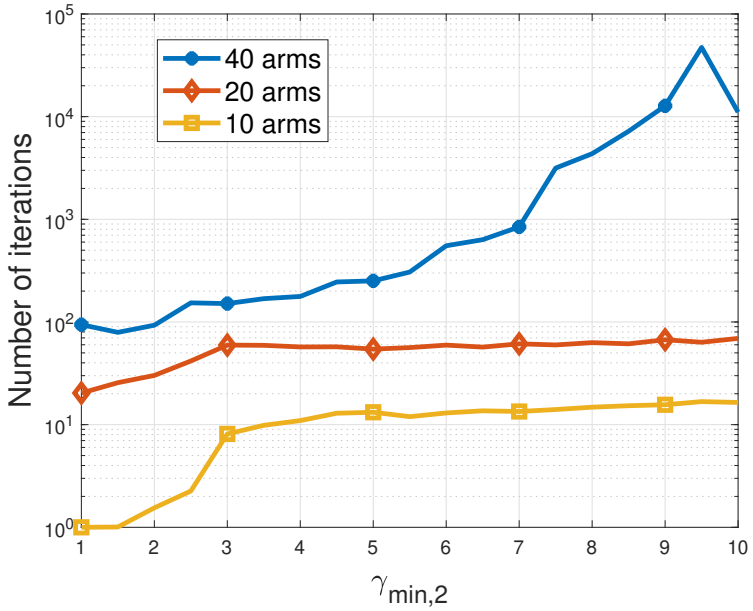

Figure 5.8: Number of iterations required for UCB to achieve 10% regret level: trade-off performance vs. complexity.

5.6 Summary

In this Chapter, we investigated the outage probability and the outage-based energy efficiency of a two-user downlink NOMA system with no CSIT/CDIT. By exploiting the Multi-Armed Bandit (MAB) framework and the well-known UCB and EXP3 algorithms, we proposed an adaptive NOMA scheme relying only on a 1-bit feedback, relevant for IoT networks. Our simulation results showed that our adaptive NOMA scheme outperforms OMA in many settings of interest including stochastic and even non-stationary (adversarial) ones. The fundamental trade-offs between performance, feedback information and complexity were highlighted, indicating that the number of arms for MAB needs to be carefully tuned depending on the specific application requirements and constraints. Our adaptive NOMA scheme can be extended to more than two users. However, the number of the decoding order possibilities and discrete power allocation policies will increase exponentially. This will imply a large amount of time to explore and exploit all the possible actions.

Chapter 6

Conclusions and Perspectives

Contents

In this Chapter, we summarize the contributions of this thesis. In addition, we present some future research topics relevant to our work.

6.1 Summary of the Contributions

In this thesis, we investigated the energy-efficient resource allocation for downlink Non-Orthogonal Multiple Access (NOMA) systems. First, we considered a multi-user NOMA system and maximized the energy efficiency under the assumption of complete knowledge of the channel state information at the transmitter (CSIT). Then we extended this investigation to include Ambient Backscatter Communication (AmBC). Since acquiring CSIT is challenging, we provided an adaptive NOMA scheme to cope with the absence of CSIT and that of the channel distribution information at the transmitter (CDIT). The contributions of each Chapter are summarized as follows

First, we investigated the energy-efficiency maximization, defined as a bi-criterion problem, in a multi-user downlink NOMA system assuming the transmitter power budget and minimum users' quality of service (QoS) constraints. Assuming perfect CSIT, we obtained a closed-form solution for the power allocation policy that optimally trade-offs between achievable sum rate and overall power consumption for any weighting factor between the two objectives. We also showed that our solution is quite useful when maximizing the ratio between the sum rate and overall power consumption by reducing the complexity of Dinkelbach's algorithm to a one-line search. Simulation results showed that NOMA is more rate-efficient than Orthogonal Multiple Access (OMA) when the

emphasis in the objective function is on the sum rate. Similarly, when the emphasis in the objective function is on reducing the power consumption, NOMA is more power-efficient.

Then, we extended the above NOMA system to include AmBC. We first analyzed the system in the case of a fixed backscattering state where the energy-efficiency optimization problem was formulated as the sum rate vs. total power consumption trade-off. Even though not a convex optimization problem, we have provided the optimal closed-form solution for the joint reflection coefficient and power allocation policy leading to a simplified Dinkelbach's algorithm. This analysis was carried out further for multiple backscatter devices. In the general case where the ambient backscatter device is not in a fixed backscattering state, we first derived the information-theoretic achievable rate region and then we formulated the energy-efficiency maximization as the trade-off between the sum rate and the power consumption. By introducing a modification on the problem's constraints, we simplified the resulting non-convex problem which allowed us to obtain an analytical solution for the joint reflection coefficient and the power allocation. Our simulation results showed the negligible impact on the sub-optimality gap resulting from our modification. Also, NOMA with backscattering outperforms conventional NOMA and OMA (with and without backscattering) as benchmarks. Finally, we investigated the impact of imperfect CSI and highlighted that when the channel estimation is sufficiently high our solution is still relevant.

Finally, we investigated the outage probability and outage-based energy efficiency of a two-user downlink NOMA system in which no channel state or distribution information is available at the transmitter side. To overcome the lack of channel information, we exploited reinforcement learning and more precisely, the Multi-Armed Bandit (MAB) framework and proposed a novel adaptive NOMA scheme relying on a single bit of feedback. In our scheme, the transmitter decides both the decoding schemes of the two users (SIC or SUD, via a binary control variable) as well as its allocated transmit power, lying in a quantized version of the feasible set, based on two well-known MAB algorithms, namely UCB and EXP3. Our numerical results demonstrate the enormous potential of our adaptive NOMA scheme relying on 1-bit of feedback by outperforming OMA in many settings of interest including stochastic and even non-stationary ones. Furthermore, our simulations showed that the number of possible arms needs to be chosen sufficiently large to compensate for the power allocation quantization, but not too large to allow a fast outage decay.

6.2 Perspectives

In this Section, we will discuss some possible future research directions related to our work.

Limitations of Multi-Armed Bandit: in Chapter 5, we have used the MAB framework to solve the joint users decoding order i and the power allocation policy $\mathbf{p}$

for a two-user NOMA system in the absence of CSIT and CDIT. As shown in Section 5.5, this framework is a simple yet powerful tool for solving resource allocation problems in unknown environments, but is limited when dealing with only discrete sets of actions which causes optimality loss. Therefore, high resolution quantization, leading to more actions, was needed to approach the optimal action but at the cost of additional complexity and time to explore and exploit all actions.

The MAB framework could also be applied to the two-user NOMA system in the presence of an ambient backscatter device, assuming no knowledge on both the direct and the backscattered channels. In this case, the set of actions is expanded to include the reflection coefficient $\rho \in [0, 1]$ where each action would be defined as $\mathbf{a} = (i, \rho, \mathbf{p})$. Since the reflection coefficient is a continuous variable, an additional quantization is needed to make use of the MAB algorithms. This would require even more complexity and larger amount of time to reach the best performance. Therefore, we need to find ways to deal with continuous variable sets to overcome the quantization-caused loss and the computational complexity.

The use of deep learning techniques could be a great solution to deal with the aforementioned challenges where it has already been proved to be useful for various resource allocation problems [123, 124]. The investigation in Chapter 5 could also be extended to the multi-user case where user pairing is applied. In this case, the problem can be formulated as a Markov decision process (MDP) and deep reinforcement learning could be very promising [125]. Depending on the nature of the problem, one can compare the performance of classic MAB-based methods and deep learning or deep reinforcement learning methods with respect to the system performance and computational complexity similarly to [126].

NOMA and multi-antenna systems: while NOMA was originally intended for single-antenna deployments, it is inefficient in most multi-antenna deployments [127]. The first false assumption about NOMA is that it is an effective strategy in multi-antenna settings since it achieves capacity in single-antenna settings for the broadcast channels. In [128], massive multiple-input multiple-output (MIMO) was compared to NOMA where it was analytically proven that when the number of antennas at the transmitter is equal to the number of users, NOMA outperforms massive MIMO. However, when the number of antennas is much larger than the users, massive MIMO outperforms NOMA. Also in [129], the joint spectral efficiency and energy efficiency maximization was investigated where it was shown that the rate splitting multiple access (RSMA) technique outperforms NOMA in a multiple-input single-output setting.

Therefore, an interesting area of research is to extensively investigate in which situations NOMA performs better than other multi-antenna technologies. Additionally, a hybrid approach could be used to pair clusters by identifying the users that would benefit from NOMA while the rest are served via other multi-antenna technologies.

Application of Reconfigurable Intelligent Surfaces within NOMA: as discussed in Section 2.1, the performance gain of NOMA over OMA relies on the exploitation of the users' asymmetric channels condition. This gain becomes limited when the channel conditions are not suitable for its implementation (e.g., in the case of symmetric channels). The users' channel conditions have always been regarded as being fixed and non-tunable where they depend only on the propagation environment. Moreover, the users are assigned a decoding order that primarily depends on the order of their channel conditions. Therefore, users with lower decoding order, i.e., weak users, may only achieve poor data rates as a result of the uncontrolled inter-user interference, while users with higher decoding order, i.e., strong users, can obtain higher data rates by applying SIC to cancel the inter-user interference [125]. However in practice, and especially in heterogeneous networks, the QoS requirements of users may not line up with the order of their channels condition where, for example, a weak user may require a higher data rate than a strong user.

Reconfigurable Intelligent Surfaces (RIS) can help overcome these issues where, as defined in Section 2.2, they have the capability of smartly modifying the wireless communication environment. Therefore, implementing RIS with NOMA would be an attractive research direction, ensuring that the propagation environment of the multiplexed users is intelligently and efficiently customized to reap the benefits of NOMA [130]. The channel asymmetry between users can be increased rather than being dictated by the wireless environment by carefully choosing the location and the design of the reflection coefficients of the RIS, resulting in a higher gain over OMA. Moreover, the users decoding order can be arranged according to their QoS requirements while RIS can help achieve the corresponding desired arrangement of the channels condition [125].

Appendix A

Proof of Theorem 1

We denote $\theta_k(\mathbf{p}) = \sum_{i=1}^{k} p_k, \forall 1 \leq k \leq K$ with $\theta_0(\mathbf{p}) = 0$. The Lagrangian of the convex problem (3.10) is given by

$$\begin{aligned}\mathcal{L} =& \sum_{i=1}^{K} \frac{1}{2} \log_2 \left(\frac{1 + H_{i|0}\theta_i(\mathbf{p})}{1 + H_{i|0}\theta_{i-1}(\mathbf{p})} \right) - \alpha \left(\theta_K(\mathbf{p}) + P_c \right) + \lambda \left(P_{\max} - \theta_K(\mathbf{p}) \right) \\ &+ \sum_{i=1}^{K} \beta_i \left(\theta_i(\mathbf{p}) - A_i \theta_{i-1}(\mathbf{p}) - \frac{A_i - 1}{H_{i|0}} \right), \end{aligned} \tag{A.1}$$

where λ and $\boldsymbol{\beta} = (\beta_1, \ldots, \beta_K)$ are the positive Lagrange multipliers for the overall power constraint and the K minimum rate constraints, respectively. The KKT optimality conditions are necessary and sufficient for optimality for convex optimization problems and they imply that $\frac{\partial \mathcal{L}}{\partial p_k} = 0, \ \forall k$, at the solution. Thus, we also have that the difference between two consecutive Lagrange derivatives equals zero: $\frac{\partial \mathcal{L}}{\partial p_{k+1}} - \frac{\partial \mathcal{L}}{\partial p_k} = 0$, which leads to the following equations

$$A_{k+1}\beta_{k+1} = \frac{1}{2 \ln 2} \left(\frac{H_{k|0}}{1 + H_{k|0}\theta_k(\mathbf{p})} - \frac{H_{k+1|0}}{1 + H_{k+1|0}\theta_k(\mathbf{p})} \right) + \beta_k, \tag{A.2}$$

for all $k \in \{1, \ldots, K-1\}$. We discuss two cases below.

i) If $H_{1|0} > H_{2|0}$ then $\beta_1 \geq 0$ and $A_2 > 0$, the above equation for $k = 1$ implies that $\beta_2 > 0$. Since $H_{k|0} \geq H_{k+1|0}$ and $A_{k+1} > 0$, for all $k \geq 2$, the fact that $\beta_2 > 0$ has a cascading effect in the above equations and leads to $\beta_{k+1} > 0, \ \forall k \in \{2, \ldots, K-1\}$. Hence, we have that $\beta_k > 0, \ \forall k \geq 2$. This means that all QoS constraints of all weaker users, $k \geq 2$, are active at the solution and they meet no more than their minimum rate requirement

$$\theta_k(\mathbf{p}) = A_k \theta_{k-1}(\mathbf{p}) + \frac{A_k - 1}{H_{k|0}}, \quad \forall k > 1. \tag{A.3}$$

By induction, we can show that

$$\theta_k(\mathbf{p}) = \theta_1(\mathbf{p}) \prod_{i=2}^{k} A_i + \sum_{i=2}^{k-1} \frac{A_i - 1}{H_{i|0}} \prod_{j=i+1}^{k} A_j + \frac{A_k - 1}{H_{k|0}}, \quad \forall k > 1. \tag{A.4}$$

Knowing that $p_k = \theta_k(\mathbf{p}) - \theta_{k-1}(\mathbf{p})$, for all $k > 1$, and that $\theta_1(\mathbf{p}) = p_1$, the above equations allow us to express all the powers allocated to the weaker users as functions of p_1, the power allocated to the strongest user as in (3.11). Hence, the multi-variable problem in (3.10) is reduced to the following single variable problem

$$\max_{p_1} f_1(p_1) \text{ s.t. } \ell \leq p_1 \leq u, \tag{A.5}$$

where the new objective function is

$$f_1(p_1) = \frac{1}{2}\log_2(1+H_{1|0}p_1) + \frac{1}{2}\log_2\prod_{i=2}^{K} A_i - \alpha\left(p_1\prod_{i=2}^{K}A_i + \sum_{i=2}^{K-1}\frac{A_i-1}{H_{i|0}}\prod_{j=i+1}^{K}A_j + \frac{A_K-1}{H_{K|0}} + P_c\right), \tag{A.6}$$

and the lower and upper bounds on p_1, coming from the QoS and maximum power constraints, are given in (3.12) and (3.13) respectively. The second-order partial derivative of (A.6) w.r.t p_1 equals

$$\frac{\partial^2 f_1(p_1)}{\partial p_1^2} = \frac{-1}{2\ln 2} \times \frac{(H_{1|0})^2}{(1+H_{1|0}p_1)^2}. \tag{A.7}$$

Hence, the objective function $f_1(p_1)$ is concave w.r.t p_1 and the optimal solution $p_1^*(\alpha)$ is either the critical point $\overline{p_1}(\alpha)$ in (3.14) canceling the first order derivative, or one of the borders of the new feasible set.

ii) If $H_{1|0} = H_{2|0}$, the main trick is to consider receiver 1 and 2 as a single entity, having the strongest channel gains $H'_{1|0} = H_{1|0} = H_{2|0}$, and whose achievable data rate and allocated power are considered as $R'_1 = (R_1 + R_2)$ and $p'_1 = p_1 + p_2$ respectively. Having done this variable change, the same discussion follows subsequently as i); two cases arise: a) $H'_{1|0} = H_{3|0}$, and b) $H'_{1|0} > H_{3|0}$. In the latter, we obtain the analytical closed-form expressions of $p_k^*, \forall k \geq 3$ as a function of p'_1 and p'^*_1 is obtained by solving the resulting problem in (A.5). Then, we can split the power p'^*_1 such that p_2^* is the enough power required to satisfy the QoS requirement for receiver 2, and the remaining power $p_1^* = (p'_1)^* - p_2^*$. In the former case, a recurring reasoning can be applied etc.

Finally, the same reasoning applies in the fully symmetric case, in which $H_{1|0} = H_{2|0} = \ldots = H_{K|0}$. Note that such an extreme case is quite unlikely to occur in practice. Moreover, NOMA in this case would likely not outperform OMA since it exploits the channel gain difference between different receivers as shown in Section 2.1. This concludes the proof.

Appendix B

Proof of Theorem 2

Since only the sum rate term in the energy-efficiency objective depends on the reflection coefficient ρ, we can only focus on optimizing the sum rate. Let $\theta_k(\mathbf{p}) = \sum_{i=1}^{k} p_k$ with $\theta_0(\mathbf{p}) = 0$ and $f(\rho)$ denote the sum rate as a function of the reflection coefficient ρ for a fixed power allocation vector $\mathbf{p}$

$$f(\rho) = \sum_{k=1}^{K} \frac{1}{2} \log_2 \left(\frac{1 + H_{k|1}(\rho)\theta_k(\mathbf{p})}{1 + H_{k|1}(\rho)\theta_{k-1}(\mathbf{p})} \right). \tag{B.1}$$

Knowing that $H_{k|1} = \frac{(h_k + \sqrt{\rho} g g_k)^2}{\sigma_k^2}$, the first-order and second-order derivatives of $f(\rho)$ are respectively given by

$$\begin{aligned} \frac{\partial f(\rho)}{\partial \rho} =& \frac{1}{2 \ln 2} \sum_{k=1}^{K} \frac{2 h_k g g_k (\rho)^{-1/2} + (g g_k)^2}{\left(\frac{\sigma_k^2}{\theta_k(\mathbf{p})} + \left(h_k^2 + 2 h_k g g_k \sqrt{\rho} + (g g_k)^2 \rho \right) \right)} - \frac{2 h_k g g_k (\rho)^{-1/2} + (g g_k)^2}{\left(\frac{\sigma_k^2}{\theta_{k-1}(\mathbf{p})} + \left(h_k^2 + 2 h_k g g_k \sqrt{\rho} + (g g_k)^2 \rho \right) \right)} \\ \geq & 0, \end{aligned} \tag{B.2}$$

$$\begin{aligned} \frac{\partial^2 f(\rho)}{\partial \rho^2} =& \frac{1}{2 \ln 2} \sum_{k=1}^{K} \frac{-h_k g g_k (\rho)^{-3/2}}{\left(\frac{\sigma_k^2}{\theta_k(\mathbf{p})} + \left(h_k^2 + 2 h_k g g_k \sqrt{\rho} + (g g_k)^2 \rho \right) \right)} + \frac{h_k g g_k (\rho)^{-3/2}}{\left(\frac{\sigma_k^2}{\theta_{k-1}(\mathbf{p})} + \left(h_k^2 + 2 h_k g g_k \sqrt{\rho} + (g g_k)^2 \rho \right) \right)} \\ & - \frac{\left(h_k g g_k (\rho)^{-1/2} + (g g_k)^2 \right) \left(2 h_k g g_k (\rho)^{-1/2} + (g g_k)^2 \right)}{\left(\frac{\sigma_k^2}{\theta_k(\mathbf{p})} + \left(h_k^2 + 2 h_k g g_k \sqrt{\rho} + (g g_k)^2 \rho \right) \right)^2} \\ & + \frac{\left(h_k g g_k (\rho)^{-1/2} + (g g_k)^2 \right) \left(2 h_k g g_k (\rho)^{-1/2} + (g g_k)^2 \right)}{\left(\frac{\sigma_k^2}{\theta_{k-1}(\mathbf{p})} + \left(h_k^2 + 2 h_k g g_k \sqrt{\rho} + (g g_k)^2 \rho \right) \right)^2} \leq 0. \end{aligned} \tag{B.3}$$

Since $\theta_k(\mathbf{p}) \geq \theta_{k-1}(\mathbf{p})$ by construction, the sum rate $f(\rho)$ is increasing and concave in ρ. Hence, in order to maximize the sum rate, the reflection coefficient ρ must be chosen as large as possible while meeting the constraints of (**EE1**). In particular, the constraints (C2)-(C4) depend on ρ.

Since $H_{k|1}(\rho)$ is an increasing function of $\rho \in [0,1]$, we can see that the higher the value of ρ the less constrained (C2) becomes, implying a larger possible set for the other variables of the problem: $\theta_k(\mathbf{p}),\ \forall k$. Hence, choosing the largest value of ρ is optimal in terms of (C2).

Now, to compute the largest possible value of ρ, we can focus only on the constraints (C3) and (C4) with no loss of optimality. These constraints require that $\gamma_{k\to i} \geq \gamma_{k\to k}$, $\forall\ k \geq 2, \forall i \leq k-1$ and $0 \leq \rho \leq 1$.

First, note that for any user $k \geq 2$ and any $i \leq k-1$, we have the following equivalencies

$$\begin{aligned} & \gamma_{k\to i} \geq \gamma_{k\to k} \\ \Leftrightarrow \quad & \frac{H_{i|1}(\rho)p_k}{H_{i|1}(\rho)\sum_{j=1}^{k-1}p_j+1} \geq \frac{H_{k|1}(\rho)p_k}{H_{k|1}(\rho)\sum_{j=1}^{k-1}p_j+1} \\ \Leftrightarrow \quad & H_{i|1}(\rho) \geq H_{k|1}(\rho), \end{aligned} \tag{B.4}$$

where the first equivalence follows from our notations and the definitions of $\gamma_{k\to i}$ and $\gamma_{k\to k}$ in (4.6); and the second equivalence is obtained after some simple derivations. Hence, constraint (C3) is equivalent to the following set of $k-1$ constraints: $H_{1|1}(\rho) \geq H_{k|1}(\rho), \ldots,$ and $H_{k-1|1}(\rho) \geq H_{k|1}(\rho)$, for any user $k \geq 2$.

For example, for user $k=2$, the only constraint writes as $H_{1|1}(\rho) \geq H_{2|1}(\rho)$. For user $k=3$, the two constraints write as $H_{1|1}(\rho) \geq H_{3|1}(\rho),$ and $H_{2|1}(\rho) \geq H_{3|1}(\rho)$. All these constraints simplify to $H_{1|1}(\rho) \geq H_{2|1}(\rho) \geq H_{3|1}(\rho)$. The same reasoning can be extended up to user K, and all the constraints reduce to

$$H_{1|1}(\rho) \geq H_{2|1}(\rho) \geq ... \geq H_{K|1}(\rho). \tag{B.5}$$

Now we focus on a single inequality of the form $H_{k|1}(\rho) \leq H_{k+1|1}(\rho)$ in the inequality chain above. The aim is to find the largest value of $\rho \in [0,1]$ fulfilling this constraint, which can be equivalently expressed as

$$\begin{aligned} & H_{k|1}(\rho) \leq H_{k+1|1}(\rho) \\ \Leftrightarrow \quad & \frac{(h_k+\sqrt{\rho}gg_k)^2}{\sigma_k^2} \leq \frac{(h_{k+1}+\sqrt{\rho}gg_{k+1})^2}{\sigma_{k+1}^2} \\ \Leftrightarrow \quad & g(\tfrac{g_{k+1}}{\sigma_{k+1}} - \tfrac{g_k}{\sigma_k})\sqrt{\rho} \geq (\tfrac{h_k}{\sigma_k} - \tfrac{h_{k+1}}{\sigma_{k+1}}), \end{aligned} \tag{B.6}$$

where the first equivalence follows from the definition of $H_{k|1}(\rho)$ and $H_{(k+1)|1}(\rho)$ and the second one by simply rearranging the terms. Two cases can arise based on the order of g_{k+1} and g_k:

a) If $g_{k+1} > g_k$, since $\frac{h_k}{\sigma_k} \geq \frac{h_{k+1}}{\sigma_{k+1}}$ by assumption, the constraints (B.6) and $C(4)$ of the optimization problem lead to the following upper bounds

$$\rho = \min\left\{1, \left(\frac{h_k}{\sigma_k} - \frac{h_{k+1}}{\sigma_{k+1}}\right)^2 \Big/ \left(g(\frac{g_{k+1}}{\sigma_{k+1}} - \frac{g_k}{\sigma_k})\right)^2\right\}, \quad \forall k > 1. \tag{B.7}$$

b) If $g_{k+1} \leq g_k$, then (B.6) becomes trivial since $\frac{h_k}{\sigma_k} \geq \frac{h_{k+1}}{\sigma_{k+1}}$ by assumption. In this case, we only have the constraint $C(4)$ to be met: $0 \leq \rho \leq 1$.

Taking all this into account, the optimal reflection coefficient ρ^* can be expressed as in Theorem 2, which completes the proof.

Appendix C

Proof of Theorem 3

The objective function of (**EE3**) is increasing w.r.t ρ_1 for fixed $\mathbf{p}$ and ρ_2; and, is also increasing w.r.t ρ_2 for fixed $\mathbf{p}$ and ρ_1; the optimal reflection coefficients lie on the Pareto boundary, i.e., all feasible points such that none of their coordinates can be increased while remaining feasible, of the feasible set defined by the constraints $(C3) - (C4)$. After some mathematical derivations, the constraint $(C3)$ can be rewritten as $\sqrt{\rho_1}(G_{12} - G_{11}) + \sqrt{\rho_2}(G_{22} - G_{21}) \leq G_1 - G_2$.

We now provide the optimal values of (ρ_1, ρ_2) by analyzing geometrically the feasible set and its Pareto optimal boundary in the four possible cases given in Theorem 3.

Case [H1]: $(G_{12} - G_{11}) \leq 0$ and $(G_{22} - G_{21}) \leq 0$

In this case, since $(G_1 - G_2) \geq 0$ by assumption, the constraints are always fulfilled for all values of $\rho_1, \rho_2 \in [0, 1]$. Hence, the optimal solution is unique $\rho_1^* = \rho_2^* = 1$.

Case [H2]: $(G_{12} - G_{11}) \leq 0$ and $(G_{22} - G_{21}) > 0$

Under [H2], one can show that $\overline{\rho_1} < 0$; $\overline{\rho_2} \geq 0$ and $\widetilde{\rho_2} > \overline{\rho_2}$. Several cases can arise depending on the value of $\overline{\rho_2}$ as depicted in Figure C.1.
[**H21**] If $\overline{\rho_2} > 1$, which leads to $\widetilde{\rho_1} < 0$ and $\widetilde{\rho_2} > 1$, the optimal solution is unique: $\rho_1^* = \rho_2^* = 1$.
Otherwise $\overline{\rho_2} \leq 1$ leads to $\widetilde{\rho_1} \geq 0$ and $\widetilde{\rho_2} > \overline{\rho_2} \geq 0$. Two sub-cases arise: either [**H221**] if $\widetilde{\rho_2} > 1$, then $\rho_1^* = \rho_2^* = 1$; or [**H222**] if $\widetilde{\rho_2} \leq 1$, then the Pareto optimal boundary also reduces to a unique point $\rho_1^* = 1, \rho_2^* = \widetilde{\rho_2}$.

Hence to summarize, the optimal values of the reflection coefficients are given as $\rho_1^* = 1; \rho_2^* = \min\{1, \widetilde{\rho_2}\}$.

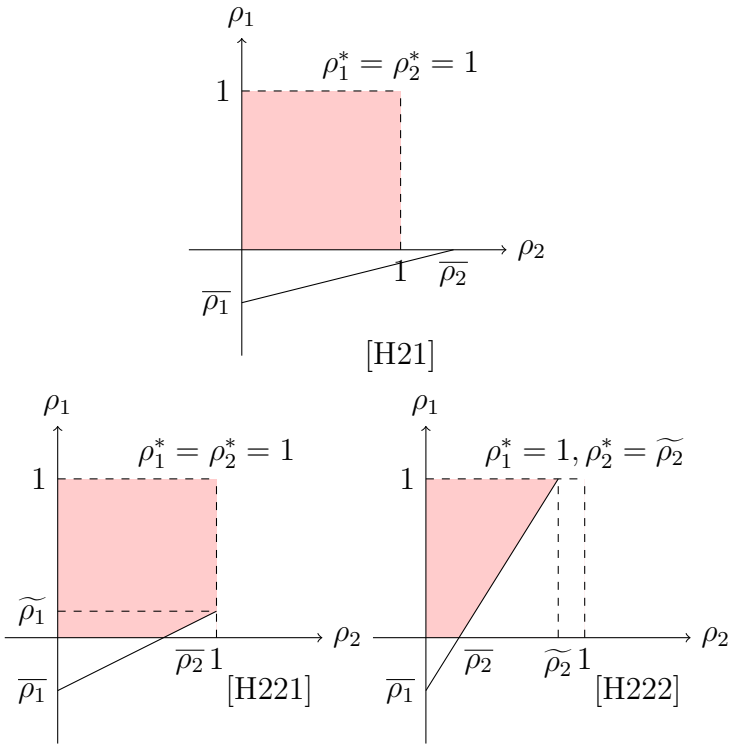

Figure C.1: The three cases that can arise under [H2]: the feasible set is depicted in red. The Pareto boundary reduces to a unique solution.

Case [H3]: $(G_{12} - G_{11}) > 0$ and $(G_{22} - G_{21}) \leq 0$

This case is similar to the previous case [H2], hence the detailed proof is omitted.

Case [H4]: $(G_{12} - G_{11}) > 0$ and $(G_{22} - G_{21}) > 0$

We can prove the following:
$\overline{\rho_i} \geq 0$ and $\widetilde{\rho}_i \leq \overline{\rho_i}$, $\forall i \in \{1, 2\}$;
If $\overline{\rho_i} > 1$, then $\widetilde{\rho_j} > 0$, $\forall i, j \in \{1, 2\}$ s.t. $j \neq i$;
If $\overline{\rho_i} < 1$, then $\widetilde{\rho_j} < 0$, $\forall i, j \in \{1, 2\}$ s.t. $j \neq i$;
If $\widetilde{\rho}_i > 1$, then $\widetilde{\rho_j} > 1$, $\forall i, j \in \{1, 2\}$ s.t. $j \neq i$;
If $\widetilde{\rho}_i < 1$, then $\widetilde{\rho_j} < 1$, $\forall i, j \in \{1, 2\}$ s.t. $j \neq i$.

The optimal solution lies on the Pareto boundary of the feasible set depicted in red in Figure C.2. Note that except for the sub-case [H41], the Pareto boundary of the feasible set is not unique but a continuous segment (in blue) of the line between $\overline{\rho_1}$ and $\overline{\rho_2}$. This set can be characterized in a parametric manner as $\rho_1 = \beta\overline{\rho_1}$, $\rho_2 = (1 - \beta)\overline{\rho_2}$, where β ranges over the interval specified in each subcases of Figure C.2. Note that except for subcase [H41], $H_{1|1,1}(\boldsymbol{\rho}) = H_{2|1,1}(\boldsymbol{\rho})$.

In [H41], both $\overline{\rho_i}$ and $\widetilde{\rho}_i$, $i \in \{1, 2\}$, are larger than 1, hence the optimal solution is $\rho_1^* = \rho_2^* = 1$. In the other four cases, we need to find the reflection coefficients on the

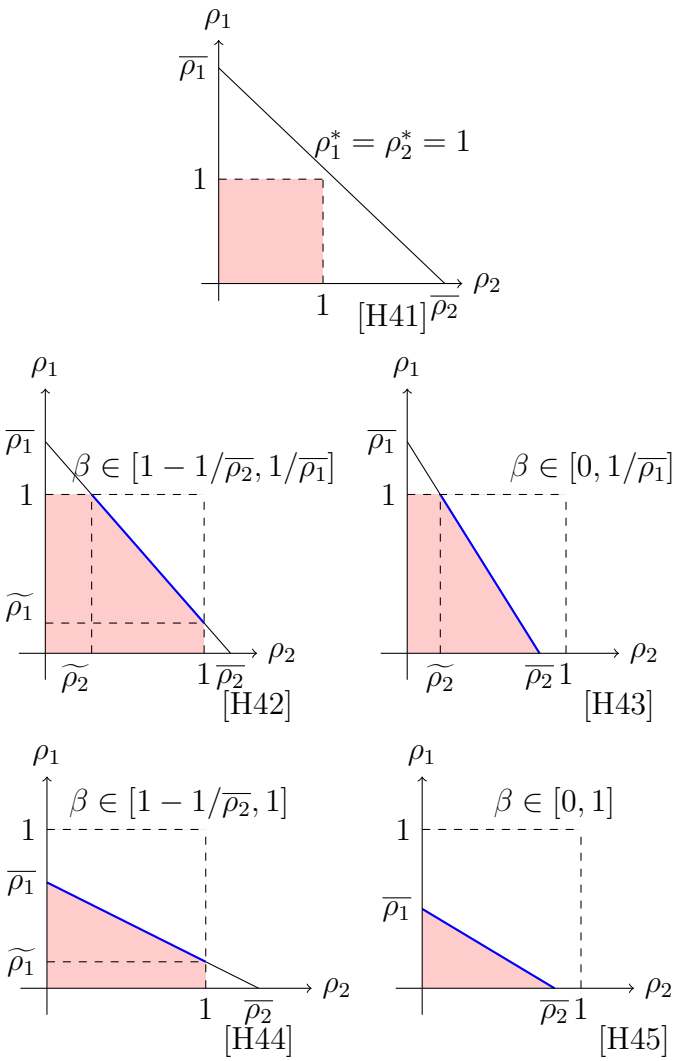

Figure C.2: The five cases that can arise under [H4]: the feasible set is depicted in red. The Pareto boundary in cases [H42]-[H44] is the blue segment given by $\rho_1 = \beta\overline{\rho_1}; \rho_2 = (1-\beta)\overline{\rho_2}$.

Pareto boundary: $\rho_1 = \beta\overline{\rho_1}$, $\rho_2 = (1-\beta)\overline{\rho_2}$, which maximize the objective function. Hence, the problem is reduced to a single variable optimization over β, whose objective is

$$f(\beta) = \log_2\left(1 + (p_1+p_2)(G_2 + \beta\overline{\rho_1}G_{12} + (1-\beta)\overline{\rho_2}G_{22})\right),$$

of derivative

$$\begin{aligned}\frac{\partial f(\beta)}{\partial \beta} &= \frac{(p_1+p_2)(G_{12}\overline{\rho_1} - G_{22}\overline{\rho_2})}{\ln 2(1 + (p_1+p_2)H_{2|1,1}(\beta))} \\ &\propto (G_{12}\overline{\rho_1} - G_{22}\overline{\rho_2}) \\ &\propto \frac{(G_1 - G_2)(G_{22}G_{11} - G_{12}G_{21})}{(G_{12} - G_{11})(G_{22} - G_{21})}.\end{aligned}$$

Hence, the objective function is either decreasing or increasing w.r.t β depending on the sign of $(G_{22}G_{11} - G_{12}G_{21})$.

a) If $(G_{22}G_{11} - G_{12}G_{21}) \geq 0$, the objective function is increasing in β, hence its optimal value is the upper-bound of its feasible interval, specified in each sub-case.

b) If $(G_{22}G_{11} - G_{12}G_{21}) < 0$, the objective function is decreasing in β, hence its optimal value is the lower-bound of its feasible interval, specified in each sub-case.

This completes the Proof.

Appendix D

Information-theoretic achievable rate region

D.1 Proof of Theorem 4

First, we have to introduce the proper information-theoretic definitions needed for the coding and decoding procedures. We consider a two-sender K-receiver discrete memoryless channel defined by the tuple $(\mathcal{X} \times \mathcal{B}, p(y_1, \ldots, y_K|x, b), \mathcal{Y}_1 \times \ldots \times \mathcal{Y}_K)$ that consists of $K + 2$ finite sets: $\mathcal{X}$, $\mathcal{B}$, $\mathcal{Y}_1, \ldots,$ $\mathcal{Y}_K$ and a collection of conditional probability mass functions (pmfs) $p(y_1, \ldots, y_2|x, b)$ defined on $\mathcal{Y}_1 \times \ldots \times \mathcal{Y}_K$. A $(2^{nR_0}, 2^{nR_1}, \ldots, 2^{nR_K}, n)$ code consists of:

- ▷ $K + 1$ message sets $[1 : 2^{nR_0}]$, $[1 : 2^{nR_1}], \ldots,$ $[1 : 2^{nR_K}]$,
- ▷ two encoders, where encoder 1, the source, assigns a codeword $x^n(m_1, \ldots, m_K)$ to each message $(m_1, \ldots, m_K) \in [1 : 2^{nR_1}] \times \ldots \times [1 : 2^{nR_K}]$ and encoder 2, the backscatter device, assigns a codeword $b^n(m_0)$ to each message $m_0 \in [1 : 2^{nR_0}]$,
- ▷ K decoders, where decoder $i \in \{1, \ldots, K\}$ (or receiver, or user i) assigns an estimate $(\hat{m}_{0\to i}, \hat{m}_{K\to i} \ldots \hat{m}_{i+1\to i}, \hat{m}_{i\to i}) \in [1 : 2^{nR_0}] \times [1 : 2^{nR_K}] \times \ldots \times [1 : 2^{nR_{i+1}}] \times [1 : 2^{nR_i}]$, or an error message e to each received sequence y_i^n, where $\hat{m}_{j\to i}, j \in \{K, \ldots, i\}$ represents the estimation of m_j when decoded by receiver i.

We assume that the message, which is a $K+1$ tuple: $(M_0, M_1, \ldots, M_K)$, is uniformly distributed over $[1 : 2^{nR_0}] \times [1 : 2^{nR_1}] \times, \ldots, \times [1 : 2^{nR_K}]$. The average probability of error is then defined as $P_e^n = \mathbb{P}\left\{ \bigcup_{\forall i} (\hat{M}_{0\to i}, \hat{M}_{i\to i}) \neq (M_0, M_i) \right\}$

Codebook generation

Encoder 1: Fix the pmfs $p(u_K)p(u_{K-1}|u_K) \ldots p(x|u_2, \ldots, u_K)$.
i) First, randomly and independently generate 2^{nR_K} sequences $u_K^n(m_K) \in [1 : 2^{nR_K}]$ each according to $\prod_{i=1}^n p_{U_K(u_{i,K})}$.

ii) For each $m_{k+1} \in [1 : 2^{nR_{k+1}}], k \in \{K-1, K-2, \ldots, 2\}$ successively in this order, randomly and conditionally independently generate 2^{nR_k} sequences $u_k^n(m_k, m_{k+1}, \ldots, m_K)$, for all $m_k \in [1 : 2^{nR_k}]$, each according to
$\prod_{i=1}^n p_{U_k|U_{k+1},\ldots,U_K}(u_{i,k}|u_{i,k+1}(m_{k+1}, \ldots, m_K), \ldots, u_{i,K}(m_K))$.
iii) For each $m_2 \in [1 : 2^{nR_2}]$ randomly and conditionally independently generate 2^{nR_1} sequences $x^n(m_1,\ldots, m_K), m_1 \in [1 : 2^{nR_1}]$ each according to $\prod_{i=1}^n p_{X|U_2,..,U_K}(x_i|u_{i,2}(m_2,..., m_K),..., u_{i,K}(m_K))$. To send message $(m_1, \ldots, m_K)$, encoder 1 transmits codeword $x^n(m_1, \ldots, m_K)$.

Encoder 2: Randomly and independently generate 2^{nR_0} sequences $b^n(m_0), m_0 \in [1 : 2^{nR_0}]$, each according to $\prod_{i=1}^n p_B(b_i)$. To send message m_0, encoder 2 transmits codeword $b^n(m_0)$.

Decoding procedure

Decoder K decides that $(\hat{m}_{0\to K}, \hat{m}_{K\to K})$ was sent, if it is the unique message pair such that $(u_K^n(\hat{m}_{K\to K}), b^n(\hat{m}_{0\to K}), y_K^n) \in \mathcal{T}_\epsilon^{(n)}$; otherwise it declares an error.

Each decoder $i \in \{1, \ldots, K-1\}$ successively decodes the messages $m_j, j \in \{K, \ldots, i+1\}$ in this specific order by the following steps.
i) Each decoder i first jointly decodes U_K and B and decides that $(\hat{m}_{0\to i}, \hat{m}_{K\to i})$ was sent, if it is the unique pair such that $\{(u_K^n(\hat{m}_{K\to i}), b^n(\hat{m}_{0\to i}), y_i^n) \in \mathcal{T}_\epsilon^n\}$; otherwise it declares an error.
ii) If such $(\hat{m}_{0\to i}, \hat{m}_{K\to i})$ is found, decoder i declares that $\hat{m}_{i\to i}$ is sent if it is the unique message such that
$\{(u_K^n(\hat{m}_{K\to i}), u_{K-1}^n(\hat{m}_{K-1\to i}, \hat{m}_{K\to i}), \ldots, u_i^n(\hat{m}_{i\to i}, \ldots, \hat{m}_{K\to i}), b^n(\hat{m}_{0\to i}), y_i^n) \in \mathcal{T}_\epsilon^n\}$, where the estimates $\hat{m}_{j\to i}, j \in \{K-1,..., i+1\}$ are obtained in a successive manner starting from $\hat{m}_{K-1\to i}$ to $\hat{m}_{i+1\to i}$ as decoder i declares that $\hat{m}_{j\to i}, j \in \{K-1,..., i+1\}$ is sent if it is the unique message such that
$\{(u_K^n(\hat{m}_{K\to i}), u_{K-1}^n(\hat{m}_{K-1\to i}, \hat{m}_{K\to i}),..., u_j^n(\hat{m}_{j\to i},..., \hat{m}_{K\to i}), b^n(\hat{m}_{0\to i}), y_i^n) \in \mathcal{T}_\epsilon^n\}$; otherwise, it declares an error. Note that whenever an error has been declared, the decoding process stops.

Analysis of the probability of error

Assume without loss of generality that the message $(M_0 = M_1 = \ldots = M_K = 1)$ was sent [40]. By the symmetry of code generation, the probability of error averaged over all possible codebooks and messages is: $\mathbb{P}(\varepsilon) = \mathbb{P}(\varepsilon|M_0 = M_1 = ... = M_K = 1)$.

Let us focus on the decoder $i \in \{1, ..., K\}$. In the SIC decoding procedure, decoder i first decodes messages destined to receivers $j \in \{K, K-1, \ldots, i+1\}$ before decoding its own message. Hence, decoder i declares an error if at least one of the following error events occurs

$$
\begin{aligned}
\varepsilon_{i,1} =& \{(u_K^n(1), b^n(1), y_i^n) \notin \mathcal{T}_\epsilon^{(n)}\}, \textit{ non-joint typicality;} \\
\varepsilon_{i,2} =& \{(u_K^n(1), b^n(m_{0\to i}), y_i^n) \in \mathcal{T}_\epsilon^{(n)},\ m_{0\to i} \neq 1\}, m_{0\to i} \textit{ not successfully decoded;} \\
\varepsilon_{i,3} =& \{(u_K^n(m_{K\to i}), b^n(1), y_i^n) \in \mathcal{T}_\epsilon^{(n)},\ m_K \neq 1\}, m_{K\to i} \textit{ not successfully decoded;} \\
\varepsilon_{i,4} =& \{(u_K^n(m_{K\to i}), b^n(m_{0\to i}), y_i^n) \in \mathcal{T}_\epsilon^{(n)}, m_{0\to i} \neq 1, m_{K\to i} \neq 1\}, \\
& \quad m_{0\to i} \textit{ and } m_{K\to i} \textit{ not successfully decoded;} \\
\varepsilon_{i,j,5} =& \{(u_K^n(1), \ldots, u_j^n(1, \ldots, 1), b^n(1), y_i^n) \notin \mathcal{T}_\epsilon^{(n)}, \quad i+1 \leq j \leq K-1\}, \textit{ non-joint typicality;} \\
\varepsilon_{i,j,6} =& \{(u_K^n(1), \ldots, u_j^n(m_{j\to i}, 1, \ldots, 1), b^n(1), y_i^n) \in \mathcal{T}_\epsilon^{(n)},\ m_{j\to i} \neq 1\}, m_{j\to i} \textit{ not successfully decoded;} \\
\varepsilon_{i,i,7} =& \{(u_K^n(1), \ldots, u_i^n(m_{i\to i}, 1, \ldots, 1), b^n(1), y_i^n) \notin \mathcal{T}_\epsilon^{(n)}\},\ \textit{non-joint typicality;} \\
\varepsilon_{i,i,8} =& \{(u_K^n(1), \ldots, u_i^n(m_{i\to i}, 1, \ldots, 1), b^n(1), y_i^n) \in \mathcal{T}_\epsilon^{(n)}, m_{i\to i} \neq 1\}, m_{i\to i} \textit{ not successfully decoded.}
\end{aligned}
$$

By the union bound of events, we obtain $\mathbb{P}(\varepsilon_i) \leq \mathbb{P}(\varepsilon_{i,1}) + \ldots + \mathbb{P}(\varepsilon_{i,i,8})$. Let us now bound each term individually. By the law of large numbers (LLN), the probabilities $\mathbb{P}(\varepsilon_{i,1})$, $\mathbb{P}(\varepsilon_{i,j,5})$ and $\mathbb{P}(\varepsilon_{i,i,7})$ can be shown to tend to zero as $n \to \infty$. By the packing lemma [40, Lemma 3.1], $\mathbb{P}(\varepsilon_{i,2})$ tends to zero as $n \to \infty$ if $R_{0\to i} \leq \mathbb{I}(B; U_K, Y_i) - \delta(\varepsilon)$. Furthermore, since B is independent of U_K, then $\mathbb{I}(B; U_K, Y_i) = \mathbb{I}(B; Y_i|U_K)$. Hence, $\mathbb{P}(\varepsilon_{i,2})$ tends to zero as $n \to \infty$ if $R_{0\to i} \leq \mathbb{I}(B; Y_i|U_K) - \delta(\varepsilon),\ \forall\ 1 \leq i \leq K$. Similarly, the error probabilities $\mathbb{P}(\varepsilon_{i,3})$, $\mathbb{P}(\varepsilon_{i,4})$, $\mathbb{P}(\varepsilon_{i,j,6})$, and $\mathbb{P}(\varepsilon_{i,i,8})$ tend to zero as $n \to \infty$, if the following conditions are met

$$
\begin{aligned}
R_{K\to i} &\leq \mathbb{I}(U_K; Y_i|B) - \delta(\epsilon), \quad \forall\ 1 \leq i \leq K, && \text{(D.1)} \\
R_{0\to i} + R_{K\to i} &\leq \mathbb{I}(U_K, B; Y_i) - \delta(\epsilon), \quad \forall\ 1 \leq i \leq K, && \text{(D.2)} \\
R_{j\to i} &\leq \mathbb{I}(U_j; Y_i|B, U_K, \ldots, U_{j+1}) - \delta(\epsilon), \quad \forall\ 1 \leq j \leq K-1, \forall i < j, && \text{(D.3)} \\
R_{i\to i} &\leq \mathbb{I}(U_i; Y_i|B, U_K, \ldots, U_{i+1}) - \delta(\epsilon), \quad \forall\ 1 \leq i \leq K-1. && \text{(D.4)}
\end{aligned}
$$

The message intended for receiver $j \in \{1, \ldots, K-1\}$ is decoded by receivers $i \in \{1, \ldots, j-1\}$ and receiver j with a data rate $R_{j\to i}$ and $R_{j\to j}$, respectively. Therefore, the achievable data rate for decoding M_j is $R_j \leq \min_{i<j}(R_{j\to i}, R_{j\to j}) \overset{(a)}{=} \min_{i\leq j} \mathbb{I}(U_j; Y_i|B, U_K, \ldots, U_{i+1}),\ \forall\ 1 \leq j \leq K-1$, where (a) follows from (D.3) and (D.4). Further, the achievable rate for decoding M_0 and M_K are defined as $R_0 \leq \min_{1\leq i\leq K} R_{0\to i}$ and $R_K \leq \min_{1\leq i\leq K} R_{K\to i}$ and are constrained as

$$
R_0 \leq \min_{1\leq i\leq K} \mathbb{I}(B; Y_i|U_K), \quad R_K \leq \min_{1\leq i\leq K} \mathbb{I}(U_K; Y_i|B), \quad R_0 + R_K \leq \min_{1\leq i\leq K} \mathbb{I}(U_K, B; Y_i), \quad \text{(D.5)}
$$

which completes the proof of Theorem 4.

D.2 Proof of Theorem 5

From Lemma (1), the achievable rate for decoding the message destined to receiver j satisfies

$$\begin{aligned} R_j &\leq \min_{i\leq j} \mathbb{I}(U_j; Y_i|B, U_K, \ldots, U_{j+1}), \quad \forall 1 \leq j \leq K-1, \\ &\overset{(b)}{=} qC\left(\min_{i\leq j}(\gamma_{j\to i|1})\right) + (1-q)C\left(\min_{i\leq j}(\gamma_{j\to i|0})\right), \quad \forall\ 1 \leq j \leq K-1, \end{aligned} \tag{D.6}$$

where (b) follows from $B \sim \text{Bern(q)}$, $U_k \sim \mathcal{N}(0, p_k)$, $\forall k \in \{2, ..., K\}$ and $X = \sum_{k=2}^{K} U_k + V$, with $V \sim \mathcal{N}(0, p_1)$, which maximizes the mutual information expressions in (D.6) and yields the capacity of the point-to-point additive white Gaussian noise (AWGN) channel when decoding the message intended to receiver j at decoder i in the reflecting state ($B = 1$) and transparent state ($B = 0$) respectively.

Following similar steps as above, we obtain the achievable rates R_K and R_0 as

$$R_K \leq qC\left(\min_{1\leq i\leq K}(\gamma_{K\to i|1})\right) + (1-q)C\left(\min_{1\leq i\leq K}(\gamma_{K\to i|0})\right), \tag{D.7}$$

$$R_0 \leq \min_{1\leq i\leq K} \mathbb{H}(Y_i|U_K) - \frac{q}{2}\log_2\left(2\pi e\sigma_i^2\left(H_{i|1}(\rho)\sum_{k=1}^{K-1} p_k + 1\right)\right) - \frac{1-q}{2}\log_2\left(2\pi e\sigma_i^2\left(H_{i|0}\sum_{k=1}^{K-1} p_k + 1\right)\right), \tag{D.8}$$

which concludes the proof of Theorem 5.

Appendix E

Proof of Theorem 6

E.1 Convexity of (EE7)

For the sake of simplicity of presentation, we denote $H_{k|1}(\rho^*)$ simply by $= H_{k|1}$. We also recall that $\theta_k(\mathbf{p}) = \sum_{i=1}^{k} p_k, \forall 1 \leq k \leq K$ with $\theta_0(\mathbf{p}) = 0$.

We start by showing that (**EE7**) is a convex optimization problem. For this, we analyze its objective function $\eta_{EE}(\mathbf{p})$ whose second-order partial derivative w.r.t $p_i,\ p_j,\ \forall i, j$, equals

$$\frac{\partial^2 \eta_{EE}(\mathbf{p})}{\partial p_j \partial p_i} = \begin{cases} d_j, & \text{if } j \geq i \\ d_i, & \text{otherwise,} \end{cases}$$

where

$$d_j = \sum_{k=j}^{K-1} \frac{q}{2\ln 2} \left(\frac{(H_{k+1|1})^2}{\Big(1+H_{k+1|1}\theta_k(\mathbf{p})\Big)^2} - \frac{(H_{k|1})^2}{\Big(1+H_{k|1}\theta_k(\mathbf{p})\Big)^2} \right) \tag{E.1}$$

$$+ \sum_{k=j}^{K-1} \frac{(1-q)}{2\ln 2} \left(\frac{(H_{k+1|0})^2}{\Big(1+H_{k+1|0}\theta_k(\mathbf{p})\Big)^2} - \frac{(H_{k|0})^2}{\Big(1+H_{k|0}\theta_k(\mathbf{p})\Big)^2} \right)$$

$$- \frac{q}{2\ln 2} \times \frac{(H_{K|1})^2}{\Big(1+H_{K|1}\theta_K(\mathbf{p})\Big)^2} - \frac{(1-q)}{2\ln 2} \times \frac{(H_{K|0})^2}{\Big(1+H_{K|0}\theta_K(\mathbf{p})\Big)^2}. \tag{E.2}$$

Let $\mathbf{D}$ be the Hessian matrix which has the following special structure

$$\mathbf{D} = \begin{pmatrix} d_1 & d_2 & d_3 & \dots & d_K \\ d_2 & d_2 & d_3 & \dots & d_K \\ d_3 & d_3 & d_3 & \dots & d_K \\ \vdots & \vdots & \vdots & & \vdots \\ d_K & d_K & d_K & \dots & d_K \end{pmatrix}.$$

We define $\mathbf{T} = -\mathbf{D}$ and show that it is positive semi-definite by proving that all of its leading principal minors are positive, i.e., $\det \mathbf{T}[1:j, 1:j] \geq 0, \forall j \in \{1,..., K\}$.

The first leading principal minor is $\det \mathbf{T}[1,1] = -d_1 \geq 0$. For $1 < j \leq K$, the j-th leading principal minor equals

$$\begin{aligned} \det \mathbf{T}[1:j,1:j] &= \begin{vmatrix} d_2-d_1 & d_3-d_2 & d_4-d_3 & \dots & d_j-d_{j-1} & -d_j \\ 0 & d_3-d_2 & d_4-d_3 & \dots & & -d_j \\ 0 & 0 & d_4-d_3 & \dots & & -d_j \\ \vdots & \vdots & \vdots & & & \vdots \\ 0 & 0 & 0 & \dots & & -d_j \end{vmatrix} \qquad \text{(E.3)} \\ &= -d_j \prod_{k=1}^{j-1} (d_{k+1}-d_k). \qquad \text{(E.4)} \end{aligned}$$

We write the terms $d_{k+1} - d_k$, for all $1 \leq k < K$

$$\begin{aligned} d_{k+1}-d_k &= \frac{q}{2\ln 2}\left(\frac{(H_{k|1})^2}{\left(1+H_{k|1}\theta_k(\mathbf{p})\right)^2} - \frac{(H_{k+1|1})^2}{\left(1+H_{k+1|1}\theta_k(\mathbf{p})\right)^2}\right) \\ &\quad + \frac{(1-q)}{2\ln 2}\left(\frac{(H_{k|0})^2}{\left(1+H_{k|0}\theta_k(\mathbf{p})\right)^2} - \frac{(H_{k+1|0})^2}{\left(1+H_{k+1|0}\theta_k(\mathbf{p})\right)^2}\right) \\ &\geq 0, \qquad \text{(E.5)} \end{aligned}$$

Note that since $H_{k|1} \geq H_{k+1|1}$ and $H_{k|0} \geq H_{k+1|0}, \forall k \in \{1,\dots,K-1\}$, we can show that $d_j \leq 0$, for all j and that $d_{k+1} - d_k \geq 0, \forall k$. The first leading principal minor is $\det \mathbf{T}[1,1] = -d_1 \geq 0$. For $1 < j \leq K$, the j-th leading principal minor equals $\det \mathbf{T}[1:j,1:j] = -d_j \prod_{k=1}^{j-1}(d_{k+1}-d_k) \geq 0$. Therefore, all leading principal minors of $\mathbf{T}$ are positive, which implies that $\mathbf{T} \succeq 0$ equivalent to the Hessian matrix $\mathbf{D} \preceq 0$. The latter means that the objective function is jointly concave w.r.t $\mathbf{p} = (p_1,\dots,p_K)$. Now, given the above and that all the inequality constraints are affine w.r.t $\mathbf{p}$, the optimization problem (**EE7**) is convex.

E.2 Solving the KKT conditions for (EE7)

The associated Lagrangian function of the optimization problem (**EE7**) is given by

$$\mathcal{L}(\rho^*,\mathbf{p}) = \sum_{k=1}^{K} R_k(\rho^*,\mathbf{p}) - \alpha(\theta_K(\mathbf{p})+P_{\mathrm{c}}) + \lambda(P_{\max}-\theta_K(\mathbf{p})) + \sum_{k=1}^{K}\beta_k\left(\theta_k(\mathbf{p}) - A_k\theta_{k-1}(\mathbf{p}) + \frac{(A_k-1)}{H_{k|0}}\right), \qquad \text{(E.6)}$$

where λ and $\boldsymbol{\beta} = (\beta_1,\dots,\beta_K)$ are the non-negative Lagrange multipliers associated with the constraints $(C1)$ and $(C2a)$ respectively. The necessary and sufficient KKT optimality

conditions write as

$$\begin{cases} \frac{\partial \mathcal{L}}{\partial p_i} \triangleq \sum_{k=i}^{K-1} \frac{q}{2\ln 2}\left(\frac{H_{k|1}}{1+H_{k|1}\theta_k(\mathbf{p})} - \frac{H_{k+1|1}}{1+H_{k+1|1}\theta_k(\mathbf{p})}\right) + \sum_{k=i}^{K-1} \frac{(1-q)}{2\ln 2}\left(\frac{H_{k|0}}{1+H_{k|0}\theta_k(\mathbf{p})} - \frac{H_{k+1|1}}{1+H_{k+1|1}\theta_k(\mathbf{p})}\right) \\ + \frac{q}{2\ln 2} \times \frac{H_{K|1}}{1+H_{K|1}\theta_K(\mathbf{p})} + \frac{(1-q)}{2\ln 2} \times \frac{H_{K|0}}{1+H_{K|0}\theta_K(\mathbf{p})} - (\alpha+\lambda) + \sum_{k=i}^{K} \beta_k - \sum_{k=i}^{K-1}(A_{k+1}\beta_{k+1}) = 0, & (K1) \\ \lambda(P_{max} - \theta_K(\mathbf{p})) = 0, & (K2) \\ \beta_k\left(\theta_k(\mathbf{p}) - A_k\theta_{k-1}(\mathbf{p}) + \frac{(A_k-1)}{H_{k|0}}\right) = 0, & (K3) \\ (C1'), (C2'), \lambda \geq, \boldsymbol{\beta} \geq 0 & (K4) \end{cases}$$

From $(K1)$, and by using the difference between two consecutive derivatives, $(\frac{\partial \mathcal{L}}{\partial p_i} - \frac{\partial \mathcal{L}}{\partial p_{i+1}}) = 0$, we obtain

$$\frac{q}{2\ln 2}\left(\frac{H_{i|1}}{1+H_{i|1}\theta_i(\mathbf{p})} - \frac{H_{i+1|1}}{1+H_{i+1|1}\theta_i(\mathbf{p})}\right) + \frac{(1-q)}{2\ln 2}\left(\frac{H_{i|0}}{1+H_{i|0}\theta_i(\mathbf{p})} - \frac{H_{i+1|0}}{1+H_{i+1|0}\theta_i(\mathbf{p})}\right) + \beta_i = A_{i+1}\beta_{i+1}. \tag{E.7}$$

We know that $H_{i|1} \geq H_{i+1|1}$, $H_{i|0} \geq H_{i+1|0}$, $A_{i+1} > 0$ and $\beta_{i+1} \geq 0$, $\forall i \in \{1, \ldots, K-1\}$. We discuss two cases:

a) If $H_{1|0} > H_{2|0}$, by replacing $i = 1$ in (E.7), since $A_2 > 0$, we have $\beta_2 > 0$. For $i = 2$, since $\beta_2 > 0$ and $A_3 > 0$ we obtain $\beta_3 > 0$. Recursively, for all $i \geq 2$ we find $\beta_i > 0$. Using $(K3)$, we obtain $\theta_k(\mathbf{p}) = A_k\theta_{k-1}(\mathbf{p}) - \frac{(A_k-1)}{H_{k|0}}, \forall k \geq 2$. This means that all receivers $k \geq 2$ will be allocated a power to meet exactly their minimum rate requirement. By induction, we find that

$$\theta_k(\mathbf{p}) = \theta_1(\mathbf{p}) \prod_{i=2}^{k} A_i + \sum_{i=2}^{k-1} \frac{(A_i - 1)}{H_{i|0}} \prod_{j=i+1}^{k} A_j + \frac{(A_k - 1)}{H_{k|0}}, \forall k \geq 2. \tag{E.8}$$

Notice that all variables θ_k are expressed in terms of $\theta_1(\mathbf{p}) = p_1$. Hence, we obtain the expressions of the optimal powers $p_k^*, \forall k \geq 2$ in closed-form as functions of p_1 as in Theorem 6.

b) In the case where $H_{1|0} = H_{2|0}$, the first order partial derivatives of $\eta_{EE}(\mathbf{p})$ write as

$$\frac{\partial \eta_{EE}}{\partial p_i} = \begin{cases} \Upsilon(\mathbf{p}) \triangleq \sum_{k=i}^{K-1} \frac{q}{2\ln 2}\left(\frac{H_{k|1}}{1+H_{k|1}\theta_k(\mathbf{p})} - \frac{H_{k+1|1}}{1+H_{k+1|1}\theta_k(\mathbf{p})}\right) \\ + \sum_{k=i}^{K-1} \frac{(1-q)}{2\ln 2}\left(\frac{H_{k|0}}{1+H_{k|0}\theta_k(\mathbf{p})} - \frac{H_{k+1|0}}{1+H_{k+1|0}\theta_k(\mathbf{p})}\right) \\ + \frac{q}{2\ln 2} \times \frac{H_{K|1}}{1+H_{K|1}\theta_K(\mathbf{p})} + \frac{(1-q)}{2\ln 2} \times \frac{H_{K|0}}{1+H_{K|0}\theta_K(\mathbf{p})}, & \text{if } i \geq 2 \\ \Upsilon(\mathbf{p}) + \frac{q}{2\ln 2}\left(\frac{H_{1|1}}{1+H_{1|1}\theta_1(\mathbf{p})} - \frac{H_{2|1}}{1+H_{2|1}\theta_1(\mathbf{p})}\right), & \text{if } i = 1. \end{cases}$$

In this case, the difference between two consecutive derivatives of the Lagrange

function gives

$$\frac{q}{2\ln 2}\left(\frac{H_{1|1}}{1+H_{1|1}\theta_1(\mathbf{p})}-\frac{H_{2|1}}{1+H_{2|1}\theta_1(\mathbf{p})}\right)+\beta_1=A_2\beta_2, \tag{E.9}$$

$$\frac{q}{2\ln 2}\left(\frac{H_{i|1}}{1+H_{i|1}\theta_i(\mathbf{p})}-\frac{H_{i+1|1}}{1+H_{i+1|1}\theta_i(\mathbf{p})}\right)+\frac{(1-q)}{2\ln 2}\left(\frac{H_{i|0}}{1+H_{i|0}\theta_i(\mathbf{p})}-\frac{H_{i+1|0}}{1+H_{i+1|0}\theta_i(\mathbf{p})}\right)$$
$$+\beta_i=A_{i+1}\beta_{i+1}. \tag{E.10}$$

We discuss two cases:
i) If $H_{1|1} > H_{2|1}$ then, since $\beta_1 \geq 0$ and $A_2 > 0$, we have $\beta_2 > 0$ and recursively we find $\beta_i > 0, \forall i \geq 2$, which leads to the analytical closed-form expressions of $p_k^*, \forall k \geq 2$ as functions of p_1 and given in Theorem 6, as in the case $H_{1|0} > H_{2|0}$.
ii) If $H_{1|1} = H_{2|1}$, the analysis of the solution $\mathbf{p}^*$ is delegated to the end of the appendix.

E.2.1 Finding the optimal power allocated to user 1 when $H_{1|0} > H_{2|0}$ or $H_{1|1} > H_{2|1}$

Using the above optimal expressions $p_k^*, \forall k \geq 2$ as functions of p_1, we can reformulate the multi-variable optimization problem (**EE7**) into a simple single-variable optimization problem

$$\max_{\ell \leq p_1 \leq u} f_1(p_1) \triangleq \sum_{k=1}^{K}\frac{q}{2}\log_2\left(\frac{1+H_{k|1}\theta_k(\mathbf{p})}{1+H_{k|1}\theta_{k-1}(\mathbf{p})}\right)+\frac{(1-q)}{2}\log_2\left(1+H_{1|0}p_1\right)+\sum_{k=2}^{K}(1-q)R_k^{\min}$$
$$-\alpha\left(p_1\prod_{i=2}^{K}A_i+\sum_{i=2}^{K-1}\frac{(A_i-1)}{H_{i|0}}\prod_{j=i+1}^{K}A_j+\frac{(A_K-1)}{H_{K|0}}+P_{\mathrm{c}}\right) \tag{E.11}$$

where $\ell = \frac{(A_1-1)}{H_{1|0}}$ and $u = \left(P_{\max}-P_{\min}+\ell\prod_{j=2}^{K}A_j\right)\Big/\prod_{i=2}^{K}A_i$.

The optimal solution of (E.11) is given by $p_1^*(\alpha) = \max\left(\min\left(\overline{p_1}(\alpha); u\right); \ell\right)$ where $\overline{p_1}$ is the critical point of the objective satisfying $\frac{\partial f_1(p_1)}{\partial p_1} = 0$ and can be found numerically.

E.2.2 The case in which $H_{1|0} = H_{2|0}$ and $H_{1|1} = H_{2|1}$

The expression of $\eta_{EE}(\mathbf{p})$ simplifies in this case. Similar to our discussion in Appendix A, we can consider receiver 1 and 2 as a single entity, having the strongest channel gains $H'_{1|0} = H_{1|0} = H_{2|0}$ and $H'_{1|1} = H_{1|1} = H_{2|1}$, and whose achievable data rate and allocated power are considered as $R'_1 = (R_1 + R_2)$ and $p'_1 = p_1 + p_2$ respectively. The same discussion follows subsequently as in the previous subsections of this Appendix E; two cases arise: **a)** $H'_{1|0} = H_{3|0}$ and $H'_{1|1} = H_{3|1}$, and **b)** $H'_{1|0} > H_{3|0}$ or $H'_{1|1} > H_{3|1}$. In the latter, we obtain the analytical closed-form expressions of $p_k^*, \forall k \geq 3$ as a function of p'_1 and $(p'_1)^*$ is obtained by solving the resulting (**EE7**) problem. Then, we can split the power $(p'_1)^*$ such that p_2^* is the enough power required to satisfy the minimum rate requirement for receiver 2, and the remaining power $p_1^* = (p'_1)^* - p_2^*$. In the

former case, a recurring reasoning can be applied etc. Finally, the same reasoning applies in the extreme symmetric case in which $H_{1|0} = H_{2|0} = \ldots = H_{K|0}$ and $H_{1|1} = H_{2|1} = \ldots = H_{K|1}$, which unlikely to occur.

For the sake of clarity and simplicity of presentation, and given that the main ideas and the procedure behind the proof is explained in the previous subsections of this Appendix E, we have decided to include only the case $H_{1|0} > H_{2|0}$ or $H_{1|1} > H_{2|1}$ in the main text of Theorem 6.

Bibliography

[1] A. A. Huurdeman, *The worldwide history of telecommunications*. John Wiley & Sons, 2003.

[2] A. Goldsmith, *Wireless communications*. Cambridge university press, 2005.

[3] M. Wendler and S. Guillemaut, "ETCS in PS-mode GPRS/EGPRS guideline," *Kapsch CarrierCom, Nokia: UIC ERTMS/GSM-R Operators Group*, 2014.

[4] I. R. Sector, "Requirements related to technical performance for IMT-advanced radio interface (s)," *Report ITU*, pp. 2134–2008, 2008.

[5] L. Horwitz, "The future of IoT miniguide: The burgeoning IoT market continues," *CISCO, San Jose, CA, USA, Tech. Rep*, 2019.

[6] M. Series, "Imt vision–framework and overall objectives of the future development of IMT for 2020 and beyond," *Recommendation ITU*, vol. 2083, p. 0, 2015.

[7] M. Vaezi, Z. Ding, and H. V. Poor, *Multiple access techniques for 5G wireless networks and beyond*. Springer, 2019, vol. 159.

[8] X. Chen, D. W. K. Ng, W. Yu, E. G. Larsson, N. Al-Dhahir, and R. Schober, "Massive access for 5G and beyond," *IEEE Journal on Selected Areas in Communications*, vol. 39, no. 3, pp. 615–637, 2020.

[9] V. W. Wong, R. Schober, D. W. K. Ng, and L.-C. Wang, *Key technologies for 5G wireless systems*. Cambridge university press, 2017.

[10] Y. Saito, Y. Kishiyama, A. Benjebbour, T. Nakamura, A. Li, and K. Higuchi, "Non-orthogonal multiple access (NOMA) for cellular future radio access," in *2013 IEEE 77th vehicular technology conference (VTC Spring)*. IEEE, 2013, pp. 1–5.

[11] K. Higuchi and A. Benjebbour, "Non-orthogonal multiple access (NOMA) with successive interference cancellation for future radio access," *IEICE Transactions on Communications*, vol. 98, no. 3, pp. 403–414, 2015.

[12] S. R. Islam, N. Avazov, O. A. Dobre, and K.-S. Kwak, "Power-domain non-orthogonal multiple access (NOMA) in 5G systems: Potentials and challenges," *IEEE Communications Surveys & Tutorials*, vol. 19, no. 2, pp. 721–742, 2016.

[13] Q. Wu, W. Chen, D. W. K. Ng, and R. Schober, "Spectral and energy-efficient wireless powered IoT networks: NOMA or TDMA?" *IEEE Transactions on Vehicular Technology*, vol. 67, no. 7, pp. 6663–6667, 2018.

[14] Z. Ding, X. Lei, G. K. Karagiannidis, R. Schober, J. Yuan, and V. K. Bhargava, "A survey on non-orthogonal multiple access for 5G networks: Research challenges and future trends," *IEEE Journal on Selected Areas in Communications*, vol. 35, no. 10, pp. 2181–2195, 2017.

[15] J. Malmodin and D. Lundén, "The energy and carbon footprint of the global ICT and E&M sectors 2010–2015," *Sustainability*, vol. 10, no. 9, p. 3027, 2018.

[16] F. M. Al-Turjman, M. Imran, and S. T. Bakhsh, "Energy efficiency perspectives of femtocells in Internet of Things: Recent advances and challenges," *IEEE Access*, vol. 5, pp. 26 808–26 818, 2017.

[17] V. Liu, A. Parks, V. Talla, S. Gollakota, D. Wetherall, and J. R. Smith, "Ambient backscatter: Wireless communication out of thin air," *ACM SIGCOMM Computer Communication Review*, vol. 43, no. 4, pp. 39–50, 2013.

[18] G. Wang, F. Gao, R. Fan, and C. Tellambura, "Ambient backscatter communication systems: Detection and performance analysis," *IEEE Transactions on Communications*, vol. 64, no. 11, pp. 4836–4846, 2016.

[19] N. Van Huynh, D. T. Hoang, X. Lu, D. Niyato, P. Wang, and D. I. Kim, "Ambient backscatter communications: A contemporary survey," *IEEE Communications surveys & tutorials*, vol. 20, no. 4, pp. 2889–2922, 2018.

[20] F. Jameel and S. A. Hassan, *Wireless-Powered Backscatter Communications for Internet of Things*. Springer, 2020.

[21] R. Fara, D.-T. Phan-Huy, and M. Di Renzo, "Ambient backscatters-friendly 5G networks: creating hot spots for tags and good spots for readers," in *IEEE WCNC*, 2020, pp. 1–7.

[22] Y. Kokar, D.-T. Phan-Huy, R. Fara, K. Rachedi, A. Ourir, J. de Rosny, M. Di Renzo, J.-C. Prévotet, and M. Helard, "First experimental ambient backscatter communication using a compact reconfigurable tag antenna," in *IEEE Globecom Workshops*, 2019, pp. 1–6.

[23] C. Song, Y. Ding, A. Eid, J. G. Hester, X. He, R. Bahr, A. Georgiadis, G. Goussetis, and M. M. Tentzeris, "Advances in wirelessly powered backscatter communications: From antenna/RF circuitry design to printed flexible electronics," *Proceedings of the IEEE*, vol. 110, no. 1, pp. 171–192, 2021.

[24] J. Hoydis, F. A. Aoudia, A. Valcarce, and H. Viswanathan, "Toward a 6G AI-native air interface," *IEEE Communications Magazine*, vol. 59, no. 5, pp. 76–81, 2021.

[25] B. Rong, "6G: The next horizon: From connected people and things to connected intelligence," *IEEE Wireless Communications*, vol. 28, no. 5, pp. 8–8, 2021.

[26] S. Ali, W. Saad, N. Rajatheva, K. Chang, D. Steinbach, B. Sliwa, C. Wietfeld, K. Mei, H. Shiri, H.-J. Zepernick *et al.*, "6G white paper on machine learning in wireless communication networks," *arXiv preprint arXiv:2004.13875*, 2020.

[27] Y. Saito, A. Benjebbour, Y. Kishiyama, and T. Nakamura, "System-level performance evaluation of downlink non-orthogonal multiple access (NOMA)," in *2013 IEEE 24th Annual International Symposium on Personal, Indoor, and Mobile Radio Communications (PIMRC)*. IEEE, 2013, pp. 611–615.

[28] Z. Ding, Z. Yang, P. Fan, and H. V. Poor, "On the performance of non-orthogonal multiple access in 5G systems with randomly deployed users," *IEEE signal processing letters*, vol. 21, no. 12, pp. 1501–1505, 2014.

[29] J. Choi, "Power allocation for max-sum rate and max-min rate proportional fairness in NOMA," *IEEE Communications Letters*, vol. 20, no. 10, pp. 2055–2058, 2016.

[30] S. Timotheou and I. Krikidis, "Fairness for non-orthogonal multiple access in 5G systems," *IEEE signal processing letters*, vol. 22, no. 10, pp. 1647–1651, 2015.

[31] J. Choi, "Non-orthogonal multiple access in downlink coordinated two-point systems," *IEEE Communications Letters*, vol. 18, no. 2, pp. 313–316, 2014.

[32] Q. Wu, W. Chen, D. W. K. Ng, and R. Schober, "Spectral and energy-efficient wireless powered IoT networks: NOMA or TDMA?" *IEEE Transactions on Vehicular Technology*, vol. 67, no. 7, pp. 6663–6667, 2018.

[33] D. Tse and P. Viswanath, *Fundamentals of wireless communication*. Cambridge university press, 2005.

[34] L. Song, R. C. de Lamare, and A. G. Burr, "Successive interference cancellation schemes for time-reversal space-time block codes," *IEEE transactions on vehicular technology*, vol. 57, no. 1, pp. 642–648, 2008.

[35] P. Li, R. C. De Lamare, and R. Fa, "Multiple feedback successive interference cancellation detection for multiuser MIMO systems," *IEEE Transactions on Wireless Communications*, vol. 10, no. 8, pp. 2434–2439, 2011.

[36] L. Dai, B. Wang, Y. Yuan, S. Han, I. Chih-Lin, and Z. Wang, "Non-orthogonal multiple access for 5G: solutions, challenges, opportunities, and future research trends," *IEEE Communications Magazine*, vol. 53, no. 9, pp. 74–81, 2015.

[37] S. Vanka, S. Srinivasa, Z. Gong, P. Vizi, K. Stamatiou, and M. Haenggi, "Superposition coding strategies: Design and experimental evaluation," *IEEE Transactions on Wireless Communications*, vol. 11, no. 7, pp. 2628–2639, 2012.

[38] M. Vaezi, R. Schober, Z. Ding, and H. V. Poor, "Non-orthogonal multiple access: Common myths and critical questions," *IEEE Wireless Communications*, vol. 26, no. 5, pp. 174–180, 2019.

[39] T. M. Cover, "Thomas. elements of information theory," *Wiley Series in Telecommunications*, 1991.

[40] A. El Gamal and Y.-H. Kim, *Network information theory*. Cambridge university press, 2011.

[41] J. Axnäs, Y.-P. E. Wang, M. Kamuf, and N. Andgart, "Successive interference cancellation techniques for LTE downlink," in *2011 IEEE 22nd International Symposium on Personal, Indoor and Mobile Radio Communications*. IEEE, 2011, pp. 1793–1797.

[42] G. Zhou, W. Xu, and G. Bauch, "Network assisted inter-cell codeword cancellation for interference-limited LTE-A and beyond," in *2014 IEEE Wireless Communications and Networking Conference Workshops (WCNCW)*. IEEE, 2014, pp. 52–57.

[43] S. Moon, H. Choe, M. Chu, C. You, H. Liu, J.-H. Kim, J. Kim, D. J. Kim, and I. Hwang, "Design and performance analysis of soft decision-based network-assisted interference cancellation and suppression scheme," *Wireless Personal Communications*, vol. 96, no. 4, pp. 5849–5863, 2017.

[44] A. Davydov, G. Morozov, and S. Han, "Network assisted interference cancellation and suppression with respect to interfering control channel transmissions," Jun. 28 2016, uS Patent 9,380,090.

[45] J.-Y. Hwang and S.-W. Lee, "Advanced receiver for interference cancellation in 3GPP LTE-A," *The Journal of Korean Institute of Communications and Information Sciences*, vol. 39, no. 7, pp. 389–397, 2014.

[46] L. Xiu, "Time moore: Exploiting moore's law from the perspective of time," *IEEE Solid-State Circuits Magazine*, vol. 11, no. 1, pp. 39–55, 2019.

[47] M. L. Memon, N. Saxena, A. Roy, S. Singh, and D. R. Shin, "Ambient backscatter communications to energize IoT devices," *IETE Technical Review*, vol. 37, no. 2, pp. 196–210, 2020.

[48] S. S. Afzal, R. Ghaffarivardavagh, W. Akbar, O. Rodriguez, and F. Adib, "Enabling higher-order modulation for underwater backscatter communication," in *Global Oceans 2020: Singapore–US Gulf Coast*. IEEE, 2020, pp. 1–6.

[49] R. Long, H. Guo, L. Zhang, and Y.-C. Liang, "Full-duplex backscatter communications in symbiotic radio systems," *IEEE Access*, vol. 7, pp. 21 597–21 608, 2019.

[50] R. Long, Y.-C. Liang, H. Guo, G. Yang, and R. Zhang, "Symbiotic radio: A new communication paradigm for passive Internet of Things," *IEEE Internet of Things Journal*, vol. 7, no. 2, pp. 1350–1363, 2019.

[51] H. Guo, Y.-C. Liang, R. Long, S. Xiao, and Q. Zhang, "Resource allocation for symbiotic radio system with fading channels," *IEEE Access*, vol. 7, pp. 34 333–34 347, 2019.

[52] Q. Zhang, L. Zhang, Y.-C. Liang, and P.-Y. Kam, "Backscatter-NOMA: A symbiotic system of cellular and internet-of-things networks," *IEEE Access*, vol. 7, pp. 20 000–20 013, 2019.

[53] G. Yang, Q. Zhang, and Y.-C. Liang, "Cooperative ambient backscatter communications for green internet-of-things," *IEEE Internet of Things Journal*, vol. 5, no. 2, pp. 1116–1130, 2018.

[54] M. Dai, P. Wang, S. Zhang, B. Chen, H. Wang, X. Lin, and C. Sun, "Survey on cooperative strategies for wireless relay channels," *Transactions on Emerging Telecommunications Technologies*, vol. 25, no. 9, pp. 926–942, 2014.

[55] A. Savard and C. Weidmann, "On the multiway relay channel with direct links," in *2014 IEEE Information Theory Workshop (ITW 2014)*. IEEE, 2014, pp. 651–655.

[56] S. I. Bross and M. A. Wigger, "On the relay channel with receiver–transmitter feedback," *IEEE Transactions on Information Theory*, vol. 55, no. 1, pp. 275–291, 2008.

[57] M. Di Renzo, K. Ntontin, J. Song, F. H. Danufane, X. Qian, F. Lazarakis, J. De Rosny, D.-T. Phan-Huy, O. Simeone, R. Zhang *et al.*, "Reconfigurable intelligent surfaces vs. relaying: Differences, similarities, and performance comparison," *IEEE Open Journal of the Communications Society*, vol. 1, pp. 798–807, 2020.

[58] Y.-C. Liang, R. Long, Q. Zhang, J. Chen, H. V. Cheng, and H. Guo, "Large intelligent surface/antennas (LISA): Making reflective radios smart," *Journal of Communications and Information Networks*, vol. 4, no. 2, pp. 40–50, 2019.

[59] E. Basar, M. Di Renzo, J. De Rosny, M. Debbah, M.-S. Alouini, and R. Zhang, "Wireless communications through reconfigurable intelligent surfaces," *IEEE access*, vol. 7, pp. 116 753–116 773, 2019.

[60] M. Di Renzo, A. Zappone, M. Debbah, M.-S. Alouini, C. Yuen, J. De Rosny, and S. Tretyakov, "Smart radio environments empowered by reconfigurable intelligent surfaces: How it works, state of research, and the road ahead," *IEEE journal on selected areas in communications*, vol. 38, no. 11, pp. 2450–2525, 2020.

[61] Q. Wu and R. Zhang, "Intelligent reflecting surface enhanced wireless network via joint active and passive beamforming," *IEEE Transactions on Wireless Communications*, vol. 18, no. 11, pp. 5394–5409, 2019.

[62] C. Huang, A. Zappone, M. Debbah, and C. Yuen, "Achievable rate maximization by passive intelligent mirrors," in *2018 IEEE International Conference on Acoustics, Speech and Signal Processing (ICASSP)*. IEEE, 2018, pp. 3714–3718.

[63] C. Huang, A. Zappone, G. C. Alexandropoulos, M. Debbah, and C. Yuen, "Reconfigurable intelligent surfaces for energy efficiency in wireless communication," *IEEE Transactions on Wireless Communications*, vol. 18, no. 8, pp. 4157–4170, 2019.

[64] Q.-U.-A. Nadeem, A. Kammoun, A. Chaaban, M. Debbah, and M.-S. Alouini, "Asymptotic analysis of large intelligent surface assisted MIMO communication," *Arxiv*, vol. 2019, 2019.

[65] R. Masmoudi, E. V. Belmega, I. Fijalkow, and N. Sellami, "A unifying view on energy-efficiency metrics in cognitive radio channels," in *EUSIPCO, Lisbon, Portugal*, Sep. 2014.

[66] E. Belmega, S. Lasaulce, M. Debbah, and A. Hrungnes, "A new energy efficiency function for quasi-static MIMO channels," in *International Wireless Communications and Mobile Computing Conference (IWCMC), Leipzig, Germany, invited paper*, 2009.

[67] G. Bacci, L. Sanguinetti, M. Luise, and H. V. Poor, "Energy-efficient power control for contention-based synchronization in OFDMA systems with discrete powers and limited feedback," *EURASIP Journal on Wireless Communications and Networking*, vol. 2013, no. 1, pp. 1–14, 2013.

[68] D. Goodman and N. Mandayam, "Power control for wireless data," *IEEE Personal Communications*, vol. 7, no. 2, pp. 48–54, 2000.

[69] S. Verdú, "On channel capacity per unit cost," *IEEE Transactions on Information Theory*, vol. 36, no. 5, pp. 1019–1030, 1990.

[70] A. Zappone, E. Jorswieck *et al.*, "Energy efficiency in wireless networks via fractional programming theory," *Foundations and Trends® in Communications and Information Theory*, vol. 11, no. 3-4, pp. 185–396, 2015.

[71] C. Isheden, Z. Chong, E. Jorswieck, and G. Fettweis, "Framework for link-level energy efficiency optimization with informed transmitter," *IEEE Transactions on Wireless Communications*, vol. 11, no. 8, pp. 2946–2957, 2012.

[72] S. Boyd and L. Vandenberghe, *Convex Optimization*. Cambridge University Press, 2004.

[73] J. Tang, J. Luo, D. So, E. Alsusa, K.-K. Wong, and N. Zhao, "Energy-efficient resource allocation in SWIPT enabled NOMA systems," in *2018 IEEE Global Communications Conference (GLOBECOM)*. IEEE, 2018, pp. 1–7.

[74] Y. Zhang, H.-M. Wang, T.-X. Zheng, and Q. Yang, "Energy-efficient transmission design in non-orthogonal multiple access," *IEEE Transactions on Vehicular Technology*, vol. 66, no. 3, pp. 2852–2857, 2016.

[75] R. S. Prabhu and B. Daneshrad, "An energy-efficient water-filling algorithm for OFDM systems," in *2010 IEEE International Conference on Communications*. IEEE, 2010, pp. 1–5.

[76] W. Dinkelbach, "On nonlinear fractional programming," *Management science*, vol. 13, no. 7, pp. 492–498, 1967.

[77] R. Jagannathan, "On some properties of programming problems in parametric form pertaining to fractional programming," *Management Science*, vol. 12, no. 7, pp. 609–615, 1966.

[78] R. S. Sutton and A. G. Barto, *Reinforcement learning: An introduction*. MIT press, 2018.

[79] E. V. Belmega, P. Mertikopoulos, and R. Negrel, "Online convex optimization in wireless networks and beyond: The feedback-performance trade-off," in *RAWNET 2022-International Workshop on Resource Allocation and Cooperation in Wireless Networks*, 2022, pp. 1–8.

[80] S. Bubeck and N. Cesa-Bianchi, "Regret analysis of stochastic and nonstochastic multi-armed bandit problems," *arXiv preprint arXiv:1204.5721*, 2012.

[81] P. Auer, N. Cesa-Bianchi, Y. Freund, and R. E. Schapire, "Gambling in a rigged casino: The adversarial multi-armed bandit problem," in *IEEE 36th Annual Foundations of Computer Science*, 1995, pp. 322–331.

[82] W. U. Khan, F. Jameel, T. Ristaniemi, S. Khan, G. A. S. Sidhu, and J. Liu, "Joint spectral and energy efficiency optimization for downlink NOMA networks," *IEEE Transactions on Cognitive Communications and Networking*, 2019.

[83] J. Zhu, J. Wang, Y. Huang, S. He, X. You, and L. Yang, "On optimal power allocation for downlink non-orthogonal multiple access systems," *IEEE Journal on Selected Areas in Communications*, vol. 35, no. 12, pp. 2744–2757, 2017.

[84] Z. Yang, W. Xu, C. Pan, Y. Pan, and M. Chen, "On the optimality of power allocation for NOMA downlinks with individual QoS constraints," *IEEE Communications Letters*, vol. 21, no. 7, pp. 1649–1652, 2017.

[85] F. Fang, H. Zhang, J. Cheng, S. Roy, and V. C. Leung, "Joint user scheduling and power allocation optimization for energy-efficient NOMA systems with imperfect CSI," *IEEE Journal on Selected Areas in Communications*, vol. 35, no. 12, pp. 2874–2885, 2017.

[86] S. D'Oro, A. Zappone, S. Palazzo, and M. Lops, "A learning approach for low-complexity optimization of energy efficiency in multicarrier wireless networks," *IEEE Transactions on Wireless Communications*, vol. 17, no. 5, pp. 3226–3241, 2018.

[87] Z. Chen, Z. Ding, X. Dai, and R. Zhang, "An optimization perspective of the superiority of NOMA compared to conventional OMA," *IEEE Transactions on Signal Processing*, vol. 65, no. 19, pp. 5191–5202, 2017.

[88] X. Kang, Y.-C. Liang, and J. Yang, "Riding on the primary: A new spectrum sharing paradigm for wireless-powered IoT devices," *IEEE Transactions on Wireless Communications*, vol. 17, no. 9, pp. 6335–6347, 2018.

[89] Y. Ye, L. Shi, R. Qingyang Hu, and G. Lu, "Energy-efficient resource allocation for wirelessly powered backscatter communications," *IEEE Communications Letters*, vol. 23, no. 8, pp. 1418–1422, 2019.

[90] B. Lyu, C. You, Z. Yang, and G. Gui, "The optimal control policy for RF-powered backscatter communication networks," *IEEE Transactions on Vehicular Technology*, vol. 67, no. 3, pp. 2804–2808, 2017.

[91] W. Chen, H. Ding, S. Wang, D. B. da Costa, F. Gong, and P. H. J. Nardelli, "Backscatter cooperation in NOMA communications systems," *IEEE Transactions on Wireless Communications*, vol. 20, no. 6, pp. 3458–3474, 2021.

[92] Y. Xu, Z. Qin, G. Gui, H. Gacanin, H. Sari, and F. Adachi, "Energy efficiency maximization in NOMA enabled backscatter communications with QoS guarantee," *IEEE Wireless Communications Letters*, vol. 10, no. 2, pp. 353–357, 2020.

[93] W. U. Khan, X. Li, M. Zeng, and O. A. Dobre, "Backscatter-enabled NOMA for future 6G systems: A new optimization framework under imperfect SIC," *IEEE Communications Letters*, vol. 25, no. 5, pp. 1669–1672, 2021.

[94] W. U. Khan, M. A. Javed, T. N. Nguyen, S. Khan, and B. M. Elhalawany, "Energy-efficient resource allocation for 6G backscatter-enabled NOMA IoV networks," *IEEE Transactions on Intelligent Transportation Systems*, 2021.

[95] S. Zhou, W. Xu, K. Wang, C. Pan, M.-S. Alouini, and A. Nallanathan, "Ergodic rate analysis of cooperative ambient backscatter communication," *IEEE Wireless Communications Letters*, vol. 8, no. 6, pp. 1679–1682, 2019.

[96] X. Jia and X. Zhou, "Performance characterization of relaying using backscatter devices," *IEEE Open Journal of the Communications Society*, vol. 1, pp. 819–834, 2020.

[97] S. Zeb, Q. Abbas, S. A. Hassan, A. Mahmood, R. Mumtaz, S. H. Zaidi, S. A. R. Zaidi, and M. Gidlund, "NOMA enhanced backscatter communication for green IoT networks," in *2019 16th International Symposium on Wireless Communication Systems (ISWCS)*. IEEE, 2019, pp. 640–644.

[98] A. W. Nazar, S. A. Hassan, H. Jung, A. Mahmood, and M. Gidlund, "BER analysis of a backscatter communication system with non-orthogonal multiple access," *IEEE Transactions on Green Communications and Networking*, vol. 5, no. 2, pp. 574–586, 2021.

[99] S. Gong, X. Huang, J. Xu, W. Liu, P. Wang, and D. Niyato, "Backscatter relay communications powered by wireless energy beamforming," *IEEE Transactions on Communications*, vol. 66, no. 7, pp. 3187–3200, 2018.

[100] J. Qian, F. Gao, G. Wang, S. Jin, and H. Zhu, "Noncoherent detections for ambient backscatter system," *IEEE Transactions on Wireless Communications*, vol. 16, no. 3, pp. 1412–1422, 2016.

[101] W. Liu, Y.-C. Liang, Y. Li, and B. Vucetic, "Backscatter multiplicative multiple-access systems: Fundamental limits and practical design," *IEEE Transactions on Wireless Communications*, vol. 17, no. 9, pp. 5713–5728, 2018.

[102] J. K. Devineni and H. S. Dhillon, "Ambient backscatter systems: Exact average bit error rate under fading channels," *IEEE Transactions on Green Communications and Networking*, vol. 3, no. 1, pp. 11–25, 2018.

[103] Z. Ding, R. Schober, and H. V. Poor, "Unveiling the importance of SIC in NOMA systems—part ii: New results and future directions," *IEEE Communications Letters*, vol. 24, no. 11, pp. 2378–2382, 2020.

[104] W. Shin, M. Vaezi, B. Lee, D. J. Love, J. Lee, and H. V. Poor, "Non-orthogonal multiple access in multi-cell networks: Theory, performance, and practical challenges," *IEEE Communications Magazine*, vol. 55, no. 10, pp. 176–183, 2017.

[105] L. Zhu, J. Zhang, Z. Xiao, X. Cao, and D. O. Wu, "Optimal user pairing for downlink non-orthogonal multiple access (NOMA)," *IEEE Wireless Communications Letters*, vol. 8, no. 2, pp. 328–331, 2018.

[106] F. Fang, H. Zhang, J. Cheng, and V. C. Leung, "Energy efficiency of resource scheduling for non-orthogonal multiple access NOMA wireless network," in *2016 IEEE International Conference on Communications (ICC)*. IEEE, 2016, pp. 1–5.

[107] J. Cui, Z. Ding, and P. Fan, "A novel power allocation scheme under outage constraints in NOMA systems," *IEEE Signal Processing Letters*, vol. 23, no. 9, pp. 1226–1230, 2016.

[108] X. Wang, J. Wang, L. He, and J. Song, "Outage analysis for downlink NOMA with statistical channel state information," *IEEE Wireless Communications Letters*, vol. 7, no. 2, pp. 142–145, 2017.

[109] J. Choi, "Joint rate and power allocation for NOMA with statistical CSI," *IEEE Transactions on Communications*, vol. 65, no. 10, pp. 4519–4528, 2017.

[110] P. Xu, Y. Yuan, Z. Ding, X. Dai, and R. Schober, "On the outage performance of non-orthogonal multiple access with 1-bit feedback," *IEEE Transactions on Wireless Communications*, vol. 15, no. 10, pp. 6716–6730, 2016.

[111] S. Li, M. Derakhshani, S. Lambotharan, and L. Hanzo, "Outage probability analysis for the multi-carrier NOMA downlink relying on statistical CSI," *IEEE Transactions on Communications*, vol. 68, no. 6, pp. 3572–3587, 2020.

[112] M. A. Adjif, O. Habachi, and J.-P. Cances, "Joint channel selection and power control for NOMA: A multi-armed bandit approach," in *IEEE WCNCW*, 2019, pp. 1–6.

[113] Z. Tian, J. Wang, J. Wang, and J. Song, "Distributed NOMA-based multi-armed bandit approach for channel access in cognitive radio networks," *IEEE Wireless Communications Letters*, vol. 8, no. 4, pp. 1112–1115, 2019.

[114] H. Sun, Q. Wang, R. Q. Hu, and Y. Qian, "Outage probability study in a NOMA relay system," in *2017 IEEE Wireless Communications and Networking Conference (WCNC)*. IEEE, 2017, pp. 1–6.

[115] H. Zhang, J. Zhang, and K. Long, "Energy efficiency optimization for NOMA UAV network with imperfect CSI," *IEEE Journal on Selected Areas in Communications*, vol. 38, no. 12, pp. 2798–2809, 2020.

[116] D. Ghosh, M. K. Hanawal, and N. Zlatanov, "Learning to optimize energy efficiency in energy harvesting wireless sensor networks," *IEEE Wireless Communications Letters*, vol. 10, no. 6, pp. 1153–1157, 2021.

[117] P. Auer, N. Cesa-Bianchi, and P. Fischer, "Finite-time analysis of the multiarmed bandit problem," *Machine learning*, vol. 47, no. 2-3, pp. 235–256, 2002.

[118] P. Perick, D. L. St-Pierre, F. Maes, and D. Ernst, "Comparison of different selection strategies in monte-carlo tree search for the game of tron," in *IEEE CIG*, 2012, pp. 242–249.

[119] A. Garivier and E. Moulines, "On upper-confidence bound policies for non-stationary bandit problems," *arXiv preprint arXiv:0805.3415*, 2008.

[120] Z. Ding, "Harvesting devices' heterogeneous energy profiles and QoS requirements in IoT: WPT-NOMA vs BAC-NOMA," *IEEE Transactions on Communications*, vol. 69, no. 5, pp. 2837–2850, 2021.

[121] Z. Ding, L. Lv, F. Fang, O. A. Dobre, G. K. Karagiannidis, N. Al-Dhahir, R. Schober, and H. V. Poor, "A state-of-the-art survey on reconfigurable intelligent surface-assisted non-orthogonal multiple access networks," *Proceedings of the IEEE*, 2022.

[122] E. V. Belmega, P. Mertikopoulos, R. Negrel, and L. Sanguinetti, "Online convex optimization and no-regret learning: Algorithms, guarantees and applications," *arXiv preprint arXiv:1804.04529*, 2018.

[123] H. Zhang, H. Zhang, K. Long, and G. K. Karagiannidis, "Deep learning based radio resource management in NOMA networks: User association, subchannel and power allocation," *IEEE Transactions on Network Science and Engineering*, vol. 7, no. 4, pp. 2406–2415, 2020.

[124] N. Yang, H. Zhang, K. Long, H.-Y. Hsieh, and J. Liu, "Deep neural network for resource management in NOMA networks," *IEEE Transactions on Vehicular Technology*, vol. 69, no. 1, pp. 876–886, 2019.

[125] Y. Liu, S. Zhang, X. Mu, Z. Ding, R. Schober, N. Al-Dhahir, E. Hossain, and X. Shen, "Evolution of NOMA toward next generation multiple access (NGMA) for 6G," *IEEE Journal on Selected Areas in Communications*, vol. 40, no. 4, pp. 1037–1071, 2022.

[126] I. Chafaa, R. Negrel, E. V. Belmega, and M. Debbah, "Self-supervised deep learning for mmwave beam steering exploiting sub-6 GHz channels," *IEEE Transactions on Wireless Communications*, 2022.

[127] B. Clerckx, Y. Mao, R. Schober, E. A. Jorswieck, D. J. Love, J. Yuan, L. Hanzo, G. Y. Li, E. G. Larsson, and G. Caire, "Is NOMA efficient in multi-antenna networks? a critical look at next generation multiple access techniques," *IEEE Open Journal of the Communications Society*, vol. 2, pp. 1310–1343, 2021.

[128] K. Senel, H. V. Cheng, E. Björnson, and E. G. Larsson, "What role can NOMA play in massive MIMO?" *IEEE Journal of Selected Topics in Signal Processing*, vol. 13, no. 3, pp. 597–611, 2019.

[129] G. Zhou, Y. Mao, and B. Clerckx, "Rate-splitting multiple access for multi-antenna downlink communication systems: Spectral and energy efficiency tradeoff," *IEEE Transactions on Wireless Communications*, 2021.

[130] Z. Ding, L. Lv, F. Fang, O. A. Dobre, G. K. Karagiannidis, N. Al-Dhahir, R. Schober, and H. V. Poor, "A state-of-the-art survey on reconfigurable intelligent surface-assisted non-orthogonal multiple access networks," *Proceedings of the IEEE*, 2022.